Chemical and Electrochemical Modification of Kraft Lignin to Value-added Products

ABSTRACT

Lignin is one of the most abundant biopolymers on earth, constituting approximately 30% of the dry weight of softwoods and 20% of hardwoods. It is a renewable, non-toxic, commercially available and low cost natural resource that has significant potential for being utilized as a basic raw material for the polymer industry.Ligninhas potential for serving as a reinforcement agent in rubber because of its relatively large molecular weight, low surface reactivity and high water resistance. However, unmodified kraft lignin is generally incompatible with the rubber matrix, causing well known hysterisis problems in filled tires. Therefore, modification is required to improve the potential application of kraft lignin as a rubber filler. To date, lignin has been used primarily as a low-grade fuel for the pulp and paper industry due to the lack of effective modification and depolymerization methods.

In this M. Sc. project, kraft lignin was extracted from black liquor that was provided by a local pulp and paper mill located in Northwestern Ontario, Canada.Both chemical and electrochemicalapproaches have been explored in an effort to modify kraft lignin such that it may have utility and appeal in value-added products. Chemical modifications of kraft lignin were carried out in order to improve itsreinforcing characteristics in rubber. Formaldehyde, glyoxal, epichlorohydrin, acetic anhydride, benzoyl chloride, myristoyl chloride, and benzyl bromide were used as modification reagents. Fourier Transform Infrared (FTIR) Spectroscopy was employed to analyze structuralchangesinthe modified

lignin. A Brunauer Emmett and Teller (BET) Surface Area Analyzerand Scanning Electron Microscope (SEM) were used to characterize the surface area and morphology of variouslignin samples. In addition, hydrophobicity tests were carried out for the determination of the wetting properties of the Kraft lignin both prior and subsequent to modifications. Lignin that was modified with glyoxal and epichlorohydrinexhibited a different structure and more dispersive particles, with a ~10 times larger surface area than unmodified kraft lignin, whereas lignin that was modified with aceticanhydrideresulted in improved hydrophobic properties. We further prepared glyoxal and epichlorohydrin-modified and acetic anhydride- modified lignin samples for industrial analysis to study the reinforcing effects of modified lignin in rubber, in comparison with its unmodified counterpart. The results indicate that modified lignin might serve as a prospective cost effective material for partially substituting the traditional and expensive rubber filler, carbon black.

In another facet of this work, we fabricated lead dioxide nanoparticles supported on TiO_2 nanotubes (TiO_2NT/PbO_2), where the TiO_2 nanotubes were directly grown on Ti substrates by electrochemical anodization and the PbO_2nanoparticles were formed by combination of photochemicalandelectrochemical deposition. Scanning Electron Microscopy (SEM) and Energy Dispersive X-ray Spectrometry (EDS) were employed to study the surface morphologyand composition of the TiO_2NT/PbO_2 electrodes. The resulting electrode was utilized as a novel approach for the oxidationof lignin; UV-Vis spectroscopy was used to in situ monitor thelignin oxidation process. The effect of concentration, current and temperature on the oxidation of lignin has been investigated, as well as post-oxidationchanges in theChemical Oxygen Demand (COD) of the lignin

solution. Fourier Transform Infrared Spectroscopy (FTIR) and High Performance Liquid Chromatography (HPLC) were employed to characterize the oxidized lignin and resultingproducts. Our study shows that the electrochemical oxidation of lignin via the fabricated TiO_2NT/PbO_2 electrode is a promising approach for the generation of lignin-derived added value products.

ACKNOWLEDGEMENTS

First and foremost, I wish to express my gratitude to my research supervisors Dr. Aicheng Chen and Dr. Zi-Hua Jiang, and the co-supervisor Dr. Bruce Kjartanson for their guidance and support throughout my studies. Without their help, this thesis would not have been possible.

I would also like to thank my fellow students and the staff of the Electrochemical and Organic Chemical Laboratories, especially Dr. Min Tian, for their help with the experiments, as well as the staff of the instrumentation laboratory for their technical expertise in regard toallanalyticalaspects of my research.

Financial support from the Natural Sciences and Engineering Research Council (NSERC) and Ontario Graduate Scholarship (OGS) are gratefully acknowledged.

Last, but certainly not least, my deepest gratitude goes out to my parents and in particular, my girlfriend, Jessica, for their support, encouragement and understanding, which have allowed me to accomplish this work. It is to them that this thesis is dedicated. Thanks and I love you!

TABLE OF CONTENTS

LIST OF SCHEMES

LIST OF FIGURES

LIST OF TABLES

Chapter 1 Introduction

1.1 Lignin

Lignin is the second most abundant biopolymer on earth, which constitutes ~30% of the dry weight of softwood and ~20% of hardwood. It plays the role of a binding agent in wood and plants and is comparable in this respect to the steel reinforcement of concrete [1]. Lignin is a primary constituent of wood in conjunction with cellulose and hemicelluloses. Cumulatively, they form the matrix which is reinforced by cellulosic fibers. In trees, lignin facilitates various functions that minimize the effects of mechanical stress. The presence of lignin in woody plants enhances their resistance against attack by microorganisms. On the other hand, lignin is also a major participant in regard to energy flows within the biosphere. Most absorbed solar energy is stored within the lignin of woody plants. Complementary to being a major component in plant systems for the storage of solar energy, lignin plays a major role as a composite material component in woods [2].

1.1.1 Physical and Chemical Properties of Lignin

Structurally, lignin is a poly phenolic macromolecule that is comprised of 9-carbon phenol propane units, non-uniformly linked together by different types of bonds. However, since the last century, although the study of lignin is ongoing, its specific structure remains uncertain, resulting in a nebulous concept and thus an inability to properly define it [3-6]. This is because lignin does not exist as a homogeneous compound with a definite molecular size but rather, is a long-chain (and most likely) cross-linked polymer, which is variable in its molecular dimensions. Furthermore, lignin is formed of

monomeric units which may vary in both character and ratio. Finally, the structures of lignin are strongly affected by the isolation methods from pulp and waste water. All of these factors lead to difficulties in defining the actual structure of lignin. Currently, the most widely used methods for characterizing the structure of lignin are based on its physical properties, which include for example, its capacity for ultraviolet absorption [7], infrared absorption [8], nuclear magnetic resonance [9]. Because of these properties, physical tests are considered to be one of the most effective strategies toward the characterization of lignin's structure.

In recent years, several investigations into lignin's chemical makeup have been undertaken, and associated structural models have been considered. Lignin is traditionally considered to be a dehydrogenative polymer that is comprised of three monolignols [10, 11]: p-coumaryl alcohol, coniferyl alcohol, and sinapyl alcohol (Scheme1). Because lignin is manifest as different structural units, it has been grouped into three types; softwood, hardwood, and grass [12]. Hardwood lignin is made up of both coniferyl alcohol (also called guaiacyl propane units) and sinapyl alcohol. Softwood lignin consists mainly of coniferyl alcohol (92-95%) with small amounts of sinapyl alcohol and p-coumaryl alcohol (also called 4-hydroxylphenyl propane units) (3-8%). Grass lignin is comprised ofconiferyl alcohol, p-coumaryl alcohol and sinapyl alcohol, in ratiosthat vary from those of other types of lignin [13].

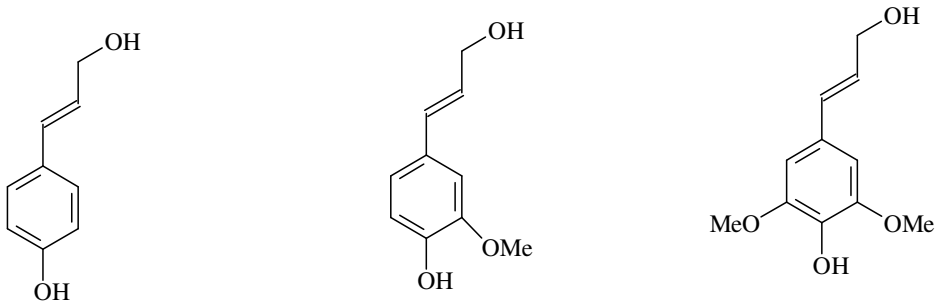

Scheme 1.Lignin building blocks, the three monolignols (Derkacheva et al. 2008)

Due to the structural complexity of lignin, there remains no standardized knowledge as relates to its chemical and physical structure. However, several molecular models have been proposed that are based on the analysis of softwood and hardwood lignin degradation products [14-17]. A schematic representation of softwood lignin is depicted in Scheme 2, showing the components derived from p-coumaryl alcohol, coniferyl alcohol and sinapyl alcohol, as well as those common linkages that are found in lignin including β-O-4, 4-O-5, and 5-5'[18]. Among them, the predominant linkage is the so-called β-O-4 linkage. About 40-60% of all inter-unit linkages in lignin are via this bond [19]. According to this scheme, the large volume of phenolic hydroxyl groups in lignin is also very important because of the reactivity of these groups and the effects that they impart to both the chemical and physical attributes of the lignin molecule [20]. The majority of ligninic active sites are comprised of phenolic or alcoholic hydroxyl groups, which greatly enhance its reactivity [21]. Furthermore, the phenolic hydroxyl groups affect the hydrophilicity of lignin, which is essential for its dissolution. They may, however, also contribute to the poor brightness stability in lignin-rich pulps, since they are prone to photonically and thermally induced oxidation reactions [22].

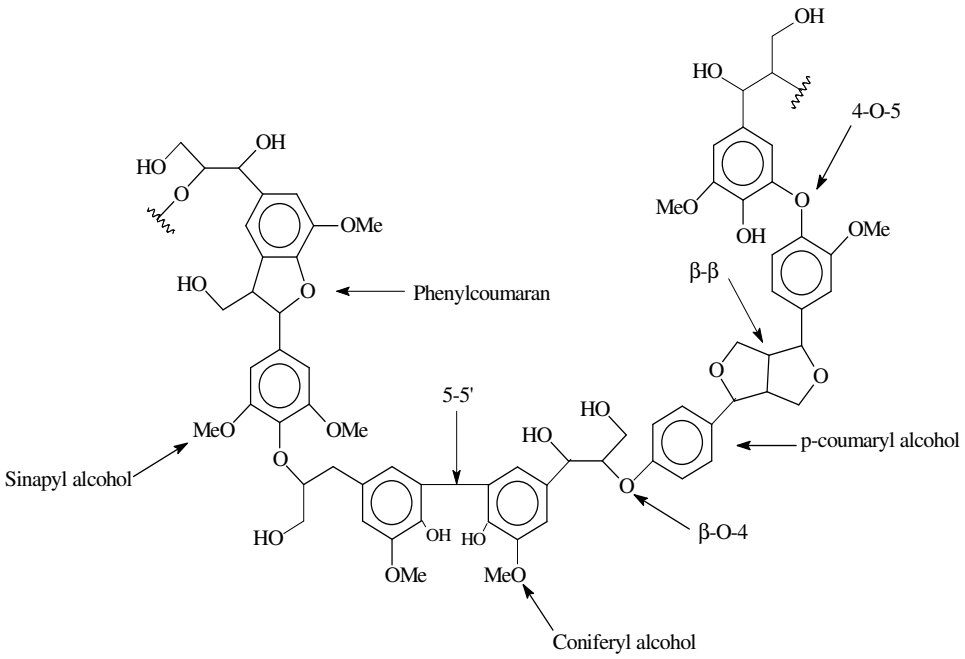

Scheme 2. A schematic representation of a softwood lignin

1.1.2 Kraft Lignin from Industrial Black Liquor

In recent years, large amounts of lignin have been generated by the pulp and paper industry, wherein vast quantities of forest biomass are used in paper mills for the manufacture of paper, while producing significant volumes of by-products, including dark residues such as black liquor [23]. Kraft pulping constitutes the most critical process in the production of pulp, which accounts for almost 60% of worldwide pulp production [24]. In kraft pulping process wood is utilized as the basic raw material to produce pulp. The major components of wood are cellulose (40-50%), hemicelluloses (25-30%) and lignin (25-30%) [25].

There are two significant pulping technologies available to produce paper pulping, which are mechanical and chemical pulping [26]. In mechanical pulping, the cellulose fibers are separated mainly through mechanical operations. The wood to pulp ratio is high;

however lignin remains in the pulp. Therefore, the mechanically processed pulps become yellow in color due to the high content of lignin. The mechanically produced pulps are mostly used for paper products that are intended for short term usage such as newspapers and magazines. It is also possible to make dense sheets for printing paper using mechanical pulps [27].

The Kraft process involves chemical treatment to separate cellulose fibers from lignin with low wood to pulp yield. The chemical pulping process includes the digestion of wood where the wood chips are cooked at a high temperature under highly alkaline conditions in the presence of sulfide. The objective is to dissolve the lignin and separate it from the cellulose fibers. Thus the pulp contains fibers with high strength and, if bleached, high brightness and long stability. Fine paper and tissue can be made from such chemical pulp [28].

The spent cooking liquor produced from the Kraft process is usually known as black liquor, which contains organics, especially lignin, from the wood and the inorganic chemicals used for delignification [29]. Black liquor may cause pollution in industrial wastewater [30]. A conventional pulp mill can produce a hundred tons of black liquor every day [31]. Despite the fact that it is rich in lignin, the heating value of black liquor is still relatively low due to the presence of inorganic chemicals [32]. Therefore, it is economically and environmentally desirable to recover and reuse industrial black liquor.

1.1.3 Applications of Lignin

As mentioned in section 1.1.2, large amounts of lignin are produced by the paper and pulp industry, which is contained in black liquor. In the pulping wastewater effluent, the

large amounts of lignin and its derivatives comprise a significant amount of biorefractory pollutants in wastewater, causing the coloration of the effluent. Furthermore, lignin contributes heavily to the oxygen consumption such as COD in pulping wastewater. Therefore, the treatment of lignin that is contained in pulping wastewater is necessary for environmental issues [33-38]. In industry, lignin is generally isolated and precipitated from pulping effluent/black liquor. Carbon dioxide and sulfuric acid are the chief reagents used for the isolation of lignin from pulp as it is dissolved in basic pulping effluent, but is precipitated in an acidic condition [39-42]. In addition, other methods such as alcohol, dioxane and phenol [43-45] have also been applied to isolate lignin. Various isolation methods of lignin from black liquor result in variable structures of extracted lignin, leading to more difficulties in the study of lignin structure [46-48]. Therefore, lignin from industrial pulping wastewater is recommended to be isolated in mild conditions, such as through the use of carbon dioxide, to retain an unchanged structure of isolated lignin [49, 50].

After isolation from wastewater, because of the lack of application potential, most of the lignin (~98%) is simply burned to recover energy or pulping chemicals. However, the combustion of lignin significantly eliminates its potential for high-value derivatives. Furthermore, the burning procedure produces large amounts of CO_2 gas, which contributes to the global warming. On the other hand, lignin has been applied for utilization in products such as adhesives, rubber fillers, and carbon fibers. [51-53]. However, the complex structures and low activities of lignin limit its potential. Because the pulping and papermaking industries are evolving rapidly, the pressures on environmental issues are

responsible for initiating research into the modification of kraft lignin from industrial wastewater to value-added products.

Because of its polymeric structure, most of the attempts to add value to lignin are based on novel innovative approaches to utilize lignin as a polymeric material, where the uniqueness of lignin as a macromolecular material might be further exploited [54]. Simmons and Eisenberg have introduced cationic and anionic groups into lignin molecules, in order to enhance the interactions among the molecules, which could improve its properties as a polymeric blend [55]. Tejado et al. found a method for fabricating lignin-modified Phenol-Formaldehyde (PF) resins by reacting lignin in an alkaline condition with formaldehyde [56]. Setua et al. studied the reinforcing effect of lignin that was modified by benzoyl peroxide in rubber, which shows its potential to improve the strength of filled rubber [57]. In respect to the competitiveness of lignin and its modified products with other polymers, the economic considerations may affect the choice of materials to be used. Lignin itself is a natural material, which generally has the advantages of low process cost with low energy requirements. For the existing plastics and rubber industries, the production of polymers is highly energy intensive. Thus the utilization of lignin from the pulping industrial waste as a polymeric material may not only reduce energy consumption, but also benefit both the forestry industry and the environment.

On the other hand, several attempts have also been made to modify lignin by changing its chemical structure, including the addition of various functional groups, or even via thorough oxidization [58]. Sun et al. have studied the acetylation of lignin molecules to enhance its dimensional stability [59]. Tolba et al. have applied an electrochemical method to convert lignin to value-added products [60]. On the whole,

various attempts have been studied to reduce the negative influence of lignin on the environment, or add value to it, to show that lignin is a prospective material to be utilized in different areas [61].

1.2 Rubber Filler

The use of fillers in rubber is almost as old as the use of rubber itself. One aspect of filler addition is the improvement of properties, where another aspect is the extension of rubber with less expensive materials [62, 63]. Carbon black is well known as the most used type of rubber filler for its low cost and ease of fabrication [64, 65]. Other kinds of rubber fillers such as organic resin fillers, etc. [66-68] have also been studied in combination with rubber. The main advantage of the predominant use of fillers, particularly carbon black, is the reinforcement that they impart to the vulcanizates [69].

Reinforcement basically relates to composites built from two or more structural elements or components of different mechanical characteristics, and whereby the strength of one of these elements is imparted to the composite combined with the set of favorable properties of the other component. This set must include easy shaping into the required form of the final article and stabilization of this shape within a reasonable time. One typical example of reinforcement is that of concrete with embedded steel rods or cable where the high tensile strength of the steel is imparted to the concrete to give it increased flexural and impact strength. In the case of the reinforcement of rubber by fillers, the best definition may be: reinforcing filler improves the modulus and failure properties (tensile strength, tear resistance, and abrasion resistance) of the final vulcanizate. On the other hand, it should be noted that there is a reduction in properties when the fillers ratio loading is too high, which may be due to a diminishing volume fraction of polymer in the

composite. If the volume percentage of filler becomes so high that there is not enough rubber matrix to hold the filler particles together, strength approaches zero [70].

1.2.1 Reinforcement Mechanism

Properties such as tensile strength of natural rubbers, for example, Styrene-Butadiene-Rubber (SBR) and nitrile rubber, is poor since there is an unequal distribution of stress within the matrix. The moving molecular chains may not be in their most favorable positions. The result is a random distribution of the chain lengths, and thus, diffused tensile stress. As a consequence, when the rubber sample is subjected to tensile or other tests, a number of chains, the shortest or most strained ones, break early on in the test, then the next most strained ones fail, until at the moment just before failure, only a few chains effectively carry the load. This is the reason for the poor tensile strength of natural rubbers [71].

When fillers such as carbon black are applied into the rubber matrix, they give the most highly strained chains a means for slippage to relieve the tensions that are caused by stretching, causing these chains to not break prematurely in the earlier part of the tensile strength experiment and to survive to the very moment before rupture.

1.2.2 Typical Filler Characteristics

Particle Size and Surface Area

The improvement of tensile strength of rubbers is strongly dependent on the particle size and surface area of the filler. Small particles usually have a much greater effect than coarse ones. Particle size is directly related to the surface area per gram of filler. Thus the effect of smaller particles actually reflects their greater extent of interface between the

polymer and rubber matrices. Surface area is usually analyzed to represent the particle size of fillers. It is usually determined by gas adsorption measurements according to the method of Brunauer Emmett and Teller (BET). The amount of gas, usually nitrogen, absorbed as a function of gas pressure, is determined at near its boiling point. Then an isotherm could be developed. The surface area of the material may finally be calculated based on the amount of nitrogen gas that is absorbed according to the isotherm.

Specific Surface Activity

The nature of the filler surface may vary in chemical composition, having different chemical groups, for example, hydroxyl, carboxyl, or carbonyl groups. The effects of surface compositions of fillers are variable in different kinds of rubber. For example, rubbers with polar natures such as neoprene and nitrile rubber, will interact more strongly with filler surfaces having dipoles such as OH and COOH groups or chlorine atoms. With general purpose hydrocarbon rubbers, however, no dramatic influences on reinforcement are noticeable when the fillers are added. Therefore, there is no confirmed method for measuring the influence of surface activity of fillers in rubbers. Only expected improvement of filled rubbers resulting from certain functional groups of fillers can be estimated.

Porosity

Porosity is mainly a characteristic of polymeric fillers such as carbon black. Properties of rubbers dependent on volume loading and inter particle distance are related to this parameter. Highly porous fillers may immobilize certain proportions of accelerator, therefore increase the viscosity and electrical conductivity of filled rubber. However,

although porosity is a factor that can be used to assess a filler's influence on rubber properties, its effect on reinforcement is a secondary.

1.2.3 Studies on the Rubber Reinforcement of Lignin

As a rubber filler, lignin displays attractive advantages over the traditional rubber fillers such as carbon black due to its polymeric structure, antioxidant properties, and low cost. However, in contrast to the great number of articles regarding its utilization, only limited studies have been made on the application of lignin as rubber filler [72]. Kumaran and De used lignin as a replacement of carbon black in SBR and natural rubber [73-76]. Nichols employed kraft lignin as a reinforcing agent in natural rubbers [77]. As a result, physical-mechanical properties were reported to be improved for the final product by using oxidized lignin instead of lignin in unmodified form. This is mainly because unmodified kraft lignin is usually incompatible with the rubber matrix, causing well known hysteresis problems in filled rubber. Therefore, most developments on lignin-reinforced rubber systems are focusing on applying various approaches to modify kraft lignin, in order to improve its reinforcing effect in filled rubber.

1.3 Chemical Modifications of Lignin

The chemical modification of lignin is an area of significant scientific work. It is largely based on the knowledge of the lignin structure. Recently, various chemical modifications of lignin have already been well-established, which are used to adjust the physical and chemical properties of this material in order to achieve enhanced solubility, increased blend compatibility, and improved mechanical properties [78-83].

According to the structure of lignin (Scheme 2), various reactive functional groups can be found in lignin molecules, which make it possible to be modified through certain chemical reactions. As mentioned in section 1.1.1, the hydroxyl groups, especially phenolic hydroxyl groups, contribute to most of the activities of lignin molecules. Therefore, most of the chemical modifications, which aim at changing the structure of lignin, are applied through the reaction related to phenolic hydroxyl groups. Adilson et al. have studied the hydroxymethylation and oxidation of lignin with formaldehyde [84]. Nour-eddine El et al. have applied glyoxal as a reagent to modify the structure of lignin [85]. Various reports in the literature have studied the chemical modification of the lignin structure for certain applications, illustrating the potential for adding value to this industrial by-product.

1.3.1 Modifications of Lignin with Electrophilic Reagents

Due to its unique chemical structure, lignin has the attractive property of being modified. One approach that has been widely explored is modifying lignin molecules with electrophilic reagents [86, 87]. Scheme 3 presents the principle reaction between lignin molecules and typical electrophilic reagents. The addition of new functional groups onto lignin molecules could modify the structure of lignin and improve its characteristics for certain applications.

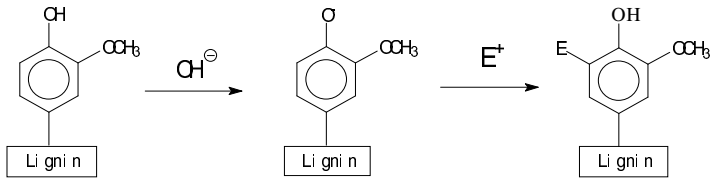

*E^+ represents electrophilic ions.

Scheme 3. A schematic representation of lignin modification with electrophilic reagent

In the past, lignin modifications with electrophilic reagents have been widely studied. Adilson and Priscila used formaldehyde to modify organosolv lignin and utilized the products as wood adhesives [88]. Theodor et al. studied the hydroxymethylation reaction of alkali lignin [89]. Carmen Martinez et al. evaluated the extent of electrophilic reactions in lignin precursors [90].The polymerization of lignin has been investigated by Stephen Y. Lin and Wausau [91].

Furthermore, cross-linking polymerization of lignin molecules is expected to occur when lignin is modified with certain electrophilic reagents such as formaldehyde [92, 93]. The cross-linking reaction can block polar functional groups or form C-C bonds between positions adjacent to the phenolic hydroxyl groups, creating networks varying in pore structure and polarity. It can also produce gels held together by secondary forces, such as hydrogen bonding and Van der Waal's forces [94, 95]. Once modified, lignin can take the form of fine powder or coarse granules. After cross-linking, the molecular weight of lignin may be further increased, while the molecular chains become longer, leading to a larger surface area of modified lignin. Such improved properties could be expected to enhance the reinforcement of lignin to filled rubber, particularly in tensile strength and tear resistance.

1.3.2 Modifications of Lignin with Acylating and Alkylating Reagents

Earlier studies have shown that lignin has a stabilizing effect on both the thermo- and photo-degradation of natural and synthetic rubbers [57]. However, one limitation of utilizing kraft lignin as a rubber filler is its hydrophilic properties because of the large amount of hydroxyl groups within lignin molecules, which contribute to the incompatibility problem of lignin with the rubber matrix. Thus the modification of these

reactive groups may result in an effective alteration of the lignin hydrophilic properties. Furthermore, the improvement of water absorbance resistance of kraft lignin could benefit its reinforcing effect in the rubber matrix.

Chemical modifications can reduce the hydrophilicity of kraft lignin. Acylating and alkylating reagents could be used to react with lignin molecules. These reagents can react with the hydroxyl groups in lignin molecules, which are mainly responsible for their hydrophilic nature, and forming new hydrophobic groups through chemical reactions [97, 98].Although such modification consumes hydroxyl groups, especially phenolic hydroxyl groups, leading to lower activity of lignin molecules, the resulting modified lignin is expected to possess highly hydrophobic properties, which could improve its reinforcing effect in the rubber matrix.

Modifications of lignin with various acylating and alkylating reagents have been widely studied [99-103]. According to Sun et al., the acetylation of lignin has been studied to reduce its hygroscopic nature [59]. Benzoyl Chloride has also been used by Haibo et al. to modify the lignin structure [104]. Ronald et al. have studied acylation reactions in grass lignin [105].All the literatures show that acylating and alkylating reagents are promising to modify the structure of lignin and change its properties.

1.4. Electrochemical Modifications of Lignin

In addition to chemical modifications, in recent years, several innovative approaches have been studied for the modification of lignin. One of these is the electrochemical approach, which aims mainly at oxidizing instead of polymerizing lignin molecules [106-108]. Given the lignin units (Scheme 2), the oxidation of lignin usually results in the

conversion of phenolic nuclei to o- or p-quinonoid structures or in the rupture of the aromatics leading to enoic or dienoic acids. Vanillin is usually obtained from the cleavage of the propanoid side chain in the presence of oxidizing agents [109-111].

In comparison to chemical oxidation, electrochemical oxidation has been described as an effective way to modify lignin due to its ease of operation, wide range of treatment conditions and environmental friendliness. Studies on the electrochemical oxidation of lignin began in the mid-1940s. When lignin is electrochemically oxidized, a considerable percentage of the mass is transformed into low-molecular weight products. The mechanism and kinetics of the oxidation of lignin have also been widely studied [112-116]. Tolba et al. studied the electrochemical oxidation of lignin at IrO_2-based oxide electrodes [60]; Tian et al. demonstrated a novel photo-electrochemical oxidation approach for degrading lignin into value-added products [117].

In industry, electrochemical oxidation has been included in the advanced oxidation processes (AOP) under the name of electrochemical advanced oxidation processes (EAOP). Comparatively among the AOP, electrochemical oxidation is very attractive due to the reduction of sludge formation and the low consumption of chemicals. However, the main drawbacks of electrochemical oxidation for the treatment of wastewater, for instance, pulping wastewater containing lignin, are the energy consumption per unit of wastewater volume and the high cost for both investment and operation of low efficiency electrodes [117]. Therefore, it will be of significant benefit to develop an electrode at low cost with high oxidation efficiency of lignin.

1.4.1 Titanium Dioxide Nanotube (TiO_2NT)

TiO_2 has been described as one of the most important materials for applications of photoelectrochemistry in semiconductors. One important property of TiO_2 is its light absorption at $\lambda \leq 385$ nm, which initiates the promotion of an electron from the valence band to the conduction band of the semiconductor. This excitation process creates an electronic charge carrier in the conduction band, as well as an electron vacancy in the valence band. Because the valence band edge of TiO_2 occurs at approximately +3.2 V vs the normal hydrogen electrode, NHE, at pH=0, the hole is a very powerful oxidizing agent for several chemicals [118]. Figure 1a illustrates the photocatalytic schematic representation. Based on its photocatalysis, TiO_2 presents as an attractive material for wastewater treatment. However, one limitation of TiO_2 electrodes is that the quantum yields for photodegradation of organics in aqueous solutions are low. Therefore, TiO_2 is always used as a substrate to fabricate electrodes with high efficiency, instead of applying it directly for wastewater treatment [118]. Figure1b illustrates the diagram of TiO_2 electrode oxidation based on its phototcatalysis, indicating that oxidation occurs not only by direct electron transfer between metallic ions and the TiO_2 substrate through the holes produced by photocatalysis, but also by hydroxyl radical attack, which is produced by the oxidation of an aqueous solution [118]. Therefore, TiO_2 is described as an attractive substrate to fabricate composite electrodes under illumination because of its high phototcatalytic properties.

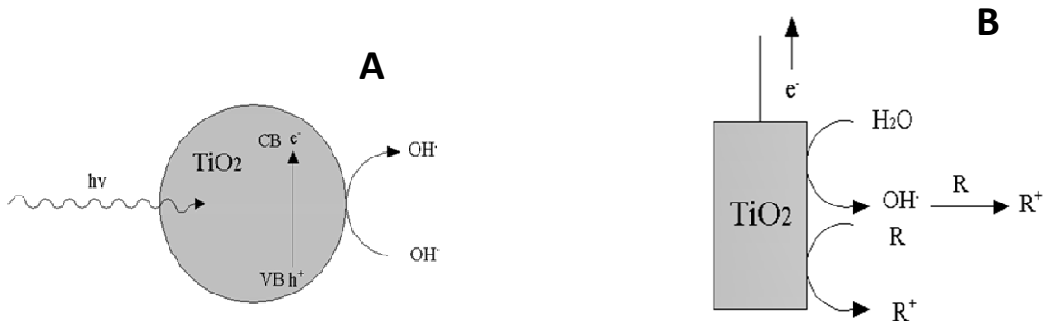

Figure 1. Schematic representation of(A)TiO_2photocatalysis; (B) TiO_2electrodeoxidation

On the other hand, in recent years, much attention has been focused on the nanostructure of TiO_2. Nanostructures comprised of TiO_2 such as nanotubes, nanofibers, nanorods may enhance its performance because of the large surface areas [119-121]. Due to this, the fabrication of nanostructures of TiO_2 has been widely investigated, including template assisted, hydrothermal, and anodic oxidation, etc. [122-125]. The facile fabrication of nanostructures and control of surface morphologies make TiO_2 an attractive material in the fabrication of high efficiency electrodes.

1.4.2 Lead Dioxide Electrode (PbO_2)

Among the most commonly used anode electrodes for the oxidation of organic compounds such as lignin, boron-doped diamond (BDD) and lead dioxide (PbO_2) show the highest oxidation power [126, 127]. Boron-doped diamond (BDD) has been widely recognized as an excellent material for electrodes in performing electrochemical oxidation, not only in electroanalysis or preparation of powerful oxidants, but also for the removal of organics from wastewater, such as lignin, due to its high anodic stability and wide potential range. Because of its unique surface properties, BDD electrodes can perform the electrochemical oxidation of lignin with high energetic efficiency under the appropriate operational conditions. Various studies have been made on the electrochemical oxidation

of organic matter using BDD electrodes [128-130]. However, a main limitation of this highly efficient electrode is its complex preparation and high cost, especially for large areas [131].

Compared with BDD, PbO_2 is a cheaper and more easily prepared electrode with stable performance in a wide range of electrolytes, which obtains high overpotential for oxygen evolution, a strong ability to produce hydroxyl radicals, and very good conductivity [132, 133]. On the other hand, PbO_2 electrodes are promising in environmental applications because if their good corrosion resistance in acidic solutions [134]. The electrochemical properties of PbO_2 are mainly determined by the conditions and mechanisms of its production [135].

$$OH^- \longrightarrow OH^{\cdot} + e$$

$$Pb^{2+} + OH^{\cdot} + OH^- \longrightarrow Pb(OH)_2{}^{2+} + e$$

$$Pb(OH)_2{}^{2+} \longrightarrow PbO_2 + 2H^+$$

Once produced, lead dioxide will accelerate with the absorbed hydroxyl radicals. Such compounds contribute mostly to the oxidation ability of organic compounds in wastewater.

However, a limitation of the PbO_2 electrode is that it does not have satisfactory electrocatalytic ability in comparison with BDD anodes. To solve this problem, recent research has focused on the modification of PbO_2 electrodes by element doping, such as Bi, Co, Ce, and Fe. Another approach is to increase the loading capacity of PbO_2 on a flat

substrate surface to enhance its electrochemical properties [134]. In general, the traditional substrate of PbO_2 anodes is typically Ti. When the vertically aligned TiO_2nanotubes are used for the substrate electrode, they can provide a larger surface area than the Ti substrate, which may serve as a novel underlay for PbO_2. The nano architecture of nanotube arrays feature a high surface-to-volume ratio, which is due to the additional area enclosed inside the hollow structures. Thus, the loading capacity of PbO_2 maybe improved with TiO_2NT [136-138]. However, because TiO_2 is a semiconductor material, which behaves as an insulator during electrochemical deposition, it is difficult to deposit PbO_2 onto TiO_2NT surfaces using normal electrochemical deposition [139]. Therefore, it is necessary to find an effective approach for the deposition of PbO_2 onto TiO_2NT electrodes.

1.4.3 Photoelectrochemcial Deposition

Until now, few studies have reported on the direct loading of PbO_2 onto TiO_2NT electrodes. It is difficult to deposit PbO_2 onto TiO_2NT arrays by constant current electrodeposition due to the high surface tension of the nanotubes. Some studies have explored novel deposition methods. For example, Chao Tan et al. have employed a pulse electrodeposition (PED) technique to synthesize an electrode with highly-ordered TiO_2NT that were loaded with PbO_2[140]. Among them, the photoelectrochemical method is an effective approach for the deposition ofPbO_2 onto TiO_2NT surfaces for its highly photoelectrochemical activity [141]. In photoelectrochemical deposition, the photo-produced hydroxyl radical on the illuminated surface of TiO_2 electrode significantly contributes to the deposition of PbO_2 because in the dark, as mentioned in section 1.4.2, TiO_2 behaves as an insulator and disturbs the electrodeposition of PbO_2.

Metallic oxides such as $PbO_2$are usually electrodeposited onto metal electrodes in an acidic electrolyte under anodic bias by the following steps [135].

On the anode:

$$Pb^{2+} + 2H_2O \longrightarrow PbO_2 + 4H^+ + 2e^-$$

$$2H_2O \longrightarrow O_2 + 4H^+ + 4e^-$$

On the cathode:

$$Pb^{2+} + 2e^- \longrightarrow Pb$$

$$2H^+ + 2e^- \longrightarrow H_2$$

In the case of the photoelectrochemical process, the light absorption of TiO_2 affects the promotion of an electron from the valence band to the conduction band of the semiconductor. This excitation process creates an electronic charge carrier in the conduction band and an electron vacancy (h^+) in the valence band. Because the hole is a very powerful oxidizing agent, the OH radical could also be generated by TiO_2 electrodes with the following step between a hole and water under illumination.

$$H_2O + h^+ \longrightarrow OH^{\cdot} + H^+$$

Therefore, the OH radical that is produced on the surface of TiO_2 under illumination might attract more metallic cations in the electrolyte, allowing a higher deposition rate of PbO_2 [142].In conclusion, the fabrication of highly efficient PbO_2 electrodes onto TiO_2

substrate is possible when the photoelectrochemcial method is used as the deposition approach.

1.5 Thesis Objectives

Large volumes of kraft lignin have been produced from the pulp and paper industries, and contributing to wastewater pollution. Most of the kraft lignin is simply burned in order to generate energy because its complex structure and low activity severely limit its potential applications. Therefore, modifications are necessary to add value to this pulp and paper industrial by-product, which will benefit both economic and environmental issues.

During my M. Sc. project, both chemical and electrochemical modifications were applied to softwood lignin, aiming to produce value-added lignin products. Firstly, chemical modifications were applied aiming to improve the reinforcing effect of kraft lignin in rubber. Kraft lignin has already been studied as a rubber filler, however the reinforcing effect was not good and they also caused hysteresis problems in rubber due to its hydrophilic properties. Therefore, in this project, electrophilic, acylating and alkylating reagents were used to modify kraft lignin and improve its reinforcement in rubber. Electrophilic reagents were used to modify the structure and add new functional groups on lignin molecules. Acylating and alkylating reagents were used to improve hydrophobic properties of kraft lignin. Fourier Transform Infrared (FTIR) Spectroscopy was employed to study the structural change of lignin. Brunauer Emmett and Teller (BET) Surface Area Analyzer and Scanning Electron Microscope (SEM) were used to study the surface morphologies of lignin. Hydrophobicity test was used to study the hydrophobic properties changes of lignin. After lab studies, we further prepared large scale lignin samples for industrial rubber reinforcing analysis.

Secondly, electrochemical modification of lignin was performed aiming to oxidize it into value-added products. Electrochemical modification has already been explored as an effective approach to oxidize the organic pollutants such as lignin in industrial wastewater. However, the high cost and low efficiency of electrode limits its potential. Therefore, in this M. Sc. project, a novel approach to fabricate a high performance PbO_2 nanoparticles supported on the TiO_2nanotubesby combining photocatalytic and electrochemical deposition was developed, and the fabricated TiO_2NT/PbO_2/ electrode was utilized to oxidize lignin. UV-Vis spectrum was employed to monitor the oxidation process. Chemical Oxygen Demand (COD) was analyzed to assess the oxidation effect of lignin. Different oxidation conditions were studied and finally the oxidized intermediates were investigated through High-Performance Liquid Chromatography (HPLC).

Chapter 2 Experimental

2.1 Materials and Chemicals

All commercial materials used in this project were purchased from commercial suppliers: Folmaldehyde (37%) (Sigma-Aldrich); Glyoxal (40%) (Sigma-Aldrich); Guaiacol (98%) (Sigma-Aldrich); Epichlorohydrin (99%) (Sigma-Aldrich); Acetic Anhydride (97%) (Caledon); Sodium Acetate (Mallinckrodt); Benzoyl chloride (99%) (Sigma-Aldrich); Potassium carbonate (Caledon); Myristoyl chloride (97%) (Sigma-Aldrich); Benzyl bromide (98%) (Sigma-Aldrich); Sodium hydroxide (97%) (Anachemia); Nitrite acid (70%) (Caledon); Lead nitrite (99%) (Sigma-Aldrich); Sulfuric acid (98%) (Caledon). Anhydrous pyridine was made by distillation over potassium hydroxide and tetrahydrofuran (THF) over sodium. ACS grade solvents were purchased from Fisher and used for chromatography without distillation. Thin Layer Chromatography (TLC) was performed on Silica Gel 60 Å F_{254} (thickness 250 µm) purchased from Silicycle Inc., Canada, with detection by fluorescence (254 nm) and by dipping into Mostaine reagent [ammonium molybdate ($(NH_4)_6Mo_7O_{24}.4H_2O$, 20 g) and cerium (IV) sulfate ($Ce(SO_4)_2$, 0.4 g) in 10% H_2SO_4 solution (400 ml)] followed by charring at ~ 120 °C. Flash column chromatography was performed on Silica Gel 60 (40-63 µm) also purchased from Silicycle Inc., Canada. In this project, kraft lignin was extracted from industrial black liquor provided by Abitibi Bowater, Thunder Bay. In this study, lignin unit was considered as a 9 carbon phenol propane structure, of which the molecular weight is estimated as ~180 g/mol. Pure water (18 MΩ cm) was obtained from a NANO pure® Diamond^{TM} UV

ultrapure water purification system. All air and moisture sensitive reactions were performed under nitrogen atmosphere.

2.2 Extraction and Purification of Kraft Lignin from Industrial Black Liquor

Lignin used in this project was extracted from commercial black liquor provided by Abitibi Bowater Inc., Thunder Bay, Canada. The softwood and hardwood lignin were isolated from industrial black liquor by different methods.

Extraction with CO_2 at pH=8

Industrial black liquor was diluted with pure water to 3:1 (w/w). The solution was then bubbled with CO_2 gas for 12 hours to adjust pH=8at 60 °C.

Extraction with H_2SO_4 at pH=4

Industrial black liquor was diluted with pure water to 3:1 (w/w). The solution was then dropped with 4 M sulfuric acid to adjust to pH=4 at room temperature.

Further precipitation with H_2SO_4 at pH = 2 after CO_2 extraction

Industrial black liquor was diluted with pure water to 3:1 (w/w). The solution was then bubbled with CO_2 gas for 12 hours. After precipitation, the remaining solution was further dropped with 4 M sulfuric acid to adjust pH=2 at room temperature.

Lignin Recovery

Once acidified, the precipitated lignin was separated and extracted from black liquor by centrifugation. The centrifugate was then washed with 0.001 M sulfuric acid several times, in order to get purified lignin products. Finally, the purified lignin was collected and

dried in an oven at 50 ºC for more than 12 hours. All the lignin products were ground into powder for further analysis.

2.3 Chemical Modifications of Kraft Lignin with Electrophilic Reagents

For the chemical modifications of lignin, all experiments were carried out in similar apparatus. In this project, only the modifications on softwood lignin extracted by CO_2 have been studied.

2.3.1 Modification with Formaldehyde

1.0 g kraft lignin powder (5.56 mmoles) was added into a 50 ml round bottom flask equipped with a condenser. About 4.3 ml sodium hydroxide solution (0.2 M) was added and the mixture was heated in an oil bath to 90 °C. After all the lignin was dissolved, 0.37 ml (5 mmole) formaldehyde solution was added drop by drop and the mixture was stirred at 90 °C for 7 hours. From time to time, NaOH solution (0.2 M) was added to keep the pH of the solution between 12 and 12.5 to prevent the precipitation of lignin product during the reaction. After reaction, the product was recovered by the same procedure as lignin recovery, with a 73% recovery yield. The lignin modified with formaldehyde is named as LF in the following sections.

2.3.2 Modification with Glyoxal

2.3.2.1 Reaction of Glyoxal with Model Compound Guaiacol

The reaction was enabled by adding 2.23 ml (20 mmoles) Guaiacol solution into 50 ml round bottom flask, followed by adding sodium hydroxide (1.0M) to adjust pH to 11. The solution was then stirred and heated at 50 °C in an oil bath. During heating, 4.56 ml (40 mmoles) Glyoxal solution was diluted to 18.24 ml and added to the round bottom flask

drop by drop. In this process, the Glyoxal solution was added in 5 hours and the reaction was left running for 2 more hours. During the process, the pH of the solution was always maintained at around 11.

After reaction, the solution was transferred to a 250 ml separating funnel. Then 1.0 M HCl was added until pH was adjusted to 2~3. Following this, Dichloromethane (DCM) was added to extract the organic phase of the solution. Na_2SO_4 solid was added after to remove the water from the extracted solution, and at last, the solution was then filtered and collected, with a 67% recovery yield.

2.3.2.2 Lignin Modification

Based on the model compound reaction, the modification of lignin was processed under a 90 °Coil bath for 7 hours at pH=12. 1.0 g lignin powder was added into a 50 ml round bottom flask with 0.29 ml (2.56 mmoles) glyoxal solution. The experimental procedure was carried out similarly to section 2.3.1, and the product showed a 63% recovery yield. The lignin modified with glyoxal is named as LG in the following sections.

2.3.3 Modification with Epichlorohydrin

This reaction was processed at 95 °C in an oil bath for 5 hours at pH=12. 1.0 g lignin powder was added into 50 ml round bottom flask with 0.0784 ml (1.00 mmoles) epichlorohydrin solution. The experimental procedure was carried out similarly to section 2.3.1, and the product showed a 74% recovery yield. The lignin modified with epichlorohydrin is named as LE in the following sections.

2.3.4 Modification with Glyoxal and Epichlorohydrin

2.3.4.1 Small Scale Reaction

In this reaction 1.0 g lignin powder was added into a 50 ml round bottom flask with 0.57 ml (5 mmoles) gloxal and 0.039 ml (0.5 mmoles) epichlorohydrin solution. The apparatus was set into an oil bath at 95 °C for 7 hours at pH=12. The experimental procedure was similar to section 2.3.1, and the product showed 82% recovery yield. The lignin modified with glyoxal and epichlorohydrin is named as LGE in the following sections.

2.3.4.2 Scale-up Preparation

After the lab study, the modified lignin with glyoxal and epichlorohydrin (LGE) was selected for industrial analysis of rubber reinforcement. 100 g kraft lignin powder was added into a 1 L round bottom flask. 57.0 ml (500 mmole) glyoxal and 3.90 ml (50 mmole) epichlorohydrin were then mixed with the lignin powder. These components were allowed to react at 95 °C for 7 hours at pH=12. The experimental procedure was the same as the small scale modification in section 2.3.4.1. The modified lignin with 92% recovery yield was dried and then sent to The Goodyear Tire & Rubber Company for rubber reinforcing analysis.

2.4 Chemical Modifications of Kraft Lignin with Acylating and Alkylating Reagents

2.4.1 Modification with Acetic Anhydride

2.4.1.1 Small Scale Reaction

1.0 g kraft lignin powder (5.56 mmoles) was added to a 50 ml round bottom flask equipped with a condenser. In the meantime, 0.6g (7.30 mmole) sodium acetate solid was mixed with lignin powder. Then 3.0 ml (31.82 mmole) acetic anhydride was added into

the flask to dissolve the solid mixture, which was stirred at 120 °C for3 hours. After reaction, the solution produced was cooled to room temperature. Around 20 ml distilled water was then added into the solution in order to hydrolyze all unreacted acetic anhydride to acetic acid. Meanwhile, 0.5 M H_2SO_4 was also used to adjust the pH of the solution to 3. Finally the acidified solution was washed with dilute H_2SO_4 solution and centrifuged to separate and purify the modified lignin. The produced modified lignin, with 82% recovery yield, was dried in an oven at 50 °C for 12 hours and ground into powder for further analysis. The lignin modified with acetic anhydride is named as LA in the following sections.

2.4.1.2 Scale-up Preparation

After the lab study, the modified lignin with acetic anhydride (LA) was selected for further industrial tests. 50 g kraft lignin powder (278 mmoles) was added to a 1 L round bottom flask equipped with a condenser. In the meantime, 30 g (365 mmole) sodium acetate solid was mixed with lignin powder. Then 150.0 ml (1591 mmole) acetic anhydride was added into the flask to dissolve the solid mixture, which was stirred at 120 °C for 3 hours. The experimental procedure was the same as the small scale modification as described in Section 2.4.1.1. The reaction was repeated 7 times with a recovery yield of 89%. The manufactured modified lignin was dried and then sent to The Goodyear Tire & Rubber Company for rubber reinforcing tests.

2.4.2 Modification with Benzoyl Chloride

1.0 g kraft lignin powder (5.56 mmoles) was added to a 50 ml round bottom flask. In the meantime, around 6.0 ml anhydrous pyridine was added as a solvent to dissolve lignin. Then 0.64 ml (5.56 mmole) benzoyl chloride was added into the flask to react with the

lignin solution. Finally, the mixture was stirred at room temperature for more than 12 hours. After reaction, around 70 ml saturated sodium bicarbonate solution was added into the flask in order to remove the remaining pyridine and other byproducts. Then the solution was washed with dilute H_2SO_4 and centrifuged to separate and purify the modified lignin. The produced modified lignin (1.02 g) was dried in an oven at 50 °C for 12 hours and ground into powder for further analysis. The lignin modified with benzoyl chloride is named as LC in the following sections.

2.4.3 Modification with Myristoyl Chloride

1.0 g kraft lignin powder (5.56 mmoles) was added to a 50 ml round bottom flask. In the meantime, 6.0 ml anhydrous pyridine was added as a solvent to dissolve lignin. Then 2.27 ml (8.34 mmole) myristoyl chloride was added into the flask to react with the lignin solution. Finally, the mixture was stirred at room temperature for more than 12 hours. After reaction, around 70 ml distilled water was added into the solution to remove the organic solvent. The precipitated mixture was washed with dilute H_2SO_4 and centrifuged. The centrifugate was then dried in an oven at 50 °C. The solid mixture was finally washed with organic solvent (6:1, hexane – ethyl acetate) and centrifuged for three more times. The modified lignin was dried in an oven at 50 °C for 12 hours. The recovery yield was not estimated as the product was not in solid phase. The lignin modified with myristoyl chloride is named as LM in the following sections.

2.4.4 Modification with Benzyl Bromide

1.0 g kraft lignin powder (5.56 mmoles) was added to a 50 ml round bottom flask equipped with a condenser. In the meantime, 1.54 g (11.12 mmole) potassium carbonate solid was mixed with the lignin powder. 6.0 ml THF was then added into the flask as a

solvent to dissolve the solid mixture. Finally 0.99 ml (8.34 mmole) benzyl bromide was added to react with the lignin. The flask was stirred at 80 °C for 8 hours. After reaction, the solution produced was cooled at room temperature. The organic solvent (6:1, hexane-ethyl acetate) was used to wash the mixture, which was then centrifuged to collect the precipitated solid. The collected solid was dried in an oven at 50 °C to remove the organic solvent and finally washed with distilled water followed by centrifugation for 3 more times to separate and purify the modified lignin. The modified lignin, with 74% recovery yield, was dried in an oven at 50 °C for 12 hours and ground into powder for further analysis. The lignin modified with benzyl bromide is named as LB in the following sections.

2.5 Electrochemical Modifications of Lignin Model Compound and Kraft Lignin

2.5.1 Fabrication of TiO_2NT/PbO_2 Electrode

The TiO_2 nanotube arrays were prepared using the electrochemical anodization of titanium plates substrates (1.25 cm x 0.8 cm x 0.5mm) were anodized in DMSO with 2% HF at 40 V for 8 hours. The electrodes were then rinsed thoroughly with pure water and dried in an argon stream. Finally, the samples were annealed at 450 °C for 3 hours.

The PbO_2 nanoparticles were subsequently directly deposited onto the TiO_2 nanotube arrays via photoelectrochemical deposition. The electrolyte contained 0.05 M $Pb(NO_3)_2$ and 0.1 M HNO_3. The prepared Ti/TiO_2NT/PbO_2 electrodes were employed as the working electrode. The counter electrode, comprised of a Pt wire coil, was cleaned prior to each experiment by flame annealing and rinsing with pure water. The reference electrode used was Ag/AgCl. An EG&G 2273 potentiostat/galvanostat was used to apply an anodic potential bias during the photoelectrochemical deposition. A BlueWave TM50 AS UV spot

lamp (main line of emission, 365 nm) was used as the UV light source with an intensity of ca. 20 mW/cm^2. The deposition was carried out under an anodic current density of 2 mA/cm^2 at 60 °C under UV illumination for 10 min. The surface morphologies and composition of the fabricated TiO_2 nanotubes and the Ti/TiO_2NT/PbO_2 electrode were characterized by a JEOL 5900LV scanning electron microscope (SEM) and energy dispersive X-ray spectrometry (EDS). The X-ray diffraction (XRD) patterns were recorded on a PW 1050-3710 diffractometer using a Cu Kα (k = 1.5405 Å) radiation source.

2.5.2 Electrochemical Oxidation of Lignin Model Compound and Kraft Lignin

2.5.2.1 Lignin Model Compound Oxidation

Before the electrochemical oxidation of lignin, the oxidation of lignin model compound was studied. Guaiacol (Scheme 4a) and 1-(4-hydroxy-3-methoxyphenyl)-2-(2-methoxyphenoxy)-1,3-propanediol (Scheme 4b) were chosen as the model compounds due to their similar structures to lignin units. 100 ppm of both model compounds were electrochemically oxidized in 0.5 M sodium hydroxide solution under 100 mA at 60 °C at the fabricated TiO_2NT/PbO_2 electrode. An EG&G 2273 potentiostat/galvanostat was used to apply an anodic potential bias for the electrochemical oxidation. The experimental apparatus was the same as electrode fabrication, except for the absence of a light source.

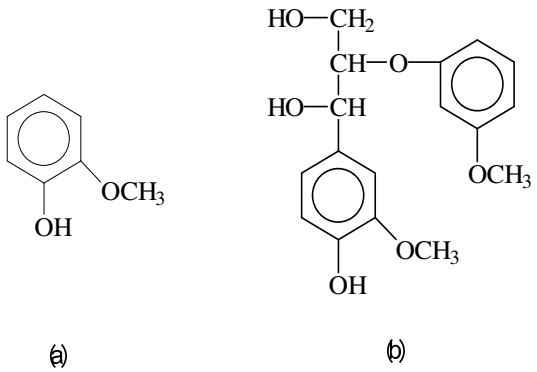

Scheme 4 Lignin model compound: (a) guaiacol; (b) 1-(4-hydroxy-3-methoxyphenyl)-2-(3-methoxyphenoxy)-1,3-propanediol

2.5.2.2Lignin Oxidation

An EG&G 2273 potentiostat/galvanostat was used to apply constant currents for the electrochemical oxidation of lignin. The fabricated Ti/TiO_2NT/PbO_2 electrode was utilized as the working electrode. A Pt coil served as the counter electrode. The reference electrode was comprised of Ag/AgCl. A Cary 50 UV-Vis spectrometer was employed to monitor the oxidation process in situ. The lignin solution was stirred using a stirring machine during all of the electrochemical oxidation processes. The resulting lignin oxidation products were analyzed using a HPLC (Varian Prostar 230, a symmetry® C8 column containing dimethyloctylsilyl bonded amorphous silica-acetonitrile), and a Nicolet 8700 FTIR spectrometer.

2.6 Analysis Techniques

2.6.1 Fourier Transform Infrared (FTIR) Spectroscopy

Infrared spectrometers can be classified into Dispersive Infrared and Fourier Transform Infrared Spectrometers. In a dispersive Infrared Spectrometer, the radiation of a polychromatic source is dispersed by a monochromater into several elements, which is then measured by a detector. The sampling procedure is tedious and the intensity of the

signal is relatively small. On the other hand, an FTIR spectrometer can collect a wide range of signals with high intensity. This shows a significant advantage over a dispersive spectrometer which measures intensity over a narrow range of wavelengths at a time.

The most commonly used interferometer for FTIR is the Michelson interferometer. In a Michelson interferometer, light from the infrared source is directed to a beam splitter. Ideally 50% of the light is reflected towards a fixed mirror and the other 50% is transmitted towards a moving mirror. Light is reflected from these two mirrors and finally back to the beam splitter. Then 50% of the original light passes into the sample. Then the light goes through the sample to the detector. The difference in optical path length between the two mirrors is considered as retardation. An interferogram is obtained by varying the retardation and collecting the data from the detector based on various retardations.

After detecting the light, the beam is modified to contain certain combinations of frequencies and produce a point. Finally the data is collected and transformed by a computer using the Fourier Transform to infer what the absorption is at each wavelength. Figure 2 shows a typical IR spectrum before and after Fourier Transform.

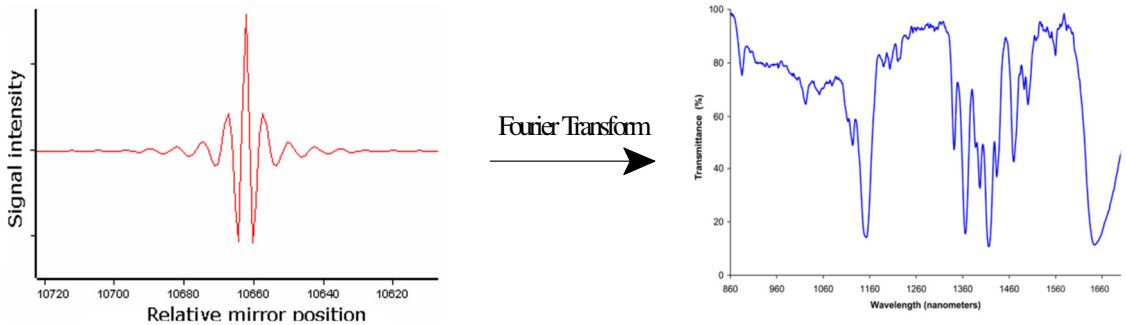

Figure 2 Fourier transform spectra (Wikipedia 2010)

In this project, a Nicolet 8700 FTIR spectrometer was employed to analyze the sample. The number of scans was set to 400 with a resolution of 8 cm^{-1}. The scanning range was set from 600 to 4000 cm^{-1}.

2.6.2 Brunauer Emmett and Teller (BET) Surface Area Analyzer

The Brunauer-Emmett-Teller (BET) method is the most widely used procedure for the determination of the surface area of solid materials and involves the use of the BET equation, in which W is the weight of gas adsorbed at a relative pressure, P/P_0, and W_m is the weight of adsorbate constituting a monolayer of surface coverage. The term C, the BET constant, is related to the energy of adsorption in the first adsorbed layer and consequently its value is an indication of the magnitude of the adsorbent/adsorbate interactions.

$$\frac{1}{W[(P_0/P)-1]} = \frac{c-1}{W_m c}\left(\frac{P}{P_0}\right) + \frac{1}{W_m c}$$

The BET equation requires a linear plot of $1/[W(P_0/P)-1]$ vs P/P_0 (φ) which for most solids, using nitrogen as the adsorbate, is restricted to a limited region of the adsorption isotherm, usually in the P/P_0 range of 0.05 to 0.35. This linear region is shifted to lower relative pressures for microporous materials. A typical BET plot is shown in Figure 3.

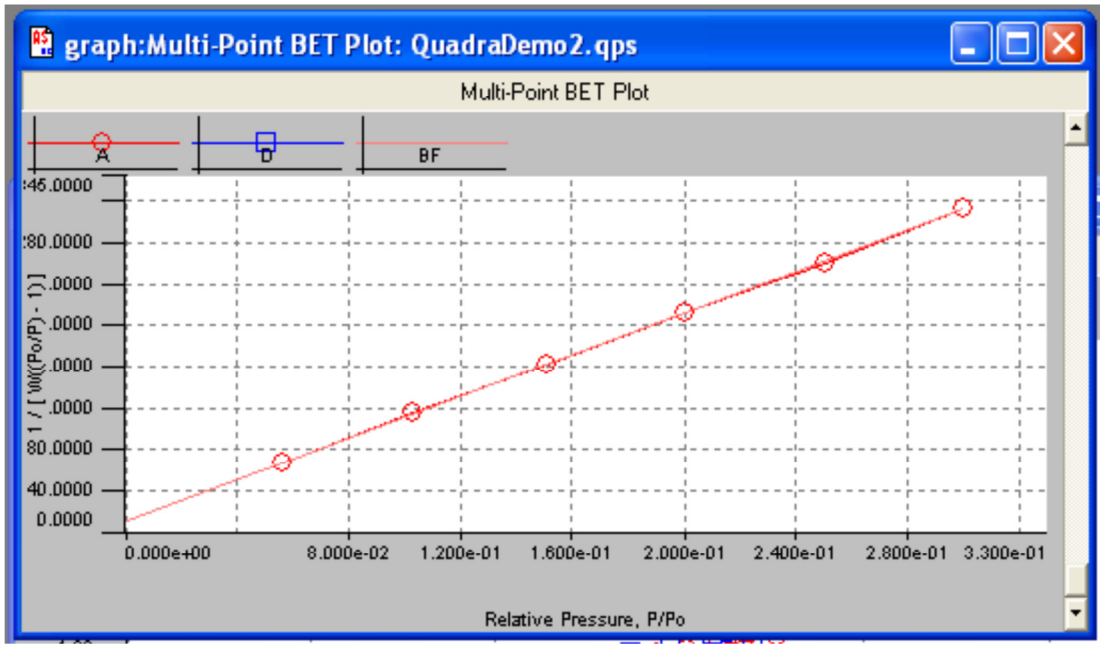

Figure 3Typical BET Plot

The standard multipoint BET procedure requires a minimum of three points in the appropriate relative pressure range. The weight of a monolayer of adsorbate W_m can then be obtained from the slope S and intercept I of the BET plot.

$$S = \frac{C-1}{W_m C} \qquad I = \frac{1}{W_m C}$$

Thus, the weight of a monolayer W_m can be obtained by combining these two equations.

$$W_m = \frac{1}{S+I}$$

The second step in the application of the BET method is the calculation of the surface area. The total surface area S_t of the sample can be expressed as followed, where N is

Avogadro's number (6.023×10^{23} molecules/mol), M is the molecular weight of the adsorbate and A_{cs} is the molecular cross-sectional area of the adsorbate molecule.

$$S_t = \frac{W_m N A_{cs}}{M}$$

The specific surface area S of the solid can be calculated from the total surface area S_t and the sample weight w.

$$S = S_t / w$$

In this project, a Quantachrome NOVA 2200e surface area and pore size analyzer was used for characterization of BET surface area in m^2/g. The samples in powder were used as adsorbent, and nitrogen as adsorbed gas.

2.6.3 Nuclear Magnetic Resonance (NMR) Spectroscopy

NMR spectroscopy is a research technique that detects the magnetic properties of certain atomic nuclei to determine the physical and chemical properties of atoms or the molecules in chemicals. The information provided by NMR is relied on the nuclear magnetic resonance of the molecules and atoms. NMR spectroscopy is most commonly used to investigate organic compounds, which have been widely used in various chemistry fields.

The principle of NMR spectroscopy is based on the nuclear magnetic resonance of different atoms and molecules. When placed in a magnetic field, NMR active nuclei (such as ^{1}H or ^{13}C) absorb electromagnetic radiation at a frequency characteristic. Different atoms and molecules present different magnetic responses in different chemical conditions. Chemical shift is known as an indicator of the frequency shift and magnetic

field, thus can indicate the chemical environment of certain molecules. In NMR spectrum, both the positions and shapes of peaks are important indicators of their chemical structures.

In this project, Varian Unity Inova 500 MHz NMR spectrometer was used for both ^{1}H and ^{13}C NMR analysis. Tetramethylsilane (TMS, δ 0.00 ppm) or solvent peaks were used as internal standards for ^{1}H and ^{13}C NMR spectrum. The chemical shifts were given in ppm and coupling constants in Hz indicated to a resolution of 0.5 Hz. Multiplicity of proton signals is indicated as follows: s (singlet), d (doublet), dd (double doublet), t (triplet), m (multiplet).

2.6.4 Scanning Electron Microscope (SEM)

A scanning electron microscope is a type of electron microscope that images a sample by scanning it with a high-energy beam of electrons in a raster scan pattern. The electrons interact with the atoms in the sample and produce signals that contain information about the surface morphology and composition of the sample. In general, SEM can produce very high resolution of images, revealing details in nanometer. Thus it is a very useful technique to lead to a better understanding of the surface structures and morphologies of samples.

In a typical SEM, an electron beam is thermionically emitted from an electron gun. Tungsten is normally used in thermionic electron guns because it has the highest melting point and lowest vapour pressure of all metals, therefore allowing it to be heated for electron emission. The beam passes through the sample and being detected to create image of the surface current of the specimen. The resulting image is a distribution map of the

intensity of the signal being emitted from the scanned area of the specimen. The image could then be digitally captured and displayed on a computer monitor.

In this study, a JEOL 5900LV Scanning Electron Microscope was used for imaging the surface structures and morphologies of samples.

2.6.5 Energy-Dispersive X-ray Spectroscopy (EDS)

Energy-Dispersive X-ray Spectroscopy is an analytical technique used for the elemental analysis or chemical characterization of a sample, which relies on the investigation of a sample through interactions between electromagnetic radiations and analyze the X-ray emitted by the charged atoms. The characterization of EDS is based on the principle that each element has a unique way to be charged and emit X-ray, allowing this technique to identify different elements in the sample.

In principle, when a high energy X-ray is focused on the sample being studied, an atom within the sample is excited and an electron in the inner shell may be injected while creating an electron hole where it was. Therefore, an electron from an outer and higher-energy shell then fills the hole, and the difference of energy between the outer and inner shell may be released in the form of X-ray. The number and intensity of X-ray emitted by a sample can be detected and analyzed by an EDS spectrometer. Because the X-ray is characterization of the energy gap between outer and inner shell inside an atom, the analysis of X-ray can provide the information on the elements contained in the sample.

In general, there are four primary components of an EDS spectrometer: The beam source, the X-ray detector, the pulse processor and the analyzer. Recently, EDS is usually combined with SEM for elemental and structural analysis of a sample. In this study, an EDS device associated with the SEM machine was used for surface analysis.

2.6.6 Gas Chromatography-Mass Spectrometry (GC-MS)

Gas chromatography–mass spectrometry is a method that combines the features of gas-liquid chromatography and mass spectrometry to identify different substances within a test sample. It is composed of two major building units: the gas chromatography (GC) and the mass spectrometer (MS). The gas chromatography utilizes a capillary column with various dimensions and phase properties. When the sample is traveling through the column, the different chemical properties of different molecules in a sample will separate the sample. Different molecules within the sample come out with different retention time through the gas chromatography, which allows the sequential mass spectrometer to capture, ionize, accelerate and detect them. The mass spectrometer breaks each molecule into ionized fragments and detects them using their mass to charge ratio.

The combined use of these two components allows a much better degree of identification than either unit used separately. It is not possible to make an accurate identification of a particular molecule by gas chromatography or mass spectrometry alone. The analysis of mass spectrometer usually requires a pure sample, which limits its application. And the traditional gas chromatography usually utilizes a detector that cannot identify compounds with the same travel time through the chromatography. Therefore, combining the two processes reduces the possibility of error, as it is extremely unlikely that two different molecules will behave in the same way in both a gas chromatography and a mass spectrometer.

In this study, a Varian 450 GC- 300 MS was employed for molecular analysis of our samples. A Factor Four Capillary 0.25 μm (30×0.25 mm) Column was equipped. Electron

Ionization (EI) or Positive/Negative Chemical Ionization (CI) was used as the ionization mode.

2.6.7 Liquid-Chromatography Mass Spectrometry (LC-MS)

Liquid-Chromatography Mass Spectrometry is also a technique which is used for the detection and identification of specific chemicals in the presence of other chemicals. The main difference of LC-MS from GC-MS is that it combines physical separation capabilities of liquid-chromatography with the mass spectrometer, instead of the gas-chromatography. The performance of liquid-chromatography is similar to the High-Performance Liquid chromatography (HPLC), which will be introduced in section 2.6.11.

In this project, a Bruker/Dionex LC-MS was employed for molecular analysis of samples. A Dionex Acclaim®120 C18 3 μm 120Å (2.1×150 mm) Column was equipped. Methanol/water with 0.1% formic acid was used as mobile phase, with methanol from 40-100% in a 30 minutes gradient. Electrospray Ionization (ESI) or Positive/Negative Chemical Ionization (CI) was used as the ionization mode.

2.6.8 Hydrophobicity Test

The hydrophobicity of material could be analyzed based on the measurement of its water contact angle. When a water drop stays on a solid surface, if the liquid is strongly attracted to the solid surface, the droplet will completely spread on the solid surface and give a contact angle close to 0°, thus the solid could be considered as hydrophilic. When the contact angle becomes up to 90° or even larger, the solid could be considered as hydrophobic.

Figure 4 illustrates the contact angle of a liquid sample. The theoretical description of contact angle was based on the thermodynamic equilibrium of three phases: the liquid

phase of the droplet (L), the solid phase of the substrate (S), and the gas/vapor phase (G). At equilibrium, the chemical potential in these three phases should be equal. If the solid-vapor interfacial energy is defined as γ_{SG}, the solid-liquid interfacial energy as γ_{SL}, and the liquid/vapor energy as γ, then the equation of the equilibrium in these three phases could be written as:

$$0 = \gamma_{SG} - \gamma_{SL} - \gamma \cos\theta_C$$

Where θ_C is the definition of contact angle.

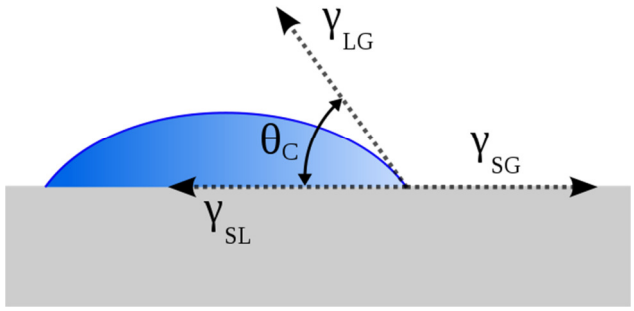

Figure 4 Contact angle schematic (Wikipedia 2010)

The latest systems usually employ high resolution cameras and software to capture the picture of contact angle for analysis. The angle formed between the liquid-solid interface and the liquid-vapor interface is the contact angle.

In this project, the hydrophobicity test was carried out by the measurement of the contact angle between water droplet and sample substrates. As the samples were all in powder, ethanol was used to disperse samples and form a flat film on a glass slide. The formed film was used as the solid substrate for the water droplet, and the contact angle was captured by a high resolution digital camera connected with computer software for analysis. The contact angle of water droplet was calculated by measuring the angle

between the liquid phase and solid phase by angle ruler from the pictures taken by the camera.

2.6.9 Cyclic Voltammetry (CV)

Cyclic voltammetry is a potentiodynamic electrochemical technique for studying the electrochemical properties of electrodes in electrolyte solutions. In cyclic voltammetry, the working electrode potential follows a linearly ramping potential versus time. The potential is measured between the reference electrode and the working electrode, and the current is measured between the working electrode and the counter electrode. The results are then plotted as current versus potential, as illustrated in Figure5. These plots are termed "polarization curves" or "cyclic voltammograms", and they can be used for determining the formal redox potentials of the electroactive species present in the solution, detecting chemical reactions, and evaluating electron transfer kinetics.

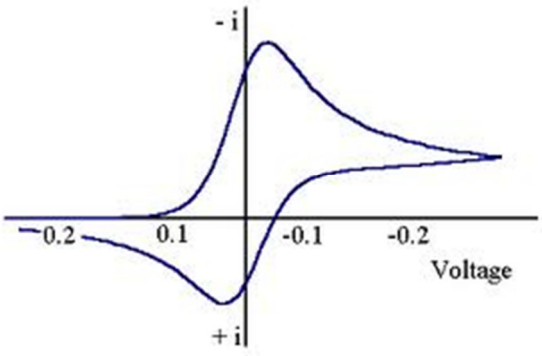

Figure 5 Typical CV curve

The measurement of CV is usually carried out using a three-electrode setup, including the working electrode, counter electrode and reference electrode. Electrolyte is

also used to ensure the high electrical conductivity of the test solution. Therefore, the combination of the electrolyte and electrodes determines the potential range of CV.

In this project, a computer-controlled EG&G 2273 potentiostat/galvanostatsystemwas used to in-situ monitor the potential and analyze the cyclic voltammetric results in all electrochemical experiments. A typical three-electrode setup was used for measurements.

2.6.10 Ultraviolet-Visible (UV-Vis) Spectroscopy

The Ultraviolet-Visible Spectrometer is an instrument to measure the intensities of light passing through the sample in UV-visible range. The basic parts of UV-Vis spectrometer are a light source, a holder for the sample, a diffraction grating in a monochromator to separate the different wavelengths of light, and a detector. The monochromator can move the diffraction grating to go through each wavelength, which allows the light intensities to be measured as a function of wavelength.

After measuring the intensities of transmitted light, the absorbance of the sample could be calculated based on Beer-Lambert law:

$$A = \log_{10}(I_0 / I) = \varepsilon.c.L$$

where A is the measured absorbance; I_0 is the intensity of light before passing through the sample' I is the transmitted intensity of light; L is the path length through the sample; ε is constant known as the extinction coefficient; and c is the concentration of the absorbing species.

In this project, a Cary 50 UV-Vis spectrometer was employed to monitor the experimental process. A rectangular transparent quartz glass container was used as a

cuvette to place the sample for UV-Vis analysis. The absorbance of samples was recorded in correlation with the wavelength in nm^{-1}.

2.6.11 High-Performance Liquid Chromatography (HPLC)

High-Performance Liquid Chromatography is a technique that can separate a mixture of compounds for purification and analysis. HPLC typically uses different types of stationary phases, a pump that moves the mobile phases, the sample passing through the column, and a detector to provide the information on characteristics of samples based on retention time. The retention time of the sample depends on the interaction between the sample and column, the ratio of solvent used to prepare the sample, and the flow rate of the mobile phase. Compared with normal column chromatography, HPLC employs a pump to provide a higher pressure to move the mobile phases, and thus the sample could flow through the densely packed column. This allows a better separation of sample through the column chromatography. In addition, HPLC also utilizes a smaller column size with smaller particle size for the media inside the column.

In this project, a Varian Pro star 230 HPLC, equipped with a Waters symmetry® C8 column containing dimethyloctylsilyl bonded silica, and a Photo Diode-Array (PDA) detector, with 50% acetonitrile/water as organic mobile phase, was used for lignin oxidation intermediate analysis.

Chapter 3 Preparation and Characterization of Kraft Lignin from Industrial Black Liquor

Softwood and hardwood lignin have been extracted from industrial black liquor using three different approaches. After extraction, the BET surface area and FTIR spectra were analyzed to study the difference between different kinds of lignin extracted by various methods. In Table 1, the yield and BET surface area of extracted lignin are presented. The yield was calculated as the weight of kraft lignin per volume of black liquor (w/V).

Table 1 Kraft lignin extraction from black liquor

Extraction Method	Lignin	Yield (g/l)	Surface Area (m^2/g)
Precipitated by CO_2 (pH=8)	Softwood	90.4	2.11
	Hardwood	52.5	5.64
Precipitated by H_2SO_4 after CO_2 (pH=2)	Softwood	44.8	2.20
	Hardwood	20.6	4.70
Precipitated by H_2SO_4 (pH=4)	Softwood	112.7	2.45
	Hardwood	67.1	14.0

According to Table 1, the yields of softwood lignin are about 2 times higher than hardwood for all extraction methods. This corresponds with the higher contents of softwood lignin in papermaking and pulping industrial black liquor. On the other hand, the surface area of hardwood lignin was found to be larger than softwood from all extracting

methods, which leads to the conclusion that hardwood lignin has a smaller particle size than softwood.

When the effects of different extraction methods were studied, for example, for softwood lignin, it was found that the yields of softwood lignin were much higher when precipitated by H_2SO_4 than CO_2. This indicates that kraft lignin could be better precipitated at lower pH. However, using CO_2 to precipitate lignin is a cheaper and more environmentally-friendly method as it can reduce the content of CO_2 in the air, which causes the serious green-house effect. On the other hand, after softwood lignin being precipitated by CO_2 at pH=8, the remaining black liquor was collected and acidified by sulfuric acid to pH=2. As a result, more lignin could be gained, which again indicated that kraft lignin should be extracted in acidic condition from basic industrial black liquor.

Figures 6 and 7 present the FTIR data for both softwood and hardwood lignin extracted by different methods. According to the introduction of FTIR spectroscopy in section 2.6.1, the structures of lignin can be studied based on FTIR results. The interpretations of the infrared absorption for lignin analysis are presented in Table 2 with correlated positions in wavelength.

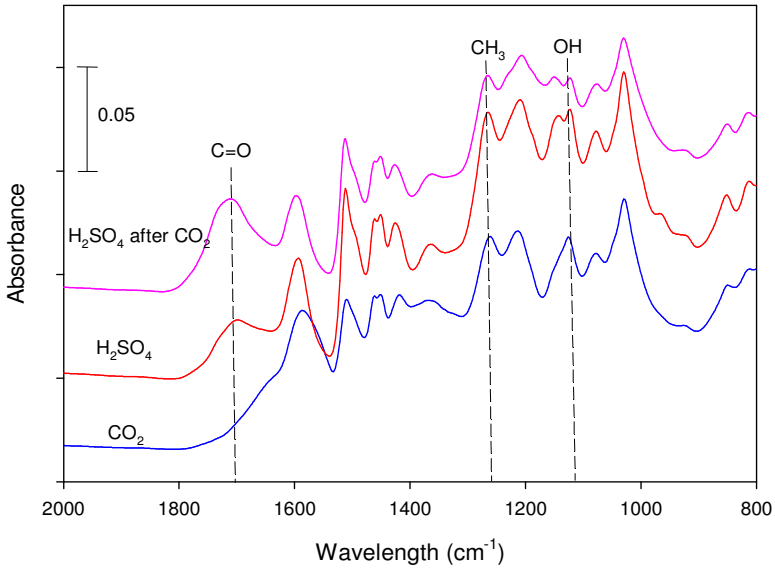

Figure 6 FTIR spectra of hardwood lignin extracted by different methods

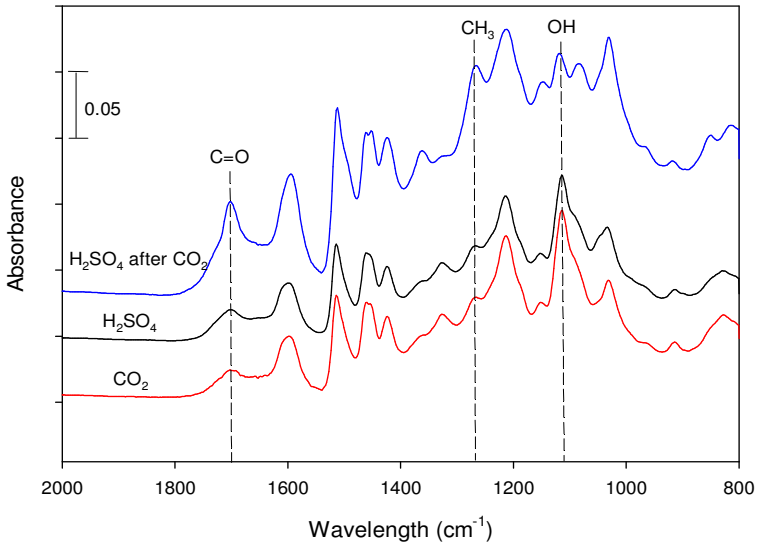

Figure 7 FTIR spectra of softwood lignin extracted by different methods

According to Figures 6 and 7, we can conclude that the structures of softwood and hardwood lignin are similar although they show some different peak intensities in the FTIR spectra. Hardwood lignin presented a larger amount of CH_3 groups while softwood

showed more OH groups content. When the effects of different extraction methods were studied, for example, in softwood lignin, the peak at 1710 cm^{-1} wavelength shows a sharper and stronger shape in the sample extracted by H_2SO_4 at lower pH. This band was assigned for the vibration of C=O groups in lignin molecules. Therefore, the higher intensity of this peak may be explained by the higher content of COOH groups when lignin was extracted at lower pH, which corresponds to the extraction method. On the other hand, we can find that both hardwood and softwood lignin display more structural differences when precipitated at low pH.

Table 2 Assignments of infrared absorption of lignin

Maximum band position (cm^{-1})	Band origin
1740-1690	C=O stretching
1600-1690	Aromatic skeletal vibration
1510	Aromatic skeletal vibration
1450-1460	CH stretching of methyl or methylene group
1425-1420	CH vibration of methyl group
1370-1270	Bending vibration of CH_3
1175-1260	C-O stretching in Alcohol, Ester, Ether, Acid
1165-1140	OH stretching of primary alcohol
1043	OH stretching of secondary alcohol
745-790	CH bending of CH_2 and CH_3 groups
650-695	Aromatic ring puckering

Chapter 4 Chemical Modifications of Kraft Lignin with Electrophilic Reagents

In this chapter, various chemical modifications of kraft lignin with electrophilic reagents were studied. Kraft lignin was modified with different kinds of electrophilic reagents, aiming to change the structures, add new functional groups on lignin molecules, and modify the surface morphologies of kraft lignin. The modified lignin was analyzed by FTIR to study the changes in structure, and BET and SEM to study the changes in surface morphologies. After lab study, scale-up preparation of modified lignin has been carried out for industrial analysis of rubber reinforcement.

Table 3 summarizes the conditions of all modifications, as well as the resultant yields and surface area. In the following parts, the principle of each modification was explained and analysis data were provided to support the explanation.

Table 3 Lignin modifications with electrophilic reagents

Type of Lignin	Reagent	Time (hr)	Temp (°C)	Yield (%)	Surface Area (m^2/g)
Unmodified	N/A	N/A	N/A	N/A	2.28
LF	Formaldehyde	7	90	73%	0.57
LG	Glyoxal	7	90	63%	2.67
LE	Epichlorohydrin	5	95	74%	2.20
LGE	Glyoxal/Epichlorohydrin	7	95	82%	26.54

*LF-Lignin modified with formaldehyde
LG-Lignin modified with glyoxal
LE-Lignin modified with epichlorohydrin
LGE-Lignin modified with glyoxal and epichlorohydrin

4.1 Modification with Formaldehyde

In previous research, formaldehyde has been studied extensively for the modification of lignin, for example, applying lignin as a substitution in phenol-formaldehyde resin or urea-formaldehyde resin. Because of this reason, in our study, formaldehyde was chosen as the first reagent for the study of lignin modifications.

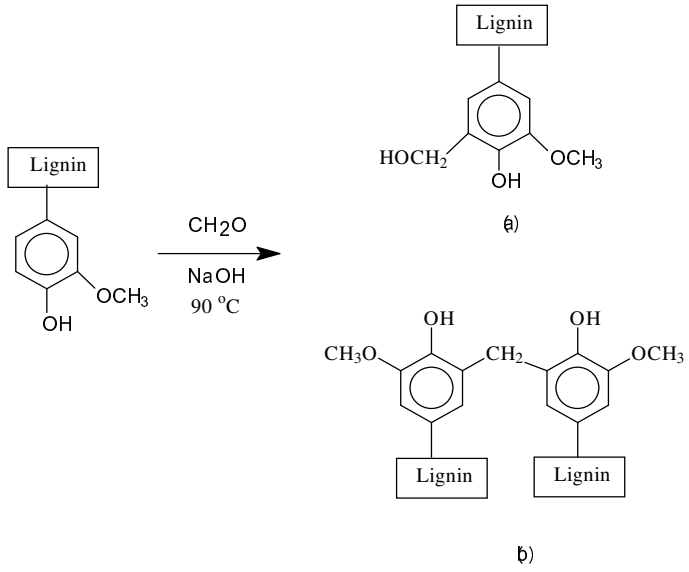

Scheme 5 Lignin modification with formaldehyde

Scheme 5 presents the fundamental reaction equations between lignin molecules and formaldehyde. Two types of linkages could result from the reaction, one leads to the hydroxymethylated product (a) before cross-linking, and (b) presents the cross-linked product.

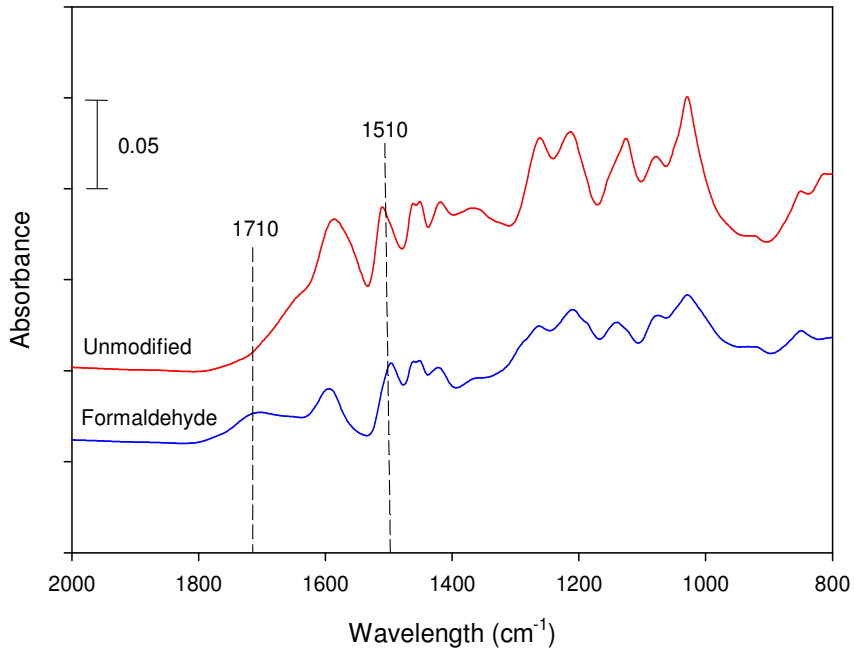

Figure 8 FTIR spectra of formaldehyde modified lignin (LF)

Table 4 Content of functional groups in formaldehyde modified lignin (LF)

	Total OH group	Ar-OH group	OCH_3 group	C=O group
Unmodified	1.08	1.01	0.81	0.32
LF	1.10	0.94	0.85	0.58

*LF-Lignin modified with formaldehyde

Figure8 illustrates the FTIR data of modified lignin compared with unmodified lignin. Among all these peaks, the aromatic skeletal vibrations occur at 1510 cm^{-1}. This bond was usually used for normalization and its intensity was set to 1.00, because it always shows a strong intensity and does not change in all modification reactions. Then the following ratios of the relative absorbance for different functional groups could be defined [89]:

Mean value of total OH groups = average (A_{1165}, A_{1043})/A_{1510}

Mean value of phenolic OH groups = A_{1043}/A_{1510}

Mean value of OCH_3 groups = average (A_{1460}, A_{1420})/A_{1510}

Mean value of C=O groups = A_{1720}/A_{1510}

Therefore, the relative contents of different functional groups in both unmodified and modified lignin were calculated and listed in Table 4. As shown in Figure8 and Table 4, the structure of lignin did not change significantly after modification. The intensities of different peaks stayed almost the same after modification, except for the increase of the band at 1710 cm^{-1} wavelength. This peak presents as the content of the C=O group in lignin molecules. As well, the relative content of C=O group also proves the increase of this functional group after lignin modification. However, according to Scheme 5, the reaction between formaldehyde and lignin could not lead to an increase of C=O group. Therefore, the increase of this functional group in modified lignin could only be explained by the oxidation and degradation of lignin by itself in alkaline conditions, which breaks ether bonds and leads to an increase of C=O groups in lignin molecules. On the other hand, the BET surface area of formaldehyde modified lignin in Table 3 also showed a negative result, which was even decreased after modification. This may result from a larger particle size and more aggregated particles in modified lignin.

4.2 Modification with Glyoxal

After modification of lignin using formaldehyde, another natural material, named glyoxal, was also used as a modification reagent for kraft lignin. In comparison with formaldehyde, glyoxal is a non-toxic, non-volatile material. But it was also less studied as a modification reagent for lignin. Thus before studying the modification of lignin, a model

compound reaction has been set to investigate the reaction between lignin molecules and glyoxal.

4.2.1 Reaction of Glyoxal with Model Compound Guaiacol

According to the structural units of lignin (Scheme 2), the main functional group is shown as methoxyphenol. For this reason, Guaiacol (Scheme 4a) was chosen as a model compound of lignin in this project, which reacts with glyoxal under alkaline conditions. After reaction, these products were purified using column chromatography and then analyzed by nuclear magnetic resonance (NMR) spectroscopy and GC/LC-MS to confirm the chemical structures. The ^{13}C and ^{1}H NMR and GC-MS data of the products is shown in Figure 9 to Figure 12.

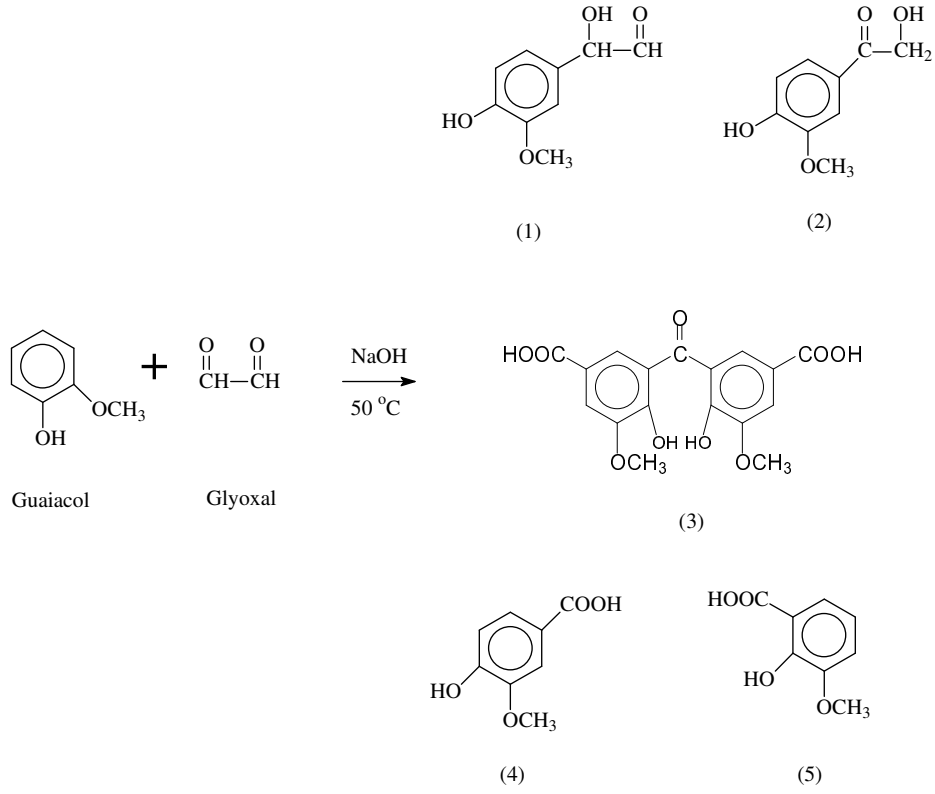

Scheme 6 Reaction of glyoxal with guaiacol

Scheme 6 presents the reaction of glyoxal with guaiacol, where the structures of products (1), (2), (4), (5) have been confirmed according to NMR and MS data. However, the compound (3) presents as the cross-linked products and the amount was small and its polarity was similar to other products. In this period of research, we have not obtained a purified sample for NMR structural analysis. According to LC-MS data (Figure 13), we found that there are several compounds that obtained a large molecular weight of more than 300 m/z in positive ionization mode, which indicates that the cross-linking reaction has occurred during the reaction between glyoxal and guaiacolto result in such large molecules. Therefore, further studies on the exact structures of cross-linked products of model compound reaction were necessary to establish the complete theory on the reaction between lignin and glyoxal.

2-hydroxy-2-(4-hydroxy-3-methoxyphenyl)-ethanal (1)

Isolated as a colorless oil: R_f 0.25(5:3:0.3 hexane-ethyl acetate-methanol); ^{1}H NMR (500 MHz, DMSO-d_6) δ_H: 10.04 (s, 1H), 7.58 (t, 1H, J=6.5 Hz), 7.47 (d, 1H, J=2.0 Hz), 6.87 (d, 1H, J=8.0 Hz), 5.60 (s, 1H), 5.05 (s, 1H), 3.80 (s, 3H), 3.30 (s, 1H);^{13}C NMR (125 MHz, DMSO-d_6) δ_C: 197.9, 152.3, 147.9, 128.4, 124.5, 115.3, 112.3, 73.3, 56.0; GC-MS: 182 m/z, calculated for $C_9H_{10}O_4$.

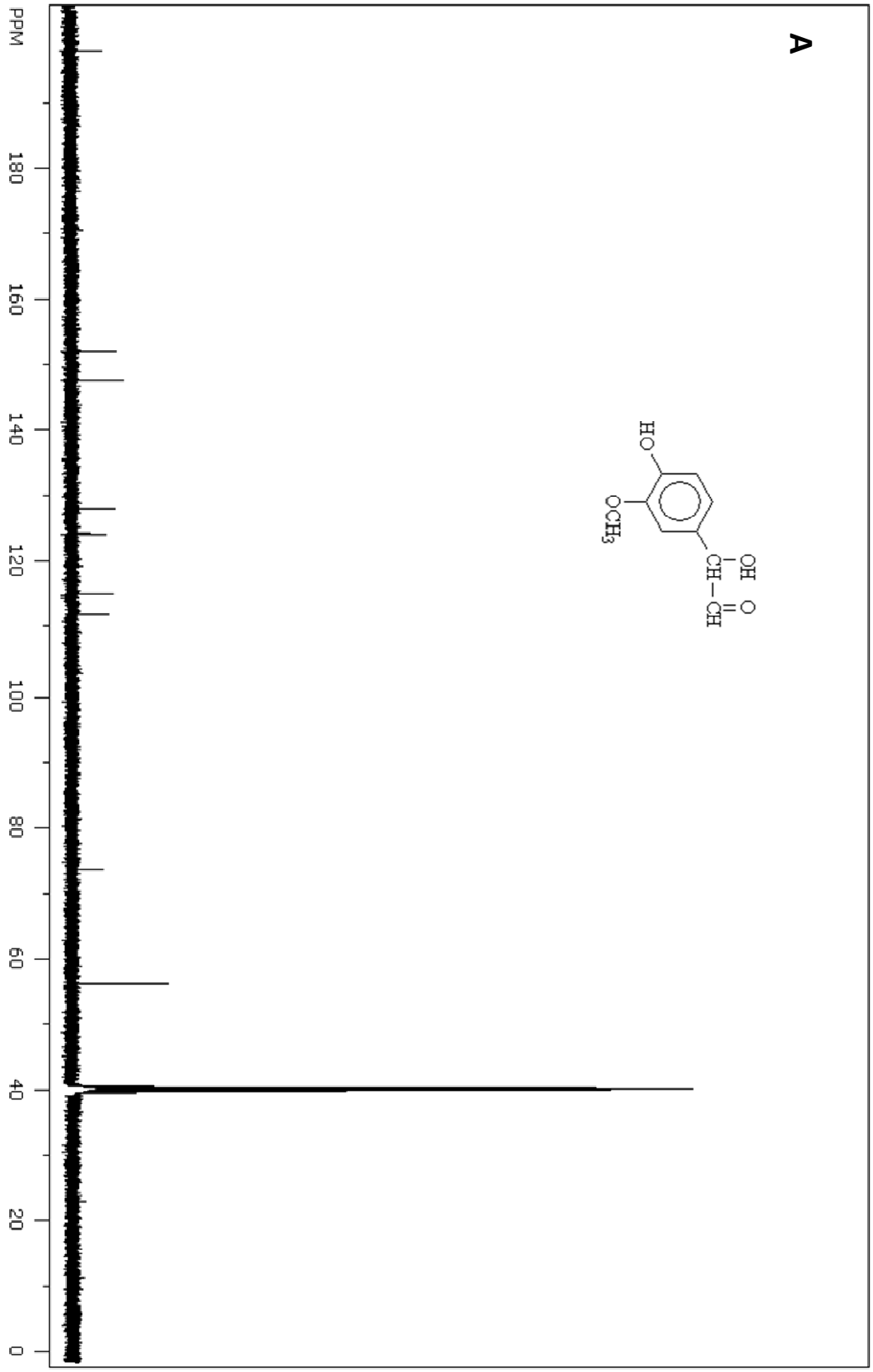
A
HO
OCH3
OH O
CH—C
CH
PPM
180
160
140
120
100
80
60
40
20
0

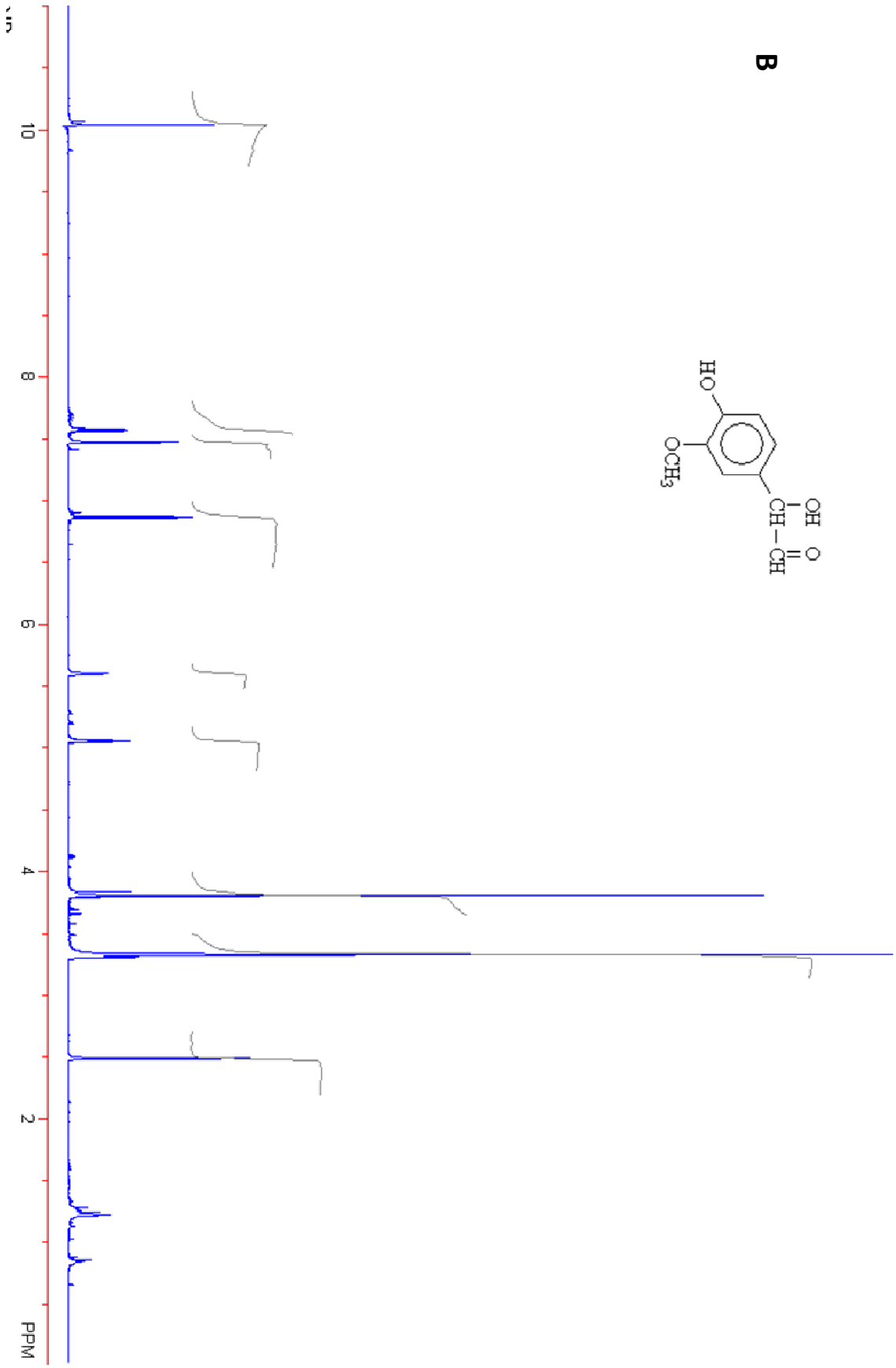
B
HO
OCH3
OH O
CH – CH
10
8
6
4
2
PPM

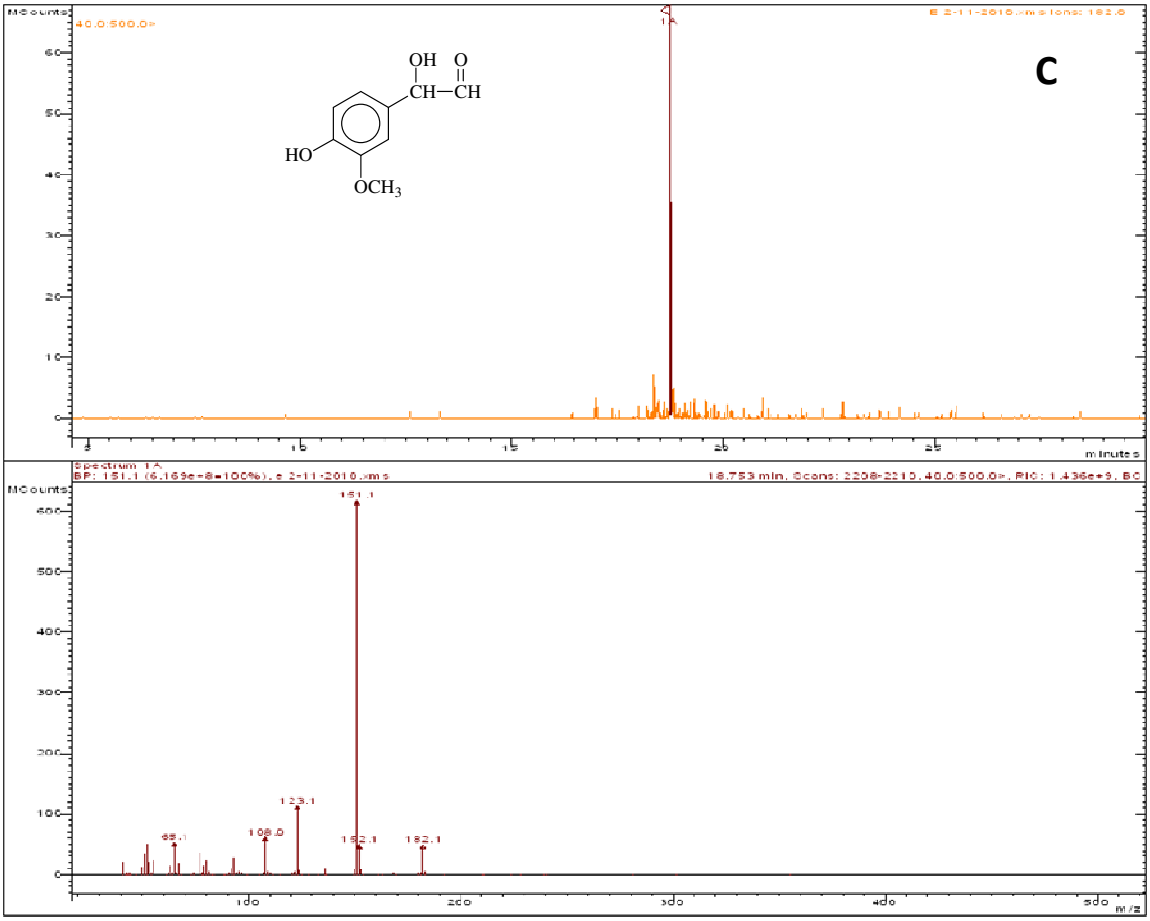

Figure 9 (A) ^{13}C NMR spectrum; (B) ^{1}H NMR spectrum; (C) GC-MS spectrum of product (1)

2-hydroxy-1-(4-hydroxy-3-methoxyphenyl)-ethanone (2)

Isolated as a colorless solid: R_f 0.45 (5:3:0.3 hexane-ethyl acetate-methanol); ^{1}H NMR (500 MHz, DMSO-d_6) δ_H: 10.00 (s, 1H), 7.48 (t, 1H, J=2.0 Hz), 7.46 (t, 1H, J=1.5 Hz), 6.88 (d, 1H, J=8.0 Hz), 4.89 (s, 1H), 4.74 (s, 2H), 3.83 (s, 3H); ^{13}C NMR (125 MHz, DMSO-d_6) δ_C: 202.4, 157.1, 152.8, 131.4, 127.6, 120.4, 116.0, 70.0, 60.8; GC-MS: 182 m/z, calculated for $C_9H_{10}O_4$. (In correspondence to Claudia et al., 2006) [143]

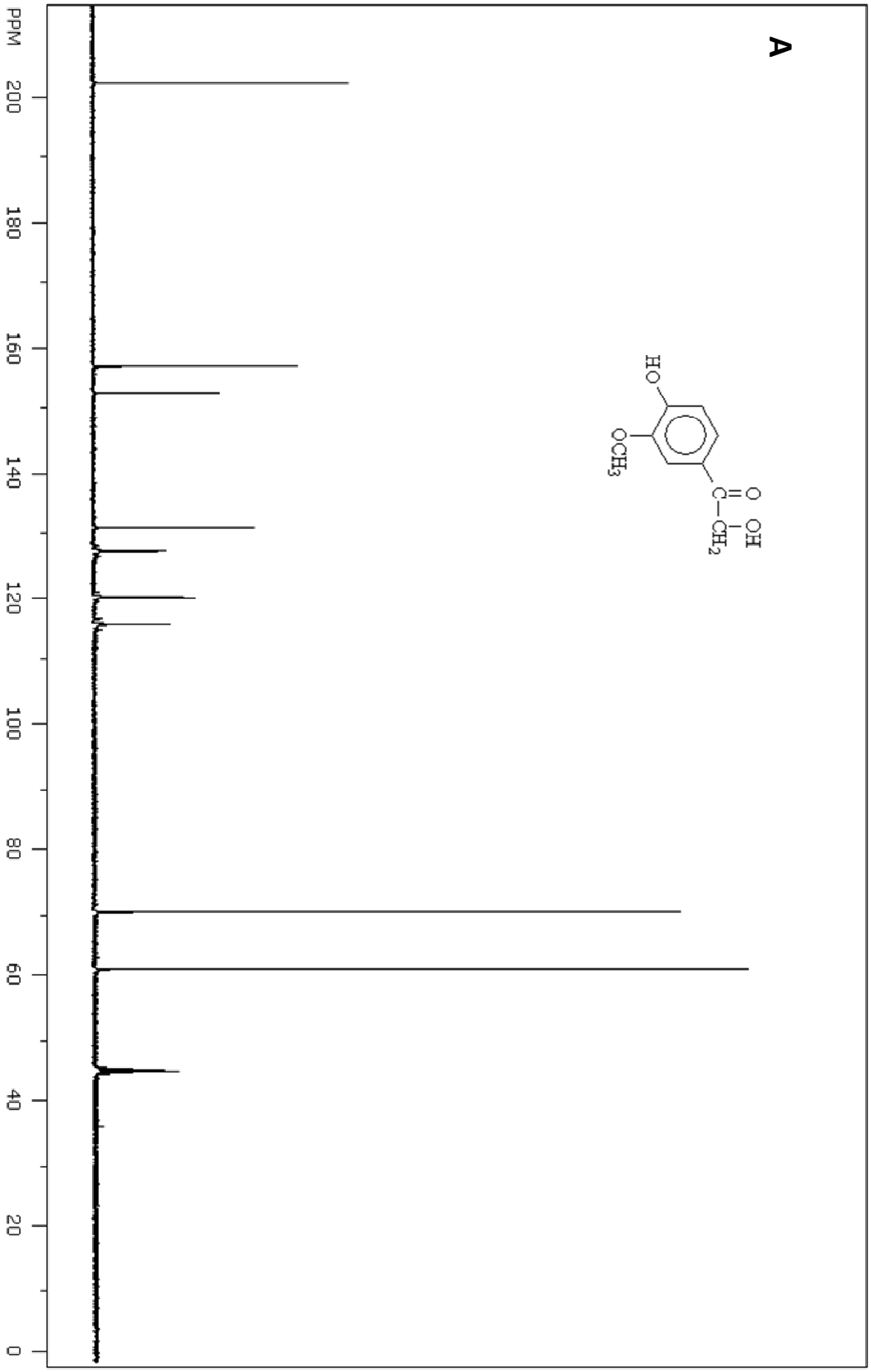
A
HO
OCH3
O
C
OH
CH2
PPM
200
180
160
140
120
100
80
60
40
20
0

B

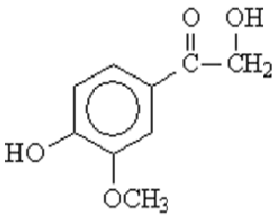

59

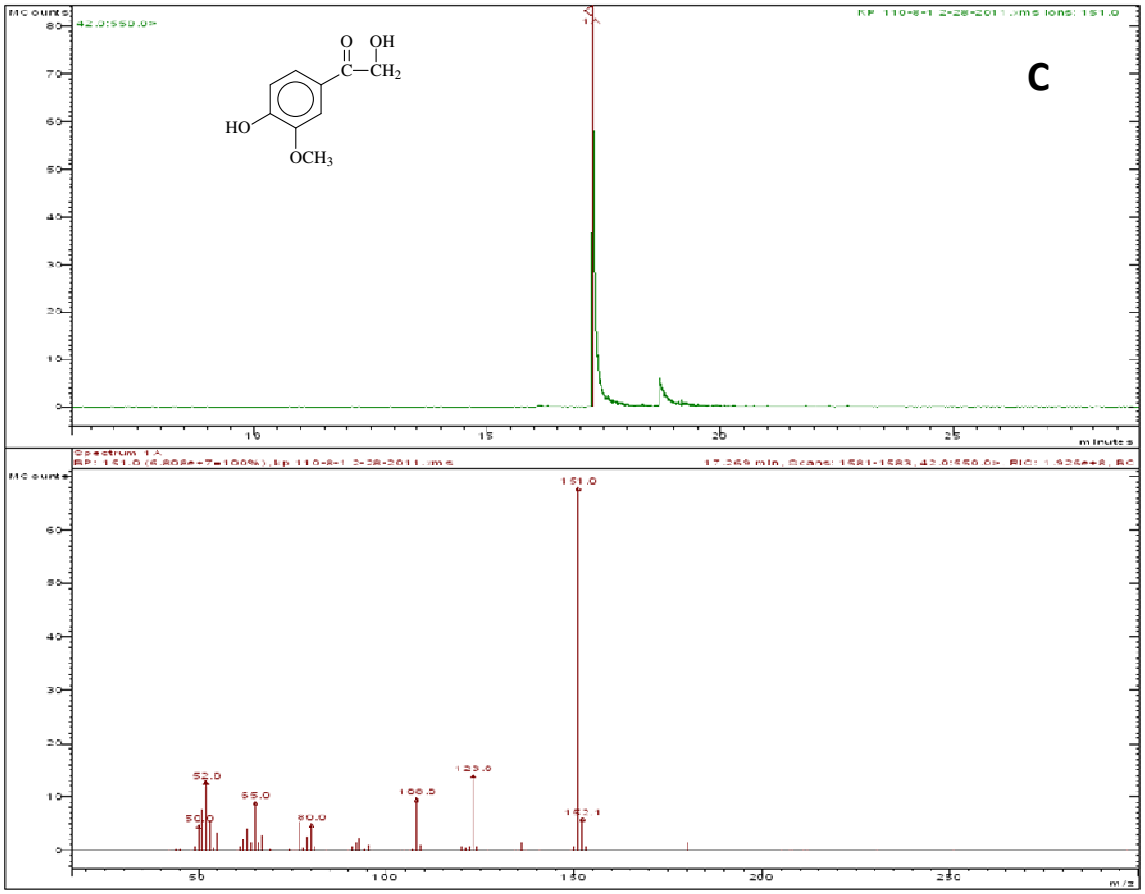

Figure 10 (A) ^{13}C NMR spectrum; (B) ^{1}H NMR spectrum; (C) GC-MS spectrum of product (2)

4-hydroxy-3-methoxy-benzoic acid (4)

Isolated as a colorless solid: R_f 0.42 (5:3:0.3 hexane-ethyl acetate-methanol); ^{1}H NMR (500 MHz, DMSO-d_6) δ_H:12.43 (s, 1H), 9.83 (s, 1H), 7.45 (d, 2H, J=7.5 Hz), 6.85 (d, 1H, J=9.0 Hz), 3.81 (s, 3H);^{13}C NMR (125 MHz, DMSO-d_6) δ_C: 167.3, 151.1, 147.2, 123.5, 121.7, 115.0, 112.7, 55.6; GC-MS (EI): 168 m/z, calculated for $C_8H_8O_4$. (In correspondence to Claudia et al., 2006) [143]

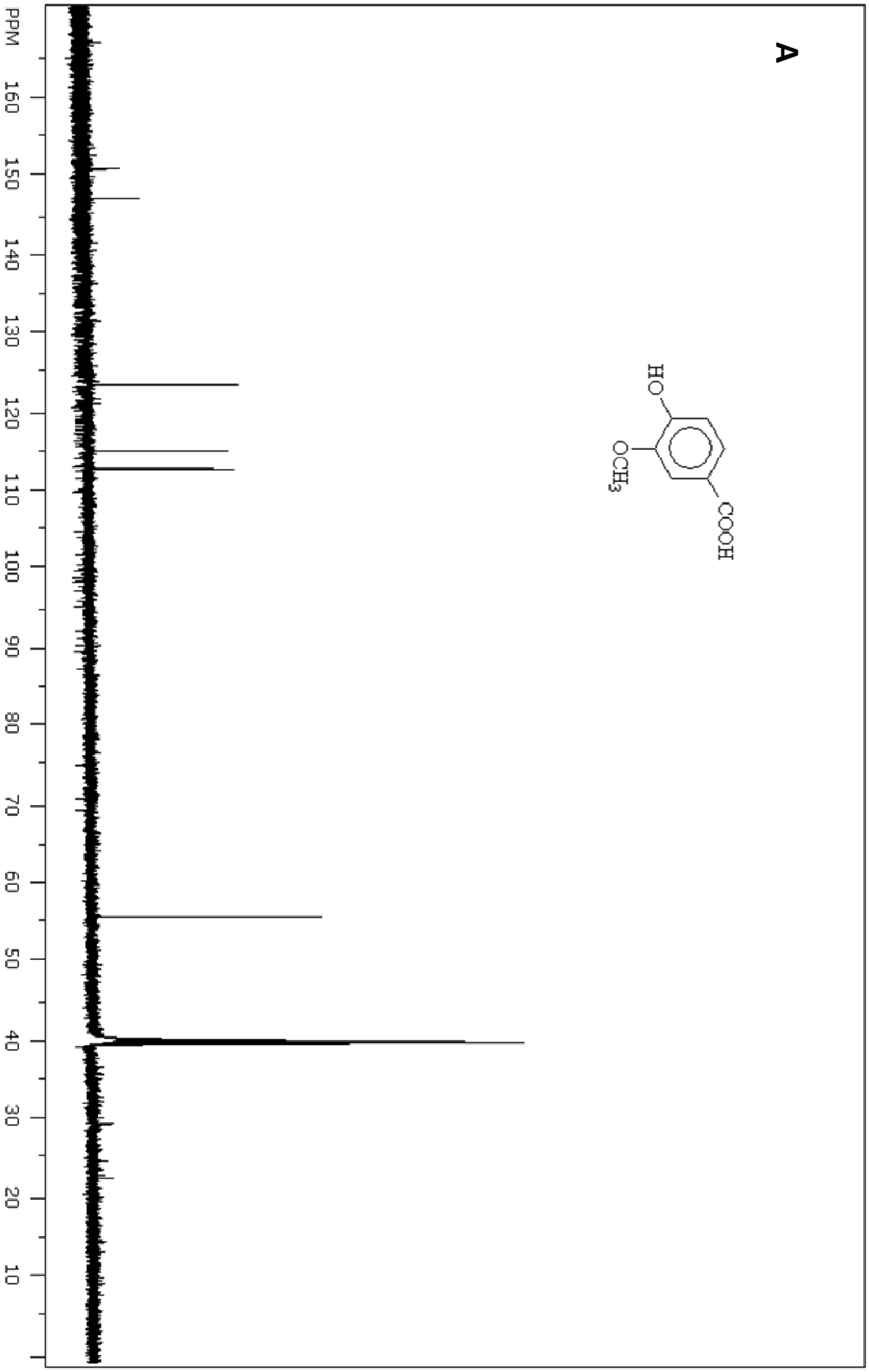
A
HO
OCH3
COOH
PPM
160
150
140
130
120
110
100
90
80
70
60
50
40
30
20
10

B

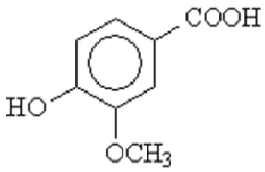

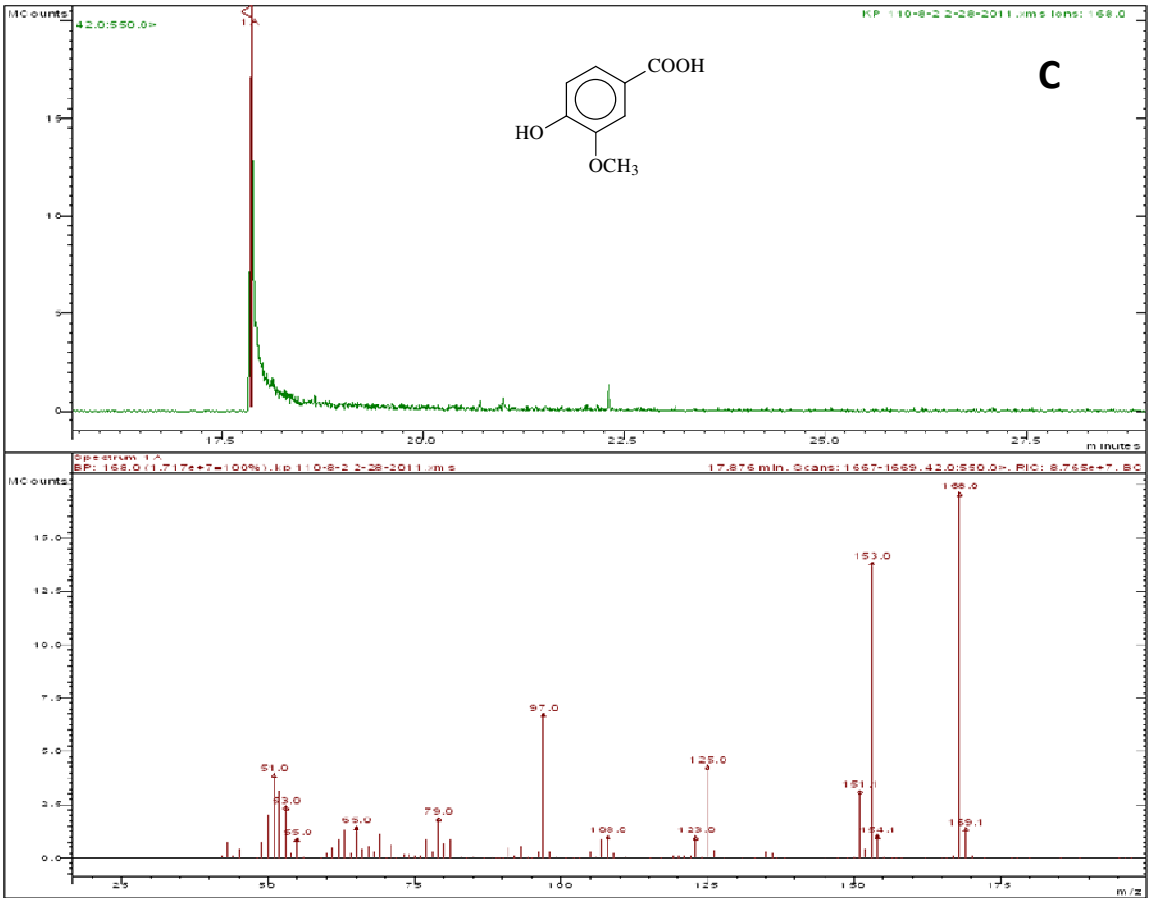

Figure 11 (A) ^{13}C NMR spectrum; (B) ^{1}H NMR spectrum; (C) GC-MS spectrum of product (4)

2-hydroxy-3-methoxy-benzoic acid (5)

Isolated as a colorful oil: R_f 0.34 (3:1:0.1 hexane-ethyl acetate-acetic acid); ^{1}H NMR (500 MHz, DMSO-d_6) δ_H: 7.35 (d, 1H, J=7.5 Hz), 7.17 (d, 1H, J=7.5 Hz), 6.82 (t, 1H, J=7.5 Hz), 3.79 (s, 3H); ^{13}C NMR (125MHz, DMSO-d_6) δ_C: 151.9, 148.2, 121.3, 118.1, 116.9, 55.8; GC-MS: 168 m/z, calculated for $C_8H_8O_4$.(In correspondence to Reszka et al., 2005) [144]

*Tertiary carbon shows weak signal and was not detected in the spectra.

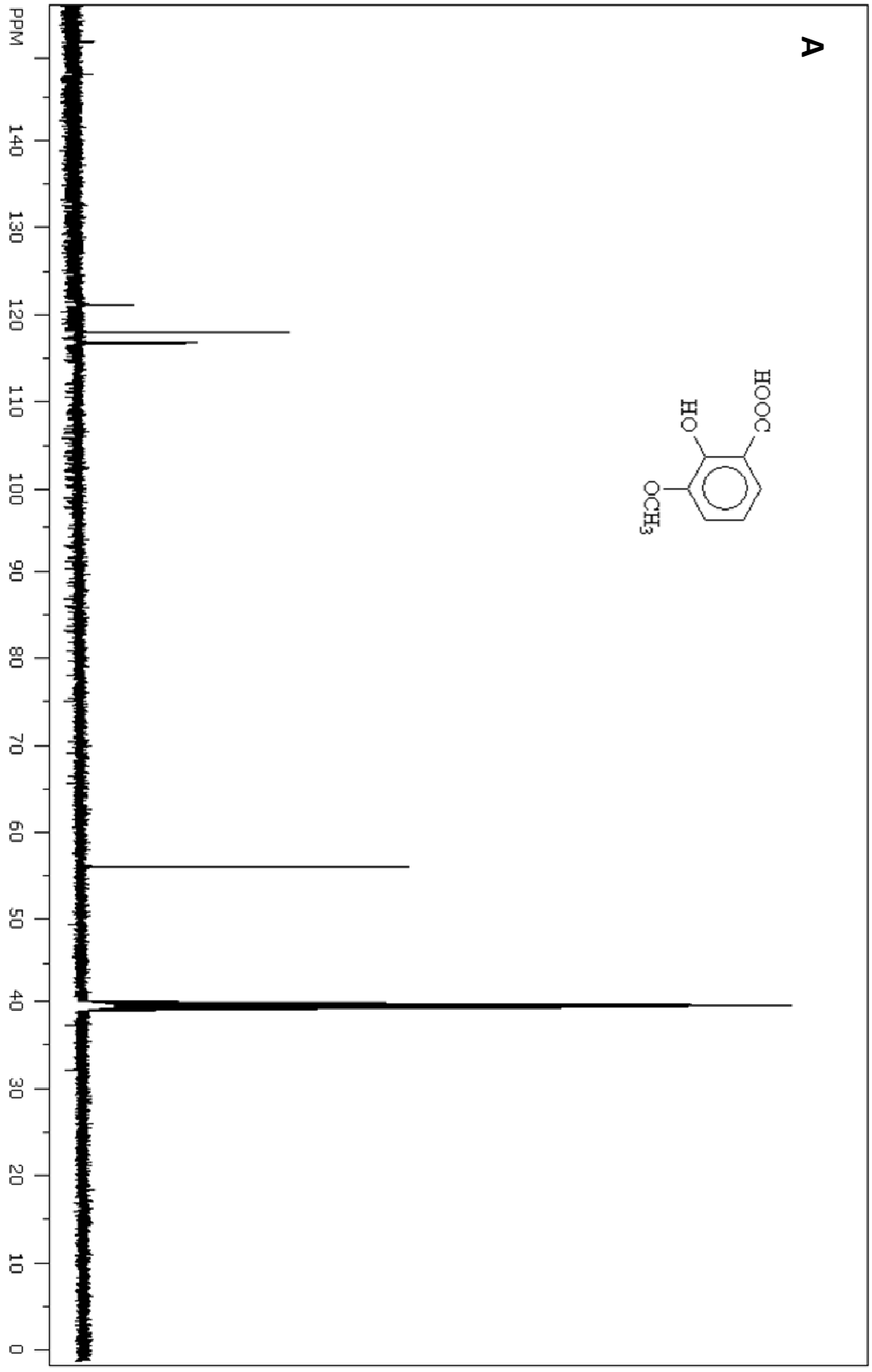
A
HOOC
HO
OCH3
PPM
0
10
20
30
40
50
60
70
80
90
100
110
120
130
140

B

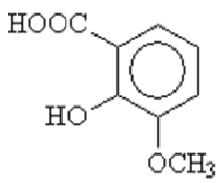

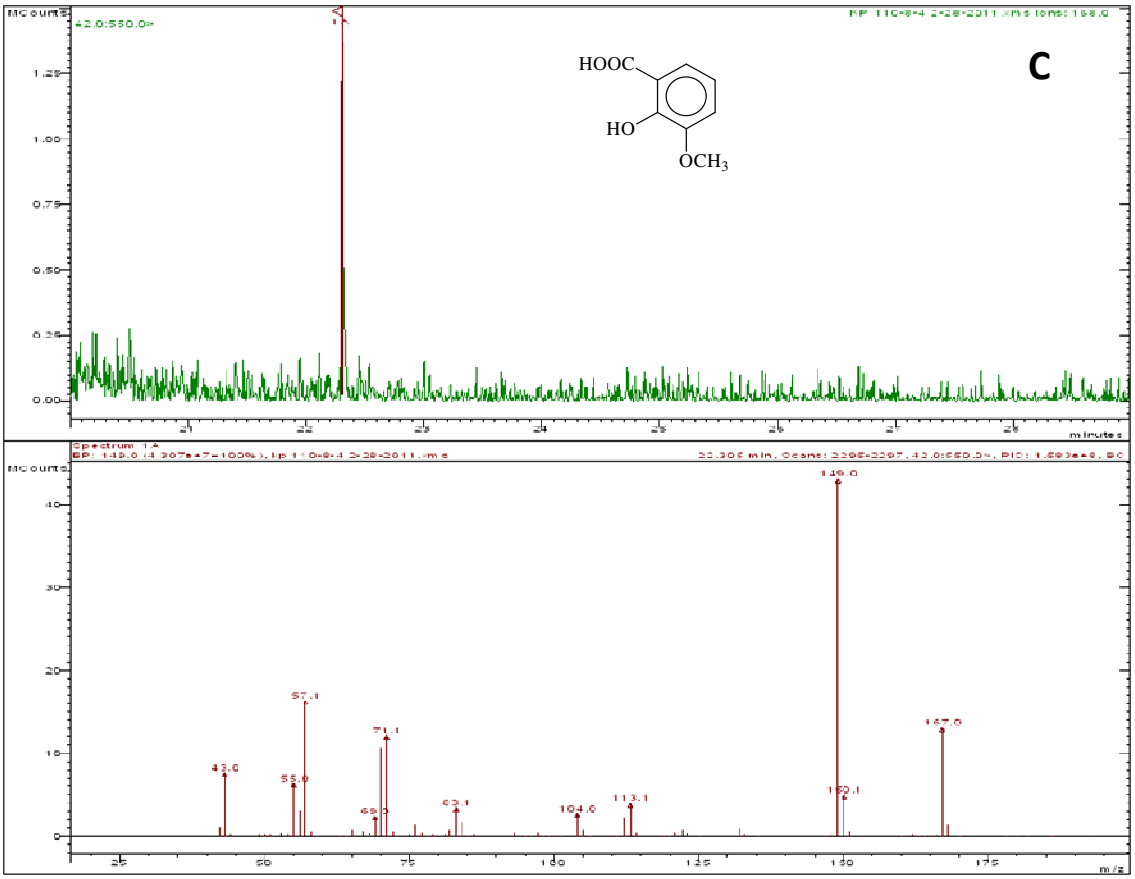

Figure 12(A) ^{13}C NMR spectrum; (B) ^{1}H NMR spectrum; (C) GC-MS spectrum of product (5)


Intens.
x10^6
5
4
3
2
1
0
167.1
181.1
360.9
356.9
A
160
180
200
220
240
260
280
300
320
340
360
m/z

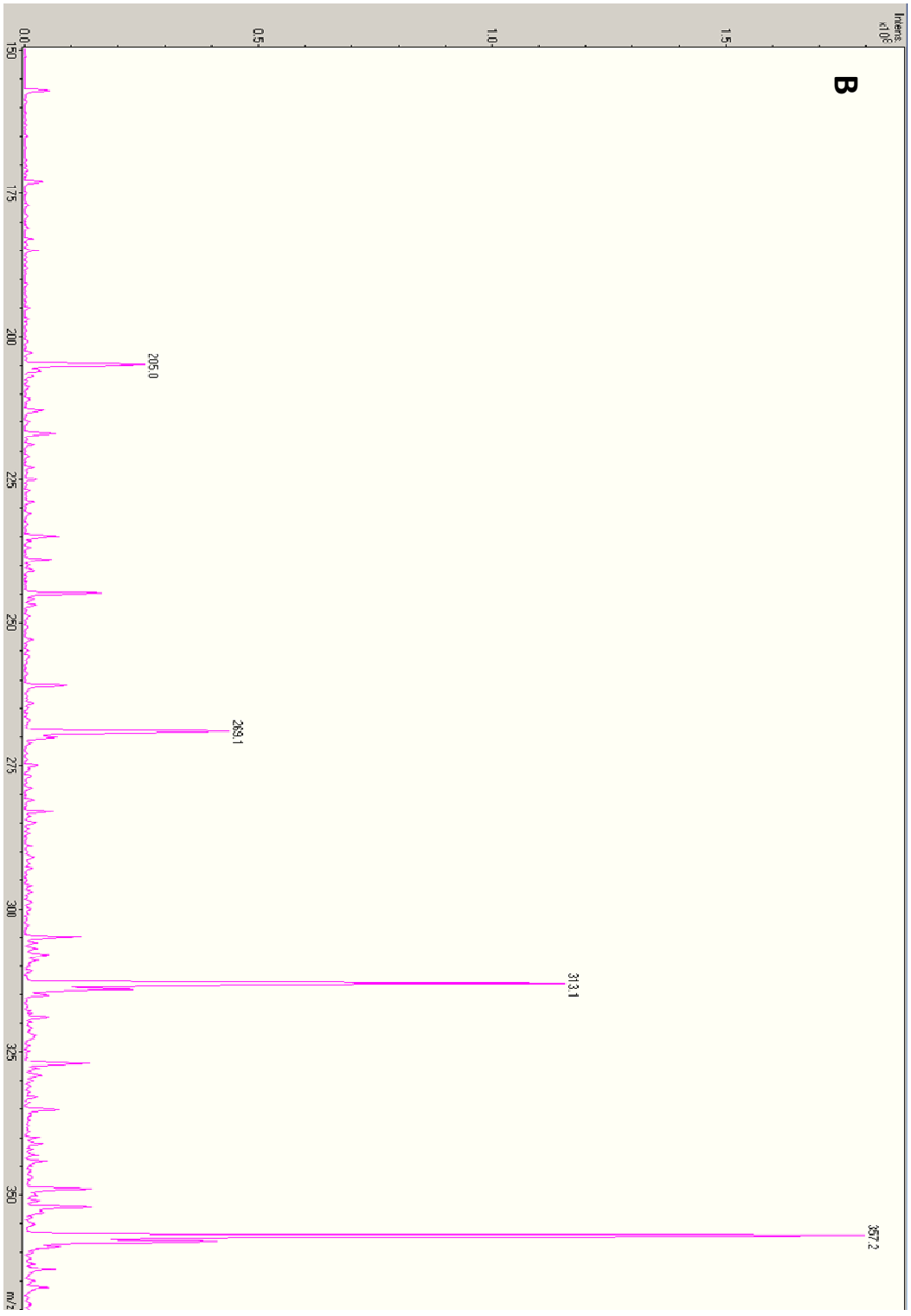

Figure 13 LC-MS spectrum of products produced in the reaction of glyoxal with guaiacol, in (A) negative ionization; (B) positive ionization

4.2.2 Lignin Modification

Although the exact structure of cross-linked product from the reaction of glyoxal with guaiacol was still not clear, the result confirmed that a reaction could occur between lignin and glyoxal. Therefore, the modification of lignin with glyoxal was then studied.

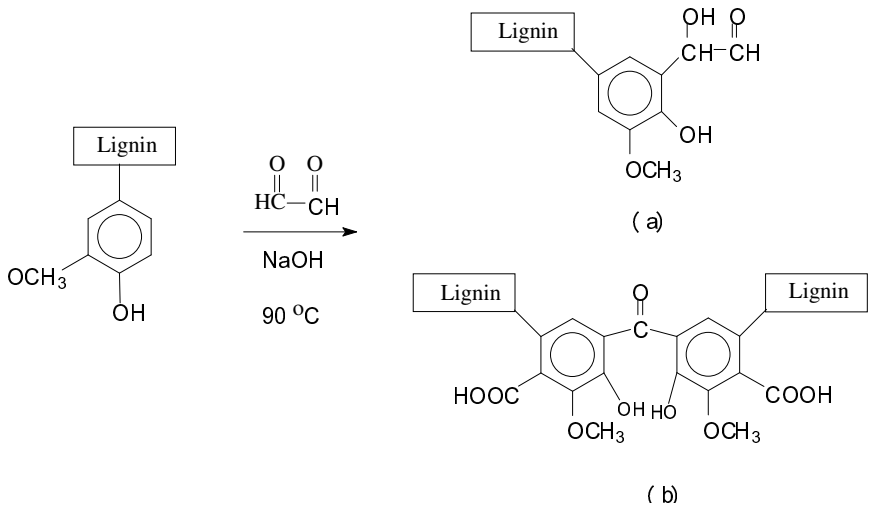

Scheme 7 Lignin modification with glyoxal

Scheme 7 presents the fundamental reaction equation between lignin molecules and glyoxal. The reaction could result in two types of linkages, (a) was the product before cross-linking, while (b) was the assumed cross-linking product.

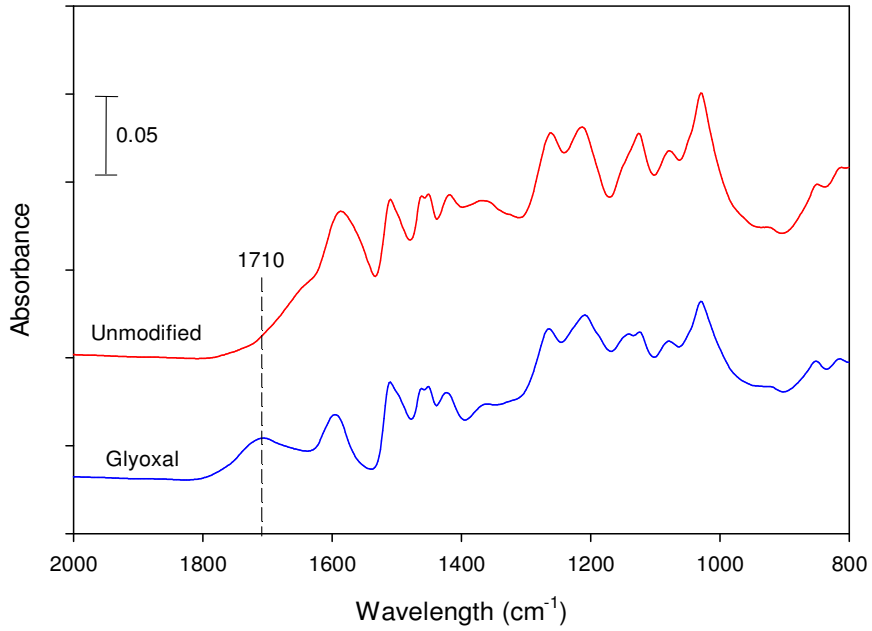

Figure 14 FTIR spectra of glyoxal modified lignin (LG)

Table 5 Content of functional groups in glyoxal modified lignin (LG)

	Total OH group	Ar-OH group	OCH_3 group	C=O group
Unmodified	1.08	1.01	0.81	0.32
LG	1.08	0.82	0.79	0.55

*LG-Lignin modified with glyoxal

Figure 14 illustrates the FTIR data of modified lignin compared with the unmodified lignin. In addition, the relative contents of different functional groups in both unmodified and modified lignin were calculated in Table 5. As shown in Figure 14 and Table 5, the primary change was the dramatic increase of the band at 1710 cm^{-1} wavelength. This peak was assigned for the intensity of C=O groups in lignin molecules. The increase of this peak thus indicates the increase of C=O groups content. When glyoxal was used as a

reagent, the increase of C=O groups could result from the connection of glyoxal with lignin molecules, as shown in Scheme 7, which will lead to a higher content of C=O groups in lignin molecules. Furthermore, the connection of glyoxal on lignin molecules could lead to sequential cross-linking reactions between these modified molecules. In addition, the surface area of modified lignin shows a similar result to the unmodified one, indicating that the surface morphologies of lignin did not change significantly after modification.

In conclusion, the model compound reaction between guaiacol and glyoxal confirmed that modification reaction could occur between lignin molecules and glyoxal. The analysis data show that the structure of lignin was changed after modification, which presented the possibility of a cross-linking reaction.

4.3 Modification with Epichlorohydrin

In this part of work, epichlorohydrin was chosen as a reagent for lignin, which can link the hydroxyl groups in lignin molecules.

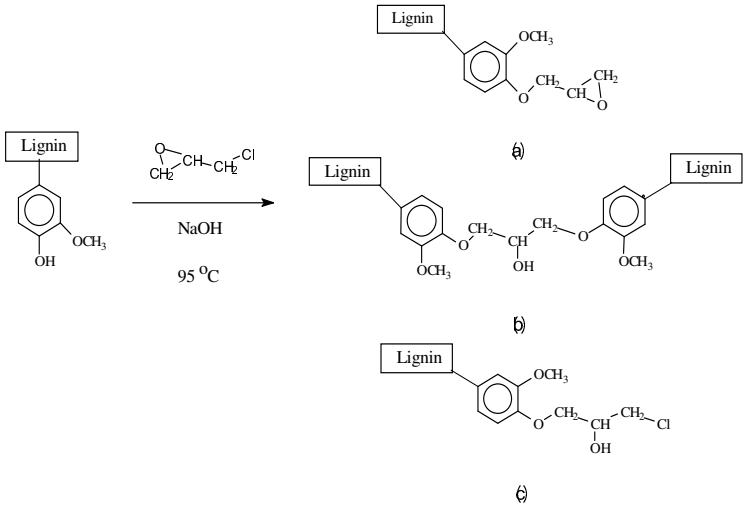

Scheme 8 Lignin modification with epichlorohydrin

Scheme 8 presents the reaction equations between lignin molecules and epichlorohydrin. The reaction resulted in three possible types of linkages. Both (a) and (c) are the products before cross-linking, while (b) is the cross-linked product.

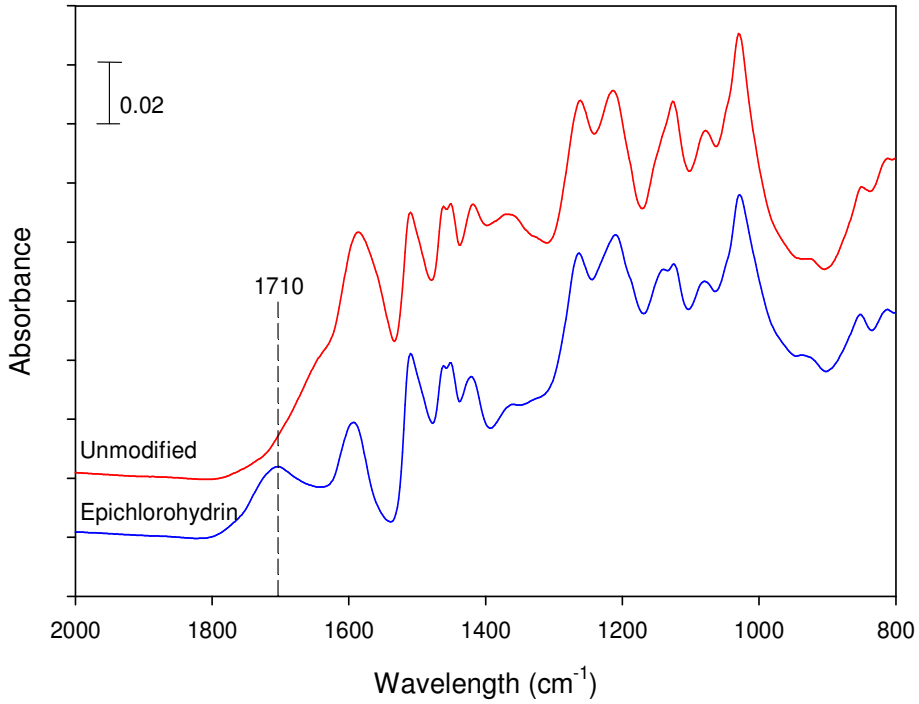

Figure 15 FTIR spectra of epichlorohydrin modified lignin (LE)

Table 6 Content of functional groups in epichlorohydrin modified lignin (LE)

	Total OH group	Ar-OH group	OCH_3 group	C=O group
Unmodified	1.08	1.01	0.81	0.32
LE	1.07	0.79	0.79	0.53

*LE-Lignin modified with epichlorohydrin

Figure 15 illustrates the FTIR data of modified lignin compared with the unmodified lignin. In addition, the relative contents of different functional groups in both unmodified

and modified lignin were calculated and listed in Table 6. As presented in Figure 15 and Table 6, the structure of lignin changed after modification. Firstly, the content of phenolic hydroxyl groups decreased in modified lignin, which corresponds with the reaction scheme. The reaction between lignin and epichlorohydrin consumes phenolic hydroxyl groups, which resulted in the approximately 30% decrease in relative absorbance of this functional group. On the other hand, the intensity of C=O groups at 1710 cm^{-1}increased after modification. Because the reaction between lignin and epichlorohydrin will not change the content of C=O groups, the increase could result from the oxidation and degradation of lignin by itself in alkaline conditions. In addition, the surface morphologies of lignin still did not change significantly after modification.

4.4 Modification with Glyoxal and Epichlorohydrin

Finally, the modification of lignin was carried out using both glyoxal and epichlorohydrin. In this reaction glyoxal was reacting with lignin molecules as a main reagent, while epichlorohydrin was used as an additional cross-linking reagent to connect the hydroxyl groups in lignin molecules, which could lead to further cross-linking reactions. The resulted modified lignin thus could be expected to be a three-dimensional cross-linked product. The reaction equations between lignin molecules, glyoxal and epichlorohydrin were shown in Scheme 7 and 8.

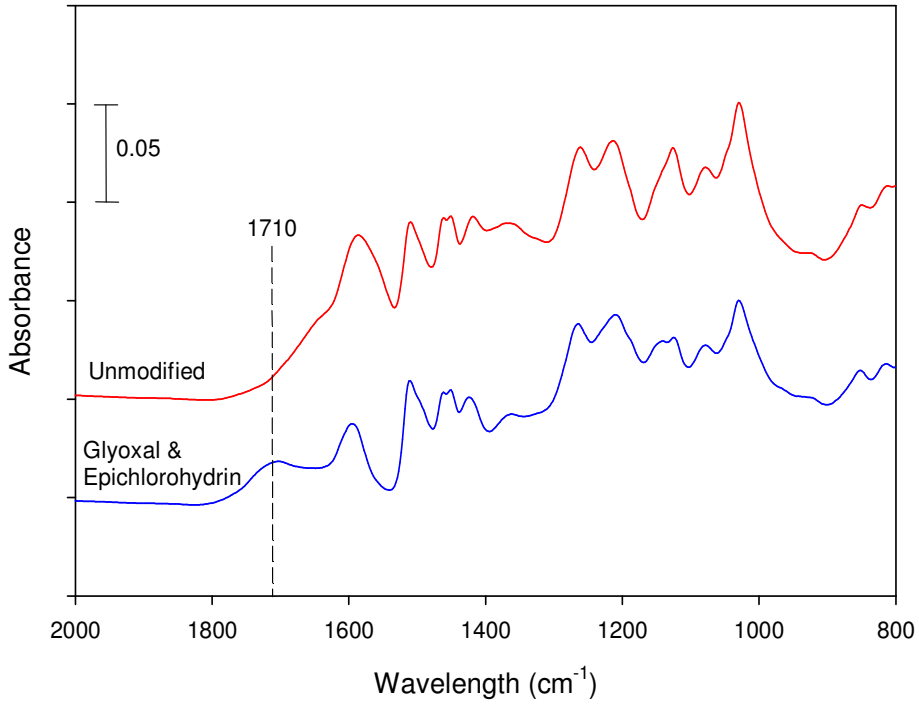

Figure 16 FTIR spectra of glyoxal and epichlorohydrin modified lignin (LGE)

Table 7 Content of functional groups in glyoxal and epichlorohydrin modified lignin (LGE)

	Total OH group	Ar-OH group	OCH_3 group	C=O group
Unmodified	1.08	1.01	0.81	0.32
LGE	1.02	0.79	0.78	0.48

*LGE-Lignin modified with glyoxal and epichlorohydrin

Figure 16 illustrates the FTIR data of modified lignin compared with the unmodified lignin. In addition, the relative contents of different functional groups in both unmodified and modified lignin were calculated and listed in Table 7. According to Figure 16 and Table 7, the structure of lignin changed after modification. The decrease of phenolic

hydroxyl groups still indicates the reaction between lignin molecules and epichlorohydrin. The increase of C=O groups content indicates that reaction between lignin and glyoxal occurred. These reactions could lead to further cross-linking reaction of lignin molecules.

In addition, according to Table 3, the surface area of lignin increased significantly, almost 10 times after modification, indicating a much smaller particle size with better dispersion. Therefore, the SEM image of modified lignin was analyzed to characterize its surface morphologies. Figure 17 presents the SEM image of modified lignin, compared with the unmodified one. According to the image, we can find that modified lignin presents a much smaller particle size and better dispersive particles, which corresponds with the BET surface area result.

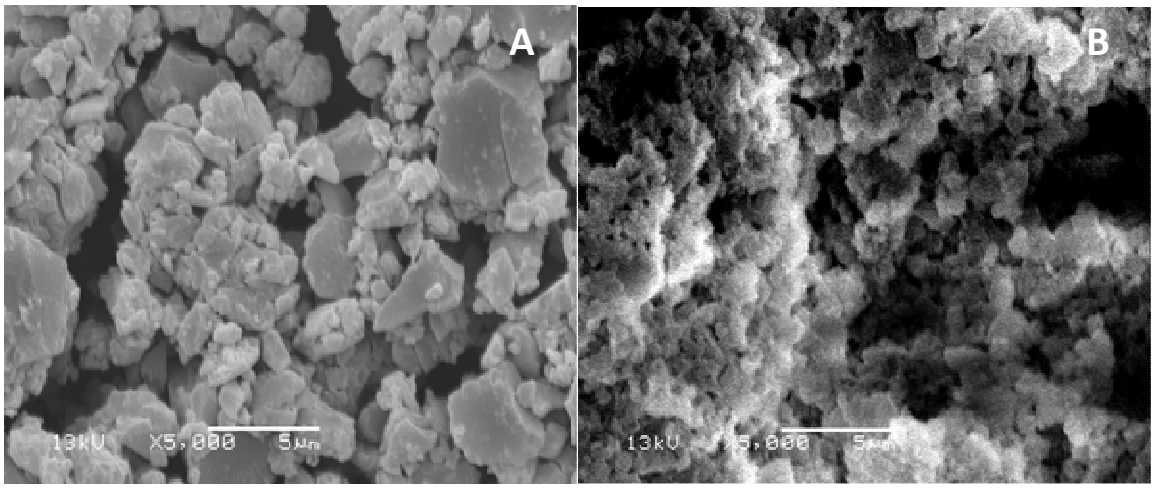

Figure 17 SEM images of (A) unmodified lignin; (B) glyoxal and epichlorohydrin modified lignin (LGE)

In conclusion, with regard to lignin modifications with various electrophilic reagents, modifications of the lignin structure have been carried out. As a result, lignin modified with both glyoxal and epichlorohydrin (LGE) shows the best result. The structure of kraft

lignin was changed after modification, where the occurrence of cross-linking reaction could be expected. On the other hand, LGE modified lignin particles obtained better surface morphology, with a small particle size and better dispersive properties. Such characteristics could be expected to improve its reinforcing effect in rubber.

4.5 Rubber Reinforcing Properties of Kraft Lignin Modified with Glyoxal and Epichlorohydrin (LGE)

According to the results of lignin modifications with different electrophilic reagents, kraft lignin modified with glyoxal and epichlorohydrin (LGE) presented the best structure and surface morphologies. In this part of work, the modified lignin with glyoxal and epichlorohydrin (LGE) was selected for further rubber reinforcing analysis, which was supported by The Goodyear Tire & Rubber Company. The analytical results of LGE filled rubber, compared with unmodified kraft lignin and traditional carbon black filled rubber, are presented in Figure 18 to Figure 22. In these figures, X-Axis presents as the amount of lignin substitutes carbon black per hundred rubber (phr), and Y-Axis presents the value of the tests.

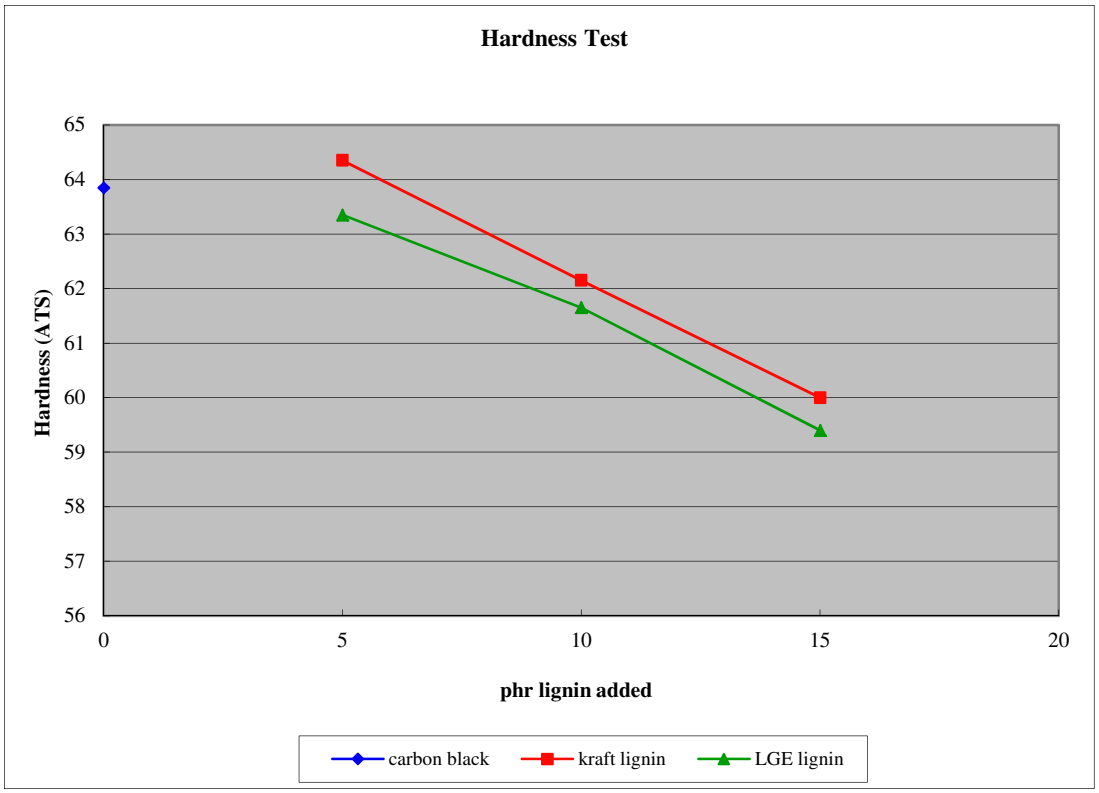

* LGE lignin indicates the lignin modified with glyoxal and epichlorohydrin
X-axis presents the amount of lignin (g) substituting carbon black in 65 g mixed filler.

Figure 18 Rubber hardness test with different fillers

In Figure18, the hardness of LGE modified lignin filled rubber was analyzed, compared with unmodified kraft lignin and traditional carbon black filled rubber. When only 5 g carbon black was substituted by LGE, the hardness of filled rubber did not change. However, when 15 g LGE was applied, the hardness of rubber decreased about 10%. Furthermore, the rubber filled with LGE obtains a lower hardness than the kraft lignin filled one. These data indicates that the larger the portion of lignin substituting carbon black, the lower the hardness of filled rubber.

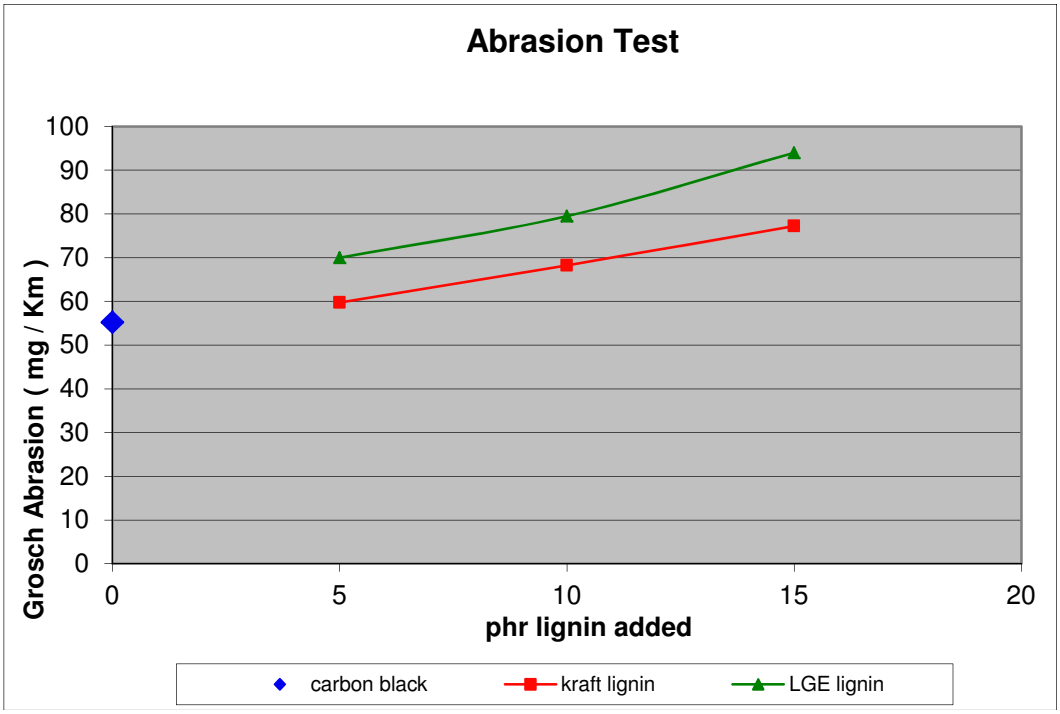

* LGE lignin indicates the lignin modified with glyoxal and epichlorohydrin
X-axis presents the amount of lignin (g) substituting carbon black in 65 g mixed filler.

Figure 19 Rubber Abrasion test with different fillers

Figure19 presents the abrasion test results of different kinds of filled rubber. The anti-abrasion ability of rubber was tested using the Grosch abrasion rate test; the lower the rate, the better the abrasion resistance. When 15 g LGE was used, the abrasion rate increased by almost 50% compared with carbon black filled rubber. In addition, the LGE filled rubber shows a higher abrasion rate than the unmodified kraft lignin filled one. The larger the substitution portion of lignin, the higher the abrasion rate, indicating that lignin filled rubber obtains a lower abrasion resistance.

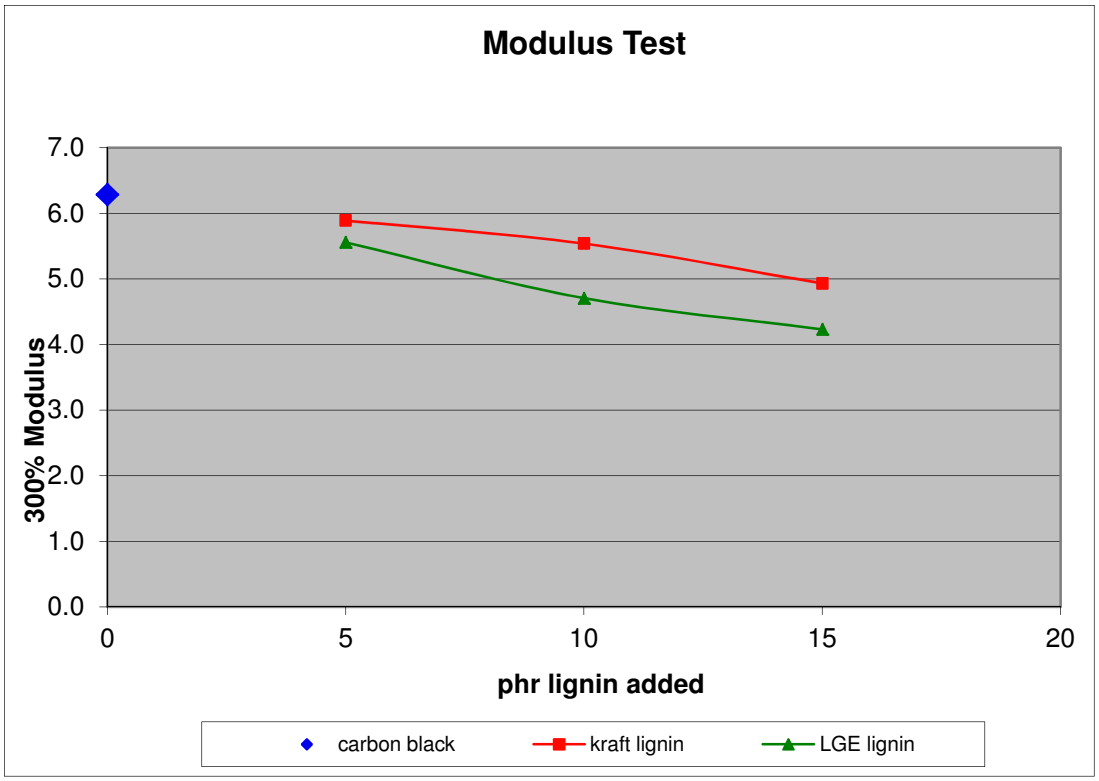

* LGE lignin indicates the lignin modified with glyoxal and epichlorohydrin
X-axis presents the amount of lignin (g) substituting carbon black in 65 g mixed filler.

Figure 20 Rubber 300% Modulus test with different fillers

Figure 20 shows the 300% Modulus data of rubber, which expresses the tensile stress on the rubber sample when it is stretched to 300% length. The lower tensile stress on the rubber, the lower the modulus, which means that the rubber has a lower stiffness. Among the results, LGE filled rubber shows the lowest modulus number, which decreased about 30% when 15 g was added, in comparison with pure carbon black filled rubber. For both kraft and modified lignin filled rubber, the higher the portion of carbon black substituted, the lower the modulus number, indicating a more compliant rubber. The better compliance of LGE filled rubber could result from the reinforcing effect of the smaller and more dispersive particles, or even cross-linked lignin particles, which will enhance the linkage between lignin particles and rubber elastomers.

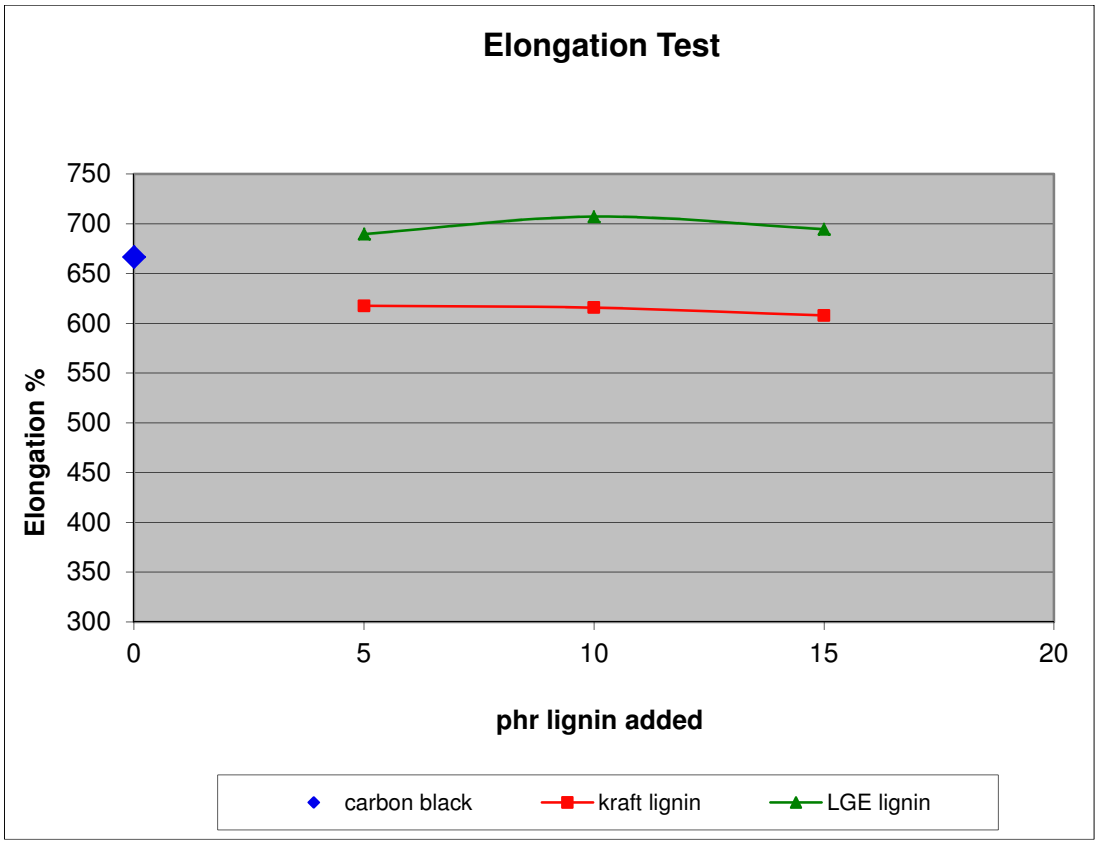

* LGE lignin indicates the lignin modified with glyoxal and epichlorohydrin
X-axis presents the amount of lignin (g) substituting carbon black in 65 g mixed filler.

Figure 21 Rubber elongation test with different fillers

Figure 21 presents the results of the elongation tests of rubber. The number shows the percentage of the original length the rubber sample could be stretched before it is broken; the larger the value, the better compliance of the rubber. The result also shows that LGE filled rubber give the best compliance, which ranges from 670% to 710% when 10 g of LGE was added. For both kraft lignin and LGE filled rubber, the data show that 10 g substitution of carbon black is the optimum amount. When more lignin was substituted for carbon black, the elongation limit starts decreasing. The superior performance of LGE filled rubber could also be explained by the enhancement of linkage between rubber

elastomers and modified lignin particles, which gives a more dispersive and cross-linked structure.

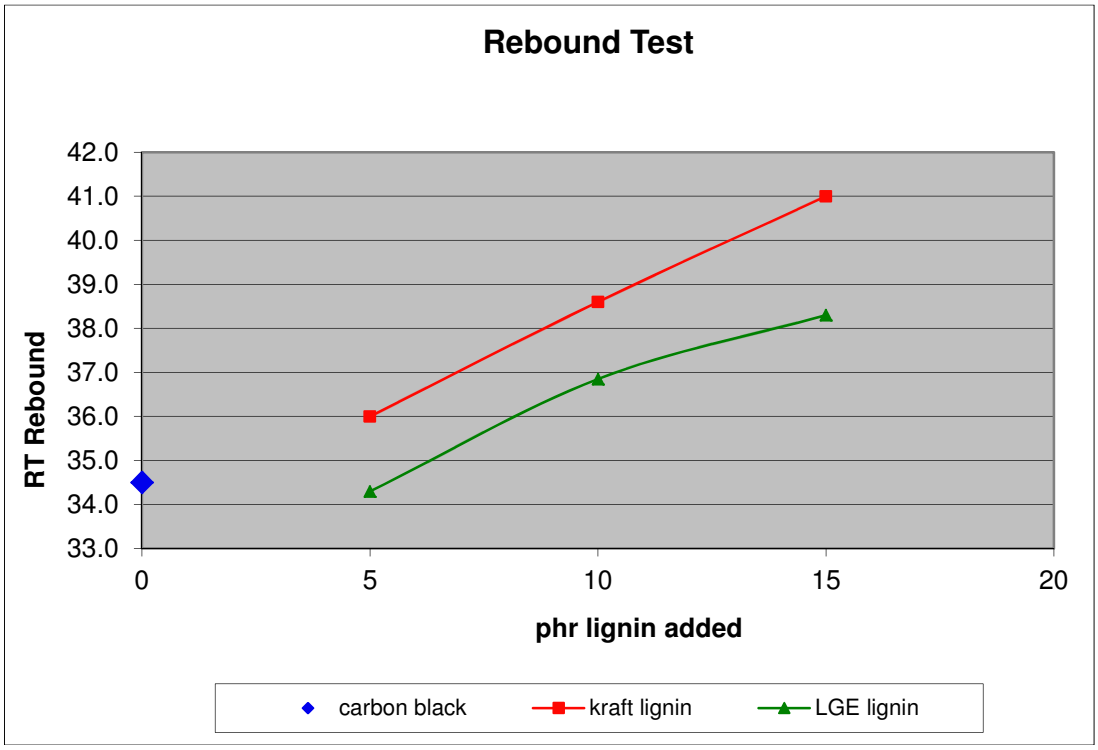

* LGE lignin indicates the lignin modified with glyoxal and epichlorohydrin
X-axis presents the amount of lignin (g) substituting carbon black in 65 g mixed filler.

Figure 22 Rubber rebound test with different fillers

Figure 22 shows the results of the rebound tests of rubber samples at room temperature; the larger the value, the better the rebound ability, but the structuring ability is compromised. The result shows that the addition of both kraft lignin and LGE could enhance the rebound ability of rubber, where kraft lignin filled rubber shows the best rebound ability, ranging from 34 to 41when 15 g of kraft lignin substitutes carbon black. It is also clear that the larger the portion of carbon black being substituted by lignin, the better the rebounding ability of filled rubber.

Chapter 5 Chemical Modifications of Kraft Lignin with Acylating and Alkylating Reagents

In this chapter, chemical modifications of kraft lignin with acylating and alkylating reagents were studied. Kraft lignin was modified with different acylating and alkylating reagents, aiming to change the structures and improve the hydrophobic properties of kraft lignin. The modified lignin was analyzed by FTIR to study the changes in structure, BET to study the surface area changes, and hydrophobicity test to study the change in hydrophobic properties. Table 8 summarizes the conditions of all modifications, as well as the resulting surface area and contact angle of lignin. In the following parts, the principle of each modification is explained and analysis data are provided to support the explanation.

Table 8 Lignin modifications with acylating and alkylating reagents

Type of Lignin	Reagent	Time (hr)	Temp (°C)	Surface Area (m^2/g)	Contact Angle (°)
Unmodified	N/A	N/A	N/A	2.28	30
LA	Aceticanhydride	3	120	6.89	120
LC	benzoyl chloride	12	RT	9.50	120
LM	myristoyl chloride	12	RT	N/A	150
LB	benzyl bromide	8	80	2.07	100

*LA-Lignin modified with acetic anhydride
LC-Lignin modified with benzoyl chloride
LM-Lignin modified with myristoyl chloride
LB-Lignin modified with benzyl bromide

5.1 Modification with Acetic Anhydride

In this chapter, modifications of lignin are aiming to improve the hydrophobic properties of kraft lignin. In principle, the hydrophilic nature of kraft lignin results from the high content of hydroxyl groups in lignin molecules. Therefore, the main objective of modifications on hydrophobic properties was to decrease the content of hydroxyl groups and add new hydrophobic groups onto lignin molecules.

In previous research, acetylation was studied widely as an effective approach to react the hydroxyl groups in lignin molecules, which means, improvement of lignin hydrophobic properties. In this study, acetic anhydride was used as the modification reagent, while sodium acetate was also added as a catalyst of the reaction. Scheme 9 presents the reaction equation.

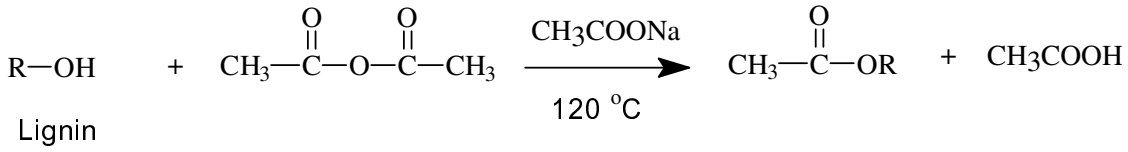

Scheme 9 Lignin modification with acetic anhydride

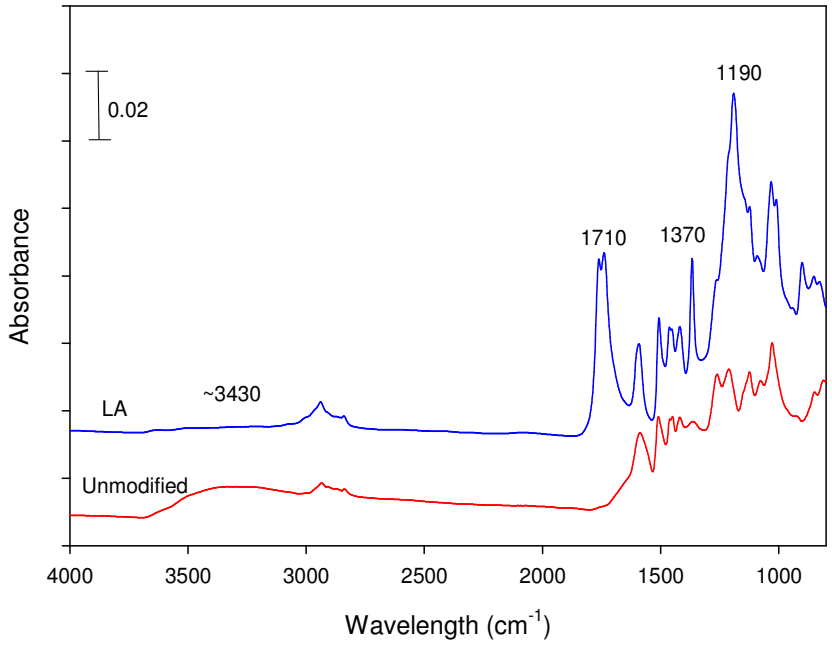

Figure 23 FTIR spectra of acetic anhydride modified lignin (LA)

Figure 23 illustrates the FTIR data of modified lignin compared with the unmodified lignin. According to the figure, the structure of lignin changed significantly after modification. The decrease of the peak around 3430 cm^{-1} indicates the decrease of OH groups. A peak at 1710 cm^{-1} wavelength appeared in modified lignin, and split into a double band. This could result from the formation of C=O groups during acetylation modification. The appearance of a peak at 1370 cm^{-1}, which was assigned to the stretching of CH bonds, could be attributed to the formation of CH_3 bonding after modification. The intense increase of the peak around 1190 cm^{-1} resulted from the large amount of C-O groups formation in acetate.

In addition, the hydrophobicity test was carried out to analyze the change of hydrophobic properties of lignin after modification. In this project, a digital camera connected to computer software was employed to capture and analyze the contact angle of

water droplets on lignin films. This technique was introduced in section 2.7.8. According to the result, the contact angle of modified lignin showed a dramatic increase to 120°, which for unmodified kraft lignin was only less than 30°. This indicates that the hydrophobicity of lignin has been improved significantly after modification.

5.2 Modification with Benzoyl Chloride

In this part of the research, benzoyl chloride was used as a modification reagent to react with the hydroxyl groups in lignin molecules, where pyridine (anhydrous) was used as a solvent. Scheme 10 presents the reaction equation.

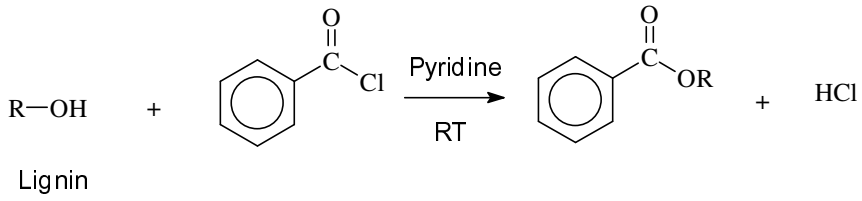

Scheme 10 Lignin modification with benzoyl chloride

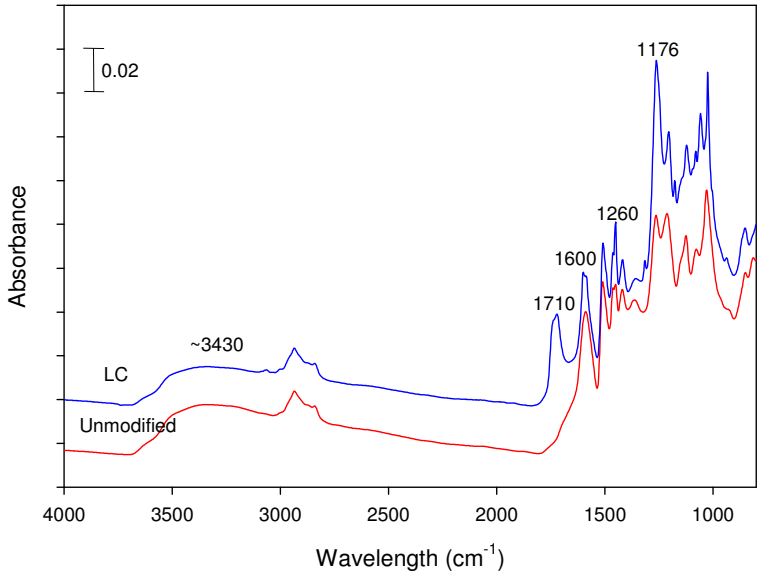

Figure 24 FTIR spectra of benzoyl chloride modified lignin (LC)

Figure 24 illustrates the FTIR data of modified lignin compared with the unmodified lignin. According to the figure, the structure of lignin changed significantly after modification. The decrease of the peak around 3430 cm^{-1} indicates the decrease of OH groups. The appearance of peak at 1710 cm^{-1} wavelength could be attributed to the formation of C=O groups after modification. The split of the band at 1600 cm^{-1} may indicate the connection of aromatic ring with lignin molecules. The intense increase of the band at 1260 cm^{-1} and the appearance of peak at 1176 cm^{-1} both could be attributed to the formation of C-O groups formed after modification.

In addition, the hydrophobicity test was carried out to analyze the change of hydrophobic properties of lignin after modification. The result showed that the contact angle of modified lignin increased from 30° to 120°, which indicates the improvement of hydrophobicity of modified lignin.

5.3 Modification with Myristoyl Chloride

Myristoyl chloride could also be used as a modification reagent for lignin to improve its hydrophobic properties. It not only reacts with the hydroxyl groups in lignin molecules, but also introduces long carbon chains onto it. Scheme 11 presents the reaction equation.

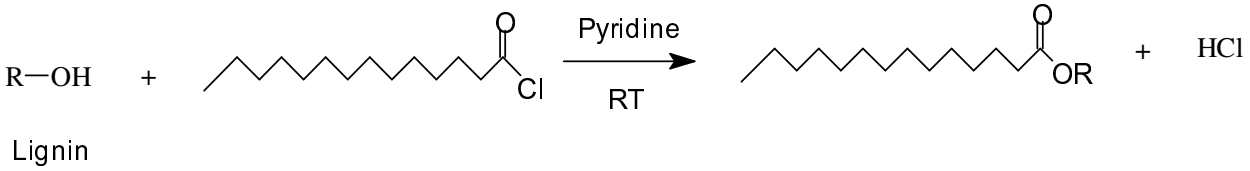

Scheme 11 Lignin modification with myristoyl chloride

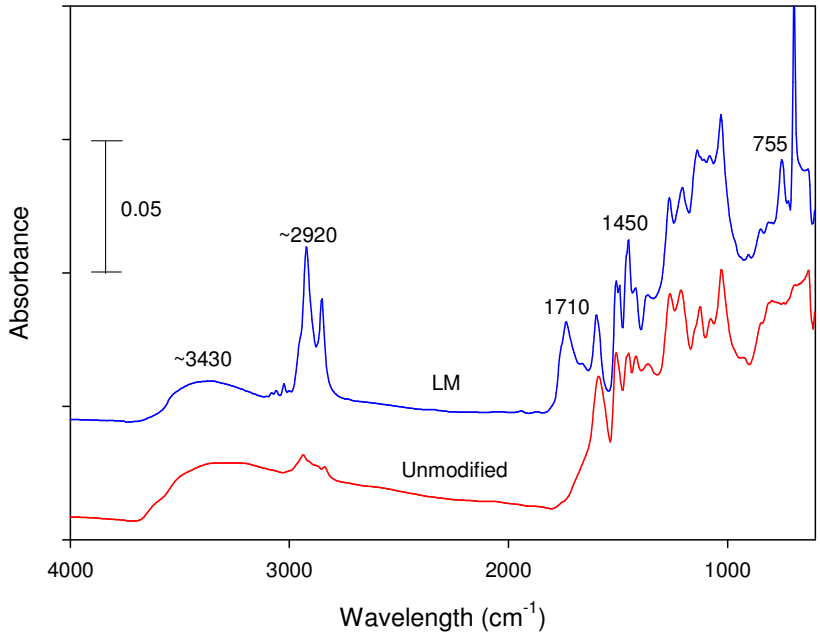

Figure 25 FTIR spectra of myristoyl chloride modified lignin (LM)

Figure 25 illustrates the FTIR data of modified lignin compared with the unmodified lignin. According to the figure, the structure of lignin changed significantly after modification. The decrease of the peak around 3430 cm^{-1} indicates the decrease of OH groups. The intense increase of the peaks around 2920 cm^{-1} could be attributed to the formation of large amounts of CH, CH_2 and CH_3 bonds from the long carbon chain. The appearance of the peak at 1710 cm^{-1} was because of the formation of C=O group after modification. The larger intensity of the band at 1450 and 755 cm^{-1} could also result from the CH bonding in CH_2, and CH_3 groups.

In addition, the hydrophobicity test was carried out to analyze the change of hydrophobic properties of lignin after modification. The contact angle of modified lignin increased dramatically from 30° to almost 150°, which improved the hydrophobic properties of kraft lignin. However, the drawback of this modification was that the

resulting modified lignin was a gel even at room temperature. This could limit its application as a rubber filler as it needs to be mixed with the rubber matrix in powder form when producing reinforced rubber products.

5.4 Modification with Benzyl Bromide

At last, benzyl bromide was used as a modification reagent to react with the hydroxyl groups in lignin molecules. Scheme 12 presents the reaction equation.

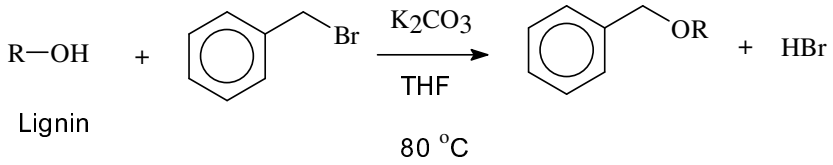

Scheme 12 Lignin modification with benzyl bromide

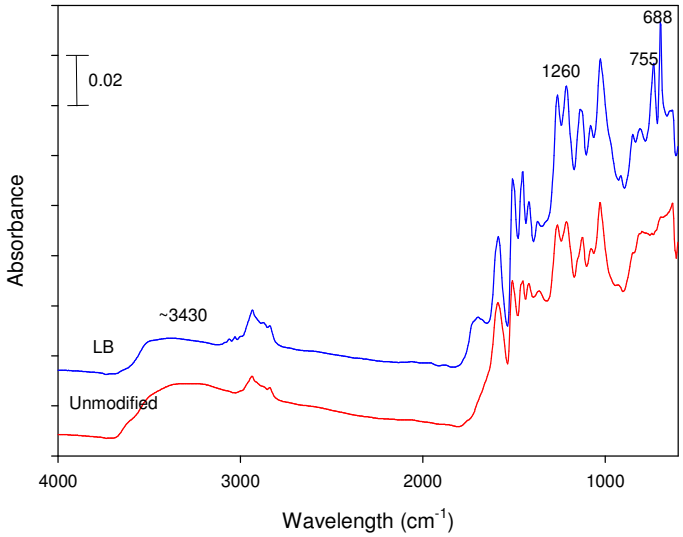

Figure 26 FTIR spectra of benzyl bromide modified lignin (LB)

Figure 26 illustrates the FTIR data of modified lignin compared with the unmodified lignin. According to the figure, the structure of lignin changed significantly after modification. The decrease of the peak around 3430 cm^{-1} indicates the decrease of OH

groups. The increasing intensity of the peak at 1260 cm^{-1} could be attributed to the formation of C-O groups after modification. The appearance of the band at 755 cm^{-1} resulted from the formation of CH_2 groups after modification, while the intense peak at 688 cm^{-1} was because of the aromatic ring puckering, which was connected to lignin molecules after modification.

In addition, the hydrophobicity test was carried out to analyze the change of hydrophobic properties of lignin after modification. The result showed that the contact angle of modified lignin increased from 30° to 100°, which indicated improvement of hydrophobicity of modified lignin.

In conclusion, all these modification reagents reacted with the lignin molecule, changing its structure and improving its hydrophobic properties. The modified lignin gives better hydrophobic properties, which could improve its reinforcing effect as a rubber filler. According to the analysis data, although lignin modified with myristoyl chloride (LM) obtained the largest contact angle, the properties of the product were not ideal as a rubber filler. Therefore, lignin modified with acetic anhydride (LA) was selected for industrial reinforcing analysis in rubber because of its high hydrophobic properties and easy preparation. However, because the test is still in process, the reinforcing results cannot be shown here.

Chapter 6 Electrochemical Modifications of Kraft Lignin

In this chapter, an electrochemical approach was studied to add value to kraft lignin. The primary objective was to oxidize kraft lignin into valuable products such as vanillin and vanllic acid. Another objective of this part of the research was to fabricate a high performance TiO_2NT/PbO_2electrode by a novel approach which combines the photocatalysis and electrochemical deposition.

6.1 Characterization of TiO_2 Nanotube

SEM was used to characterize the surface structure and morphologies of the fabricated TiO_2 nanotubes and the Ti/TiO_2NT/PbO_2 electrodes. As shown in Figure 27A, well ordered self-assembled nanotubes were produced with uniform pore diameters of ~100 nm. Figure 27B displays distinct oxygen and titanium peaks, confirming the formation of TiO_2 nanotubes. In addition, Figure 27C, presents the corresponding XRD pattern of the fabricated TiO_2 nanotubes. All diffraction peaks may be attributed to the tetragonal anatase TiO_2 phase. The peaks marked with a star are derived from the Ti substrate. The photocatalytic activity of the fabricated TiO_2 nanotubes was also tested. The time dependence of the current density of the TiO_2 nanotubes recorded in 0.1 M H_2SO_4 at a 1.4 V potential, in the presence and absence of UV illumination, is presented in Figure 28. The current density of the TiO_2 nanotubes was found to increase from ~0.01 to ~0.50 mA/cm^2 when illuminated by UV light. This data indicates that the fabricated TiO_2 nanotubes are highly activated under the application of UV light, which is desirable for the photoelectrochemical deposition of PbO_2 nanoparticles.

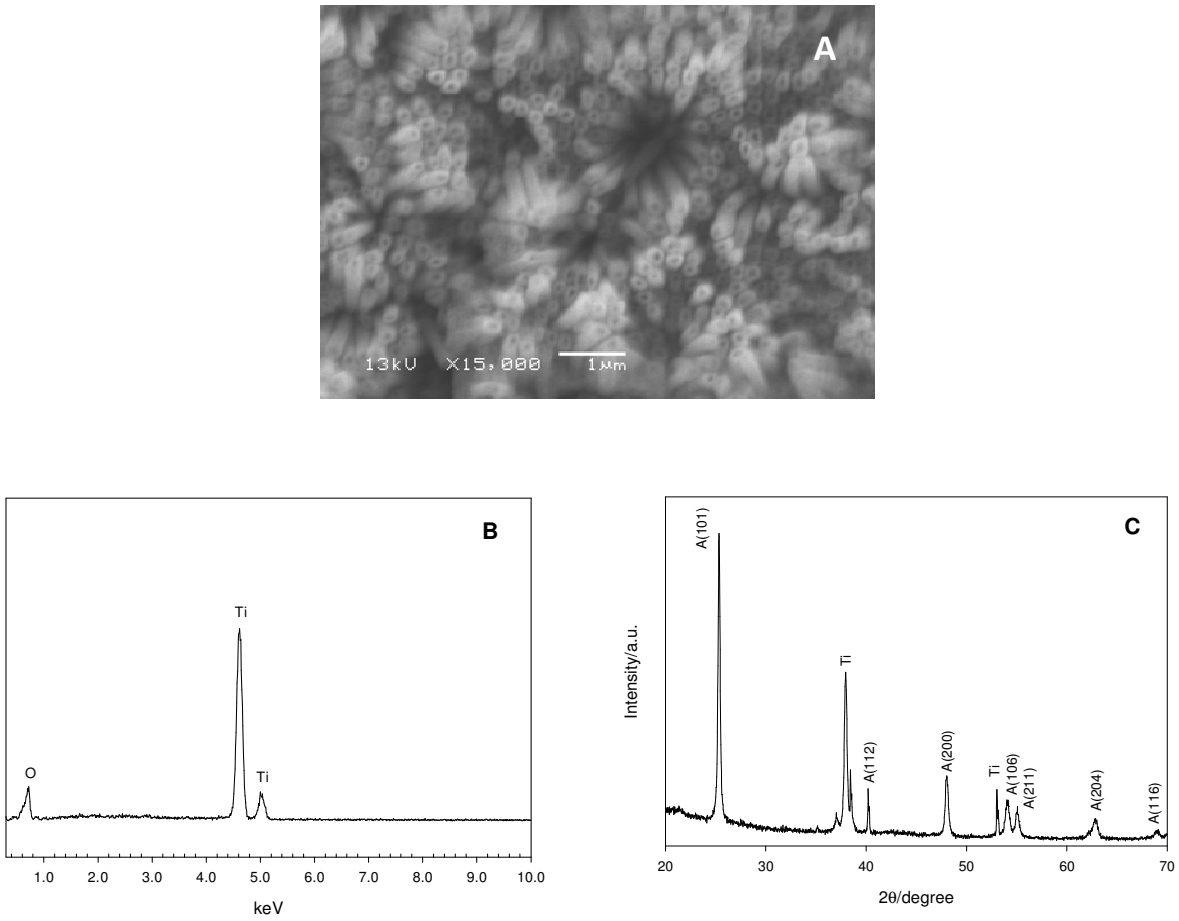

Figure 27(A) SEM image of TiO_2NT; (B) EDS spectra of TiO_2NT; (C) XRD of TiO_2NT

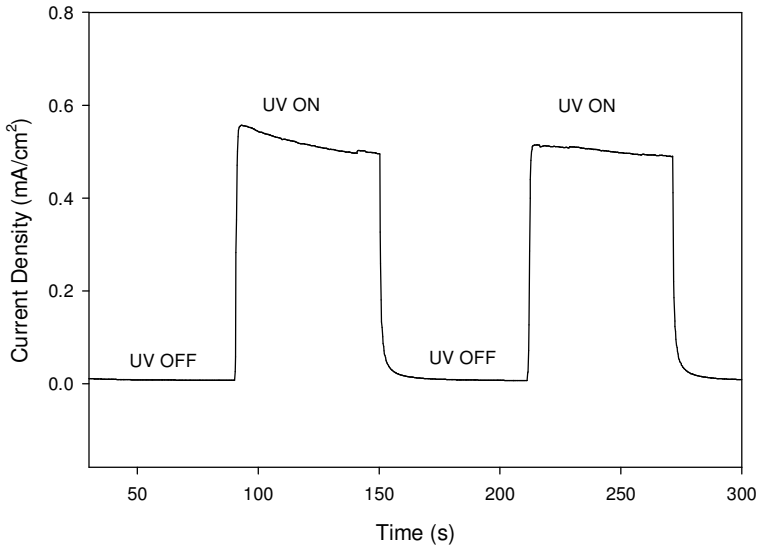

Figure 28Time-Current curve of TiO_2NT electrode under UV illumination

6.2 Characterization of TiO_2NT/PbO_2 Electrode

Figure 29A presents a SEM image of the fabricated $Ti/TiO_2NT/PbO_2$ electrode, revealing that PbO_2 nanoparticles were uniformly deposited onto the TiO_2 nanotube arrays. Besides the oxygen and titanium peaks, strong Pb peaks were observed in the EDS spectrum (Figure 29B). Figure 29C illustrates the XRD pattern of the prepared $Ti/TiO_2NT/PbO_2$ electrode, showing corresponding diffraction peaks of PbO_2 in both tetragonal and orthorhombic phases. The electrochemical performance of the fabricated $Ti/TiO_2NT/PbO_2$ electrode was then characterized. Figure 30A shows the cyclic voltammogram (CV) of the $Ti/TiO_2NT/PbO_2$ electrode recorded in 0.5 M NaOH solution in the potential range between 0 and + 1.4 V at a scan rate of 20 mV/s. For comparison, the CV of the Ti/TiO_2NT electrode is included in Figure 30A, showing that the deposited PbO_2 nanoparticles possess much higher electrocatalytic activity. The onset potential for oxygen evolution on the $Ti/TiO_2NT/PbO_2$ electrode was at ~0.8 V vs Ag/AgCl. The current increased linearly with an increase of the electrode potential when higher than 0.9 V. The steady state current of the fabricated $Ti/TiO_2NT/PbO_2$ electrode was further measured at 1.4 V for 90 min. As seen in Figure 30B, the TiO_2NT-supported PbO_2 nanoparticles possess high electrocatalytic activity (over 40 mA/cm^2) and robust stability, which is desirable for the electrochemical oxidation of lignin.

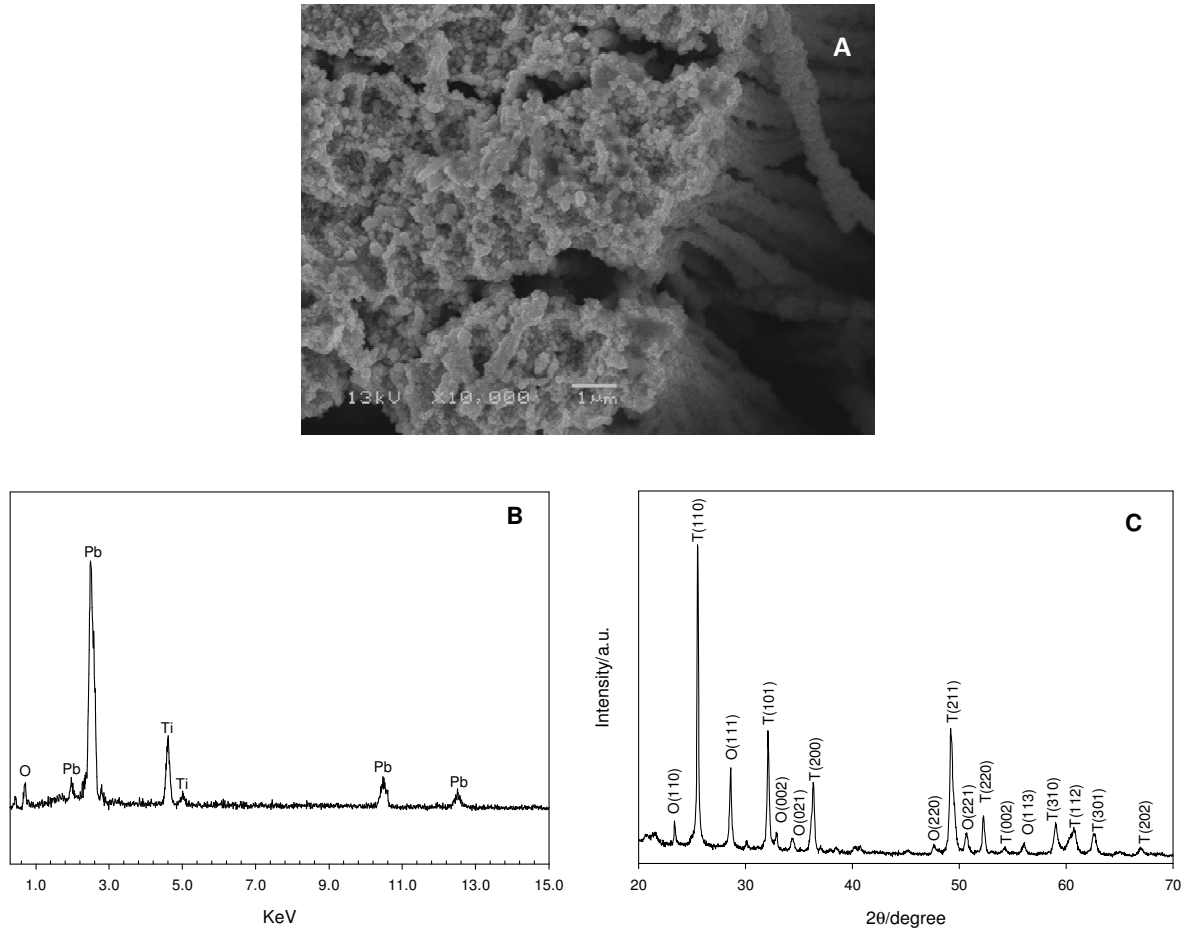

Figure 29(A) SEM images of TiO_2NT/PbO_2; (B)EDS spectra of TiO_2NT/PbO_2 electrode; (C) XRD of TiO_2NT/PbO_2 electrode

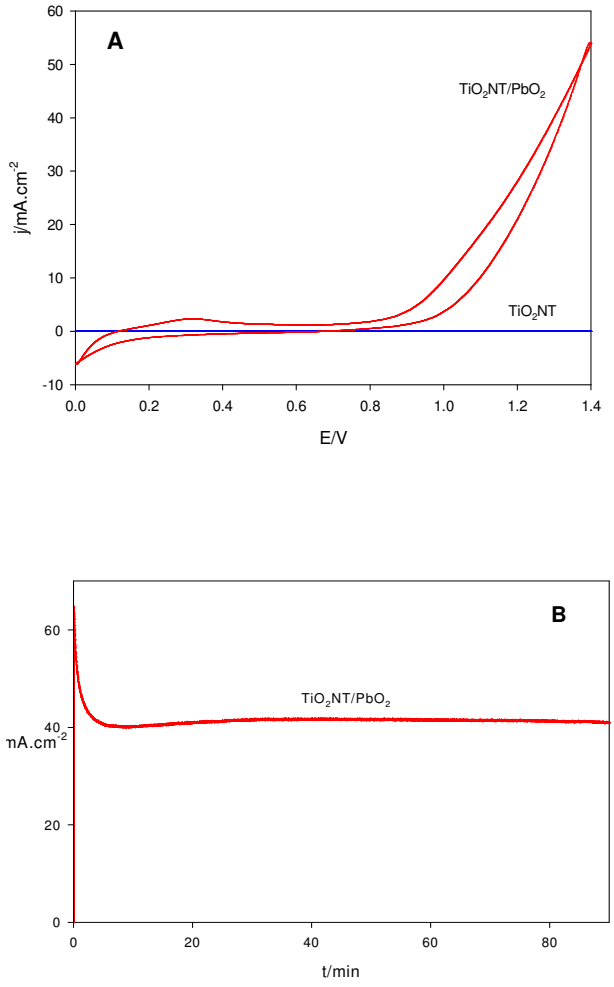

Figure 30 (A) CV curves of TiO_2NT/PbO_2 electrode compared with TiO_2NT electrode; (B) Time-current curve of TiO_2NT/PbO_2electrode for stability test

6.3 Electrochemical Oxidation of Lignin Model Compound

Before the electrochemical oxidation of lignin, the oxidation of model compound for lignin was studied. In this study, guaiacol and 1-(4-hydroxy-3-methoxyphenyl)-2-(2-methoxyphenoxy)-1,3-propanediol were chosen as the model compounds because of their similar structures to lignin. Figure 31 presents the scanning kinetics graphs taken at 15 minute intervals. The UV-Vis absorption at 240 nm^{-1} for guaiacol and 248 nm^{-1} for 1-(4-

hydroxy-3-methoxyphenyl)-2-(2-methoxyphenoxy)-1,3-propanediol were considered to represent the concentration of these model compounds, respectively. Therefore, the decrease of the absorbance over time indicates oxidation of the model compounds, confirming the ability of the fabricated TiO_2NT/PbO_2 electrode to oxidize lignin.

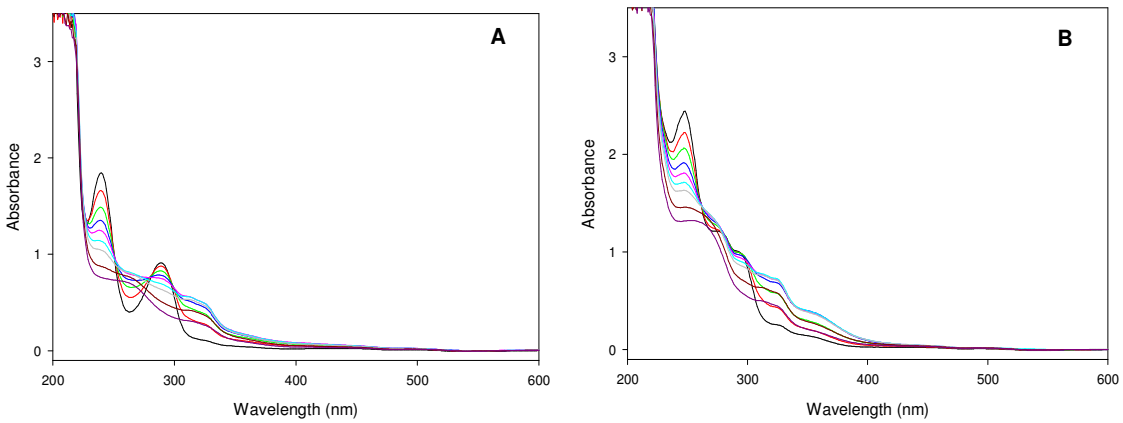

Figure 31 In-situ UV-Vis spectra of lignin model compound oxidation: (A) guaiacol; (B) 1-(4-hydroxy-3-methoxyphenyl)-2-(2-methoxyphenoxy)-1,3-propanediol

6.4 Electrochemical Oxidation of Lignin

The initial oxidation of lignin using the $Ti/TiO_2NT/PbO_2$ electrode was held under 100 mA at 60 °C. The scanning kinetics graphs taken at 15-minute intervals are presented in Figure 32. The UV-Vis absorption at 290 nm is considered to represent the concentration of lignin, and thus the decrease of the absorbance over time is confirmation of the lignin oxidation process. The influence of initial lignin concentrations on the electrochemical oxidation process was subsequently studied; and the plots of ln (C/C_0) vs. time for three different lignin concentrations 75, 100 and 125 ppm are displayed in Figure 33A. The linear relationships illustrate that the electrochemical oxidation of lignin follows pseudo first-order kinetics. The apparent kinetic rate constant k was determined from the

magnitude of the slope of the straight line at the different initial concentrations. As depicted in Figure 33A, different lignin concentrations showed similar slopes; the apparent kinetic rate constant k is ~0.0044 min^{-1}. This data indicates that the effect of the initial lignin concentration on the rate of the electrochemical oxidation process was negligible.

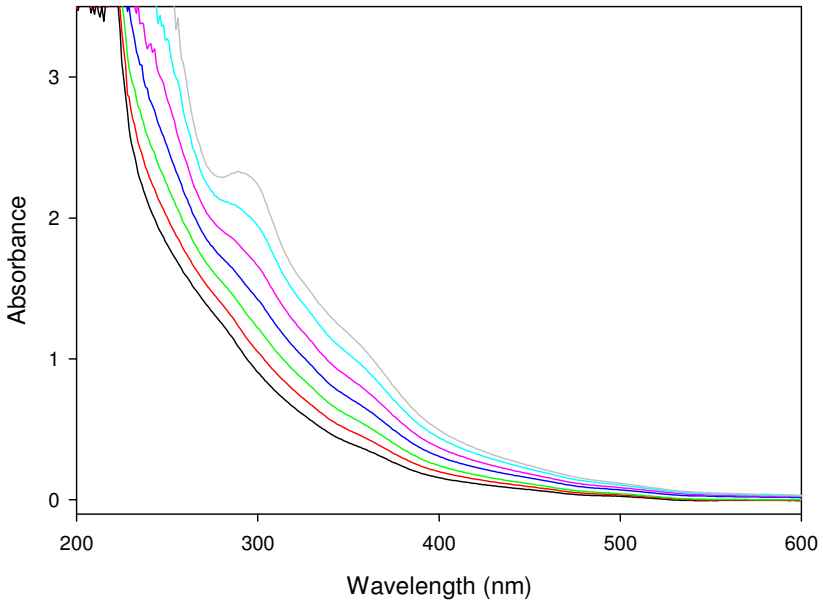

Figure 32 UV-Vis spectra of 100 ppm lignin oxidation under 100 mA in 60 °C

The impact of current on the electrochemical oxidation of lignin was also studied. The concentration of lignin was 100 ppm, and the temperature was held at 60 °C. Different currents spanning 50 to 125 mA were applied. Figure 33B presents the plots of ln (C/C_0) vs. time under the different currents. The kinetic rate constant k can be determined from the linear relationships of the plots. The slope was increased from 0.0032 to 0.0043 min^{-1} with an increase of the applied current from 50 to 100 mA, showing that higher applied currents result in more rapid lignin oxidation. However, a further increase of the current from 100 to 125 mA scarcely elevated the oxidation rate, which remained at 0.0043 min^{-1}, indicating

that 100 mA is the optimized current for the electrochemical oxidation of lignin at the Ti/TiO_2NT/PbO_2 electrode. The extra current over 100 mA is primarily utilized in competition for the oxygen evolution reaction, which exhibits no notable contribution to the oxidation of lignin.

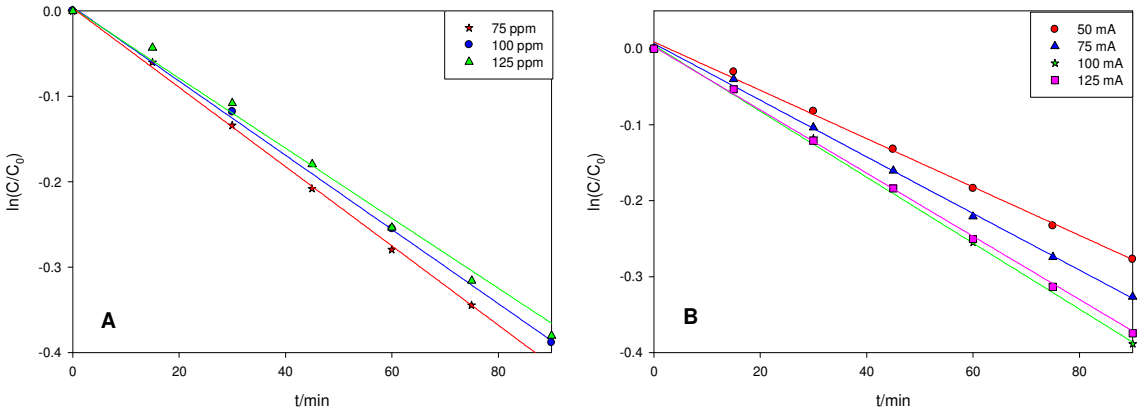

Figure 33 (A) Concentration effect on lignin oxidation under 100 mA in 60 °C; (B) Current effect on 100 ppm lignin oxidation at 60 °C

The effect of temperature on the electrochemical oxidation of lignin at the TiO_2NT/PbO_2 electrode was investigated as well. The concentration of lignin was 100 ppm under an applied current of 100 mA at different temperatures that ranged from 20 to 60 °C. Figure 34A presents the plots of ln (C/C_0) vs. time, and the kinetic rate constant k was also determined. The value of k increased concurrently with temperature from 0.0018 min^{-1} at 20 °C to 0.0043 min^{-1} at 60 °C, indicating that higher temperatures could enhance the oxidation of lignin. The activation energy (Ea) of the lignin oxidation was further studied by plotting 1/T vs. ln k, which is presented in Figure 34B. The activation energy for the electrochemical oxidation of lignin at the TiO_2NT/PbO_2 electrode was calculated to be 16.0 kJ/mol. This is smaller than that at the Ti/RuO_2-IrO_2 electrode (20.0 kJ/mol) [60],

indicating that the TiO_2NT/PbO_2 electrode possesses higher catalytic activity for the electrochemical oxidation of lignin.

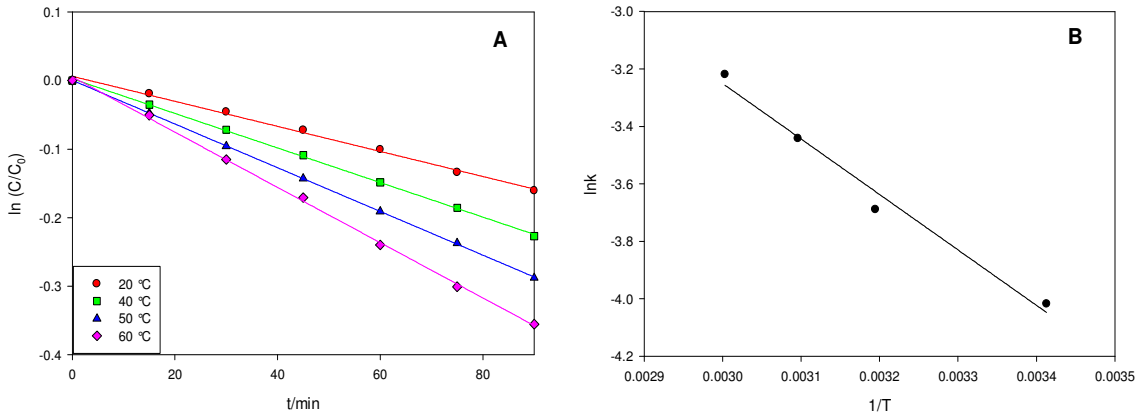

Figure 34 (A) Temperature effect on 100 ppm lignin oxidation under 100 mA; (B) Activation energy of 100 ppm lignin oxidation under 100 mA

Finally, the COD of the lignin solution was investigated during the electrochemical oxidation process. The oxidation was set under optimized conditions (e.g., 100 ppm lignin solution under 100 mA at 60 °C). The COD of the lignin solution was analyzed during the oxidation process, and the results are presented in Figure 35A. According to the graph, the COD of the lignin solution decreased linearly over the eight-hour electrochemical oxidation period. The COD dropped from 185.09 to 65.58 mg/L, showing that the fabricated TiO_2NT/PbO_2 electrode is effective for electrochemical oxidation of lignin. Furthermore, photographs of the oxidized lignin solution are shown in Figure 35B. The color of the solution was altered from an initial deep yellow to colorless following eight-hours of electrochemical oxidation. This shows that lignin, which is the source of the color in the solution, was oxidized, and further indicated that the remaining COD in the solution

is likely the result of residual organic compounds that are generated subsequent to lignin oxidation.

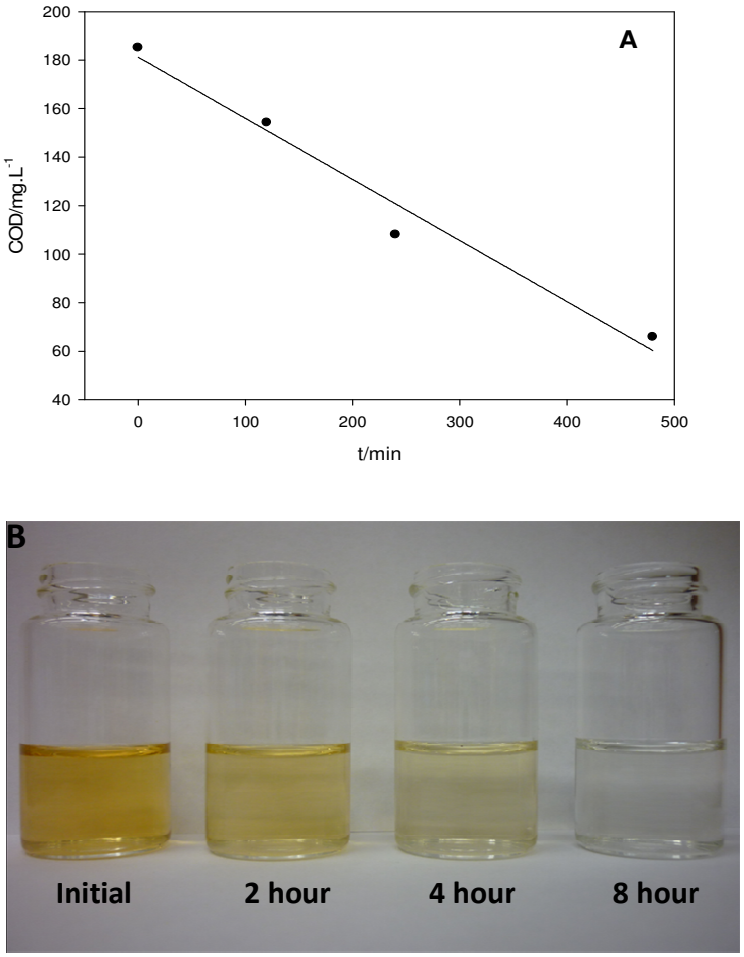

Figure 35(A) COD elimination of lignin solution with oxidation time; (B) Photographs of lignin solution after oxidation

6.5 Identification of Lignin Degradation Products

In order to study the degradation products that result from the oxidation of lignin, the complete process was carried out under different conditions using the $Ti/TiO_2NT/PbO_2$ electrode: 10 g/L lignin solution was oxidized under 100 mA at 60 °C. The status of the oxidation process at different time increments was studied. In order to analyze the residual

lignin by-products subsequent to oxidation toward the determination of the intermediates produced, the lignin solution was acidified with dilute H_2SO_4 to precipitate all lignin residues. Photographs of the lignin solution subsequent to electrochemical oxidation for four and eight hours, in comparison with the initial lignin solution are illustrated in Figure 36. The amount of lignin being precipitated was continually reduced in conjunction with the increase in oxidation time, while the color of the solution became darker. This indicates that higher volumes of lignin were being oxidized with increasing time. In a following step, the lignin solution was centrifuged to separate the residues from solution. The separated solution and solids were analyzed via HPLC and FTIR, respectively.

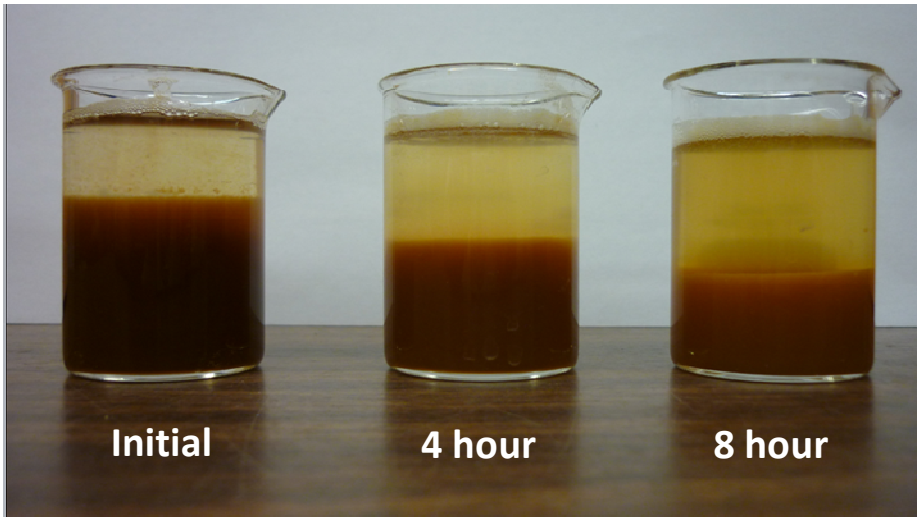

Figure 36 Photographs of lignin solution subsequent to precipitation

FTIR was employed to characterize the lignin residues following the electrochemical treatment. The FTIR data of the lignin after four and eight hours of oxidation in comparison with the initial sample is shown in Figure 37. The band centered at 1710 cm^{-1} was assigned to the stretching of carbonyl groups, unconjugated ketones, or carboxylic acids, showing an increasing intensity after the electrochemical oxidation. This might be attributed to the production of more carbonyl groups in the lignin following the oxidation.

The sharp peaks at 1600 and 1510 cm^{-1} were assigned to aromatic ring vibrations, which typically exhibit large intensities in lignin molecules. The bands at 1030, 1260, and ~1130 cm^{-1} were due to the stretching of C-O-C groups in esters, ethers and alcohols, which decrease after protracted oxidation times. This may result from the cleavage of C-O-C groups and the formation of C=O groups during oxidation. Furthermore, the content of C=O and C-O-C groups in the lignin residues was estimated and the results are presented in Table 9. Also shown here is that the occurrence of C-O-C groups decreased from 1.74 to 1.51 during the lignin oxidation, while C=O groups increased from 0.72 to 1.04, revealing the same trend of structural change that is observed in the FTIR spectra. This estimation is based on the relative absorbance intensity of functional groups to the ratio of aromatic rings at 1510 cm^{-1} wavelength. On the whole, the changes in functional group content according to FTIR reveal the formation of different species of functional groups subsequent to the electrochemical oxidation.

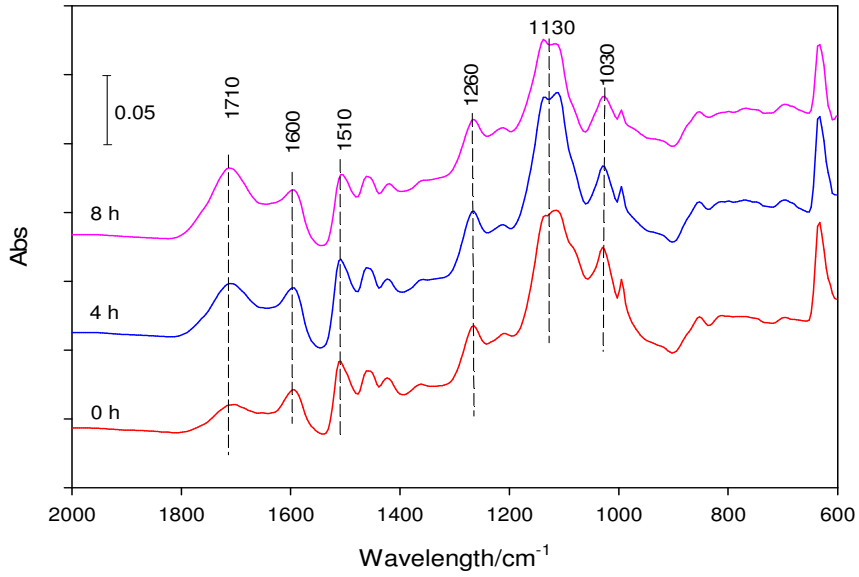

Figure 37 FTIR spectra of lignin residue

Table 9 Content of functional groups in lignin residues

Lignin Solution	C=O group	C-O-C group
Initial	0.72	1.74
4 hour	0.85	1.58
8 hour	1.04	1.51

Additionally, HPLC was employed to characterize the remaining solution, in order to determine the intermediates formed after lignin oxidation. The HPLC results are presented in Figure 38. Two primary products were characterized as vanillin and vanillic acid. These two by-products derived from the oxidation of lignin demonstrate attractive properties for myriad applications in the food, fragrance and chemical industries.

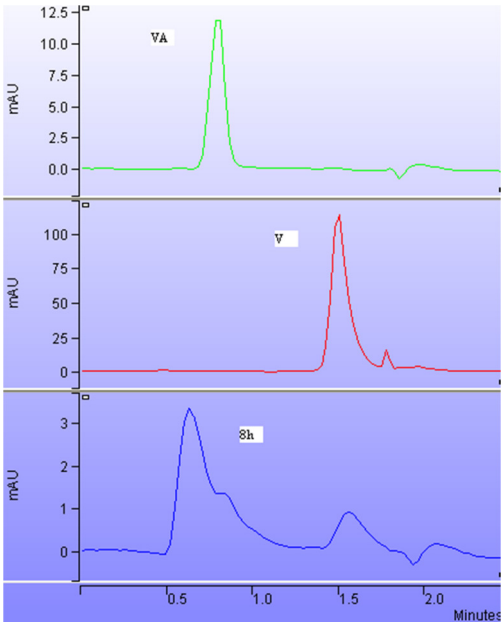

Figure 38 HPLC spectra of lignin oxidized intermediates (from above to below: vanillic acid, vanillin, lignin 8 hour oxidized product)

Chapter 7 Summaries and Future Work

In this study, we have demonstrated different approaches to modify kraft lignin, aiming to add value to this industrial by-product. Kraft lignin has been extracted from the black liquor of paper and pulping industries. Both hardwood and softwood lignin have been extracted and studied. The results show that industrial softwood black liquor contains more lignin than the hardwood black liquor. Lignin could be extracted from black liquor by lowering the pH of the black liquor using either an acid or CO_2.

The modifications of kraft lignin include chemical and electrochemical approaches, where chemical modifications have been carried out to modify the structures and hydrophobic properties, aiming to improve the potential application of kraft lignin as a rubber filler. Lignin modifications with different electrophilic reagents have been studied to add new functional groups and modify the surface morphologies of kraft lignin. The lignin modified with glyxoal and epichlorohydrin (LGE) shows some promising results. FTIR spectra indicate that the structure of kraft lignin has been changed, which could lead to further cross-linking reaction. SEM and BET results show that the modified lignin possesses a larger surface area with more dispersive particles. Because of those promising properties, the kraft lignin modified with glyoxal and epichlorohydrin (LGE) has been chosen for further rubber reinforcing study. A scale-up manufacturing of modified lignin has been carried out. LGE has been applied as a rubber filler and the reinforcing effect has been tested, compared with unmodified kraft lignin and traditional rubber filler, carbon black. The results show that the partial substitution of carbon black with lignin could lead to different properties of filled rubber. The LGE filled rubber presents a larger tensile

strength and better compliance than traditional carbon black and unmodified kraft lignin, which could be the result of its better dispersive surface morphologies, as well as the expected occurred cross-linking reactions in lignin molecules. Therefore, modified lignin shows good potential as a rubber reinforcement to partially substitute for the traditional carbon black.

Lignin modifications with various acylating and alkylating reagents have been studied to improve the hydrophobic properties of kraft lignin through reacting phenolic hydroxyl groups and add new hydrophobic groups onto lignin molecules. The FTIR results show that all modification has occurred and the structure of lignin has been modified. Then a hydrophobicity test has been employed to analyze the improvement of lignin hydrophobic properties. The results show that kraft lignin modified with acetic anhydride (LA) not only achieves a high water resistance, but also gains optimum physical properties including a powder form. Furthermore, the easy operation of this reaction shows an attractive potential for industrial use. A scale-up preparation of LA has been carried out for further rubber reinforcing tests. However, the results from our industrial partner have not been received as of the content of this thesis.

In this study, we have demonstrated a novel approach, which combines photocatalytic and electrochemical methods to fabricate high-performance Ti/TiO_2NT/PbO_2 electrodes. The fabricated Ti/TiO_2NT/PbO_2 electrode shows a high electrochemical response with an enduring stability. The SEM images reveal that the TiO_2 nanotubes are well covered by the PbO_2 nanoparticles. The electrochemical oxidation of lignin at the fabricated Ti/TiO_2NT/PbO_2 electrode has been studied, showing that the oxidation process follows the pseudo first order kinetics. We further investigated the effects of concentration, current and

temperature on the electrochemical oxidation of lignin. These results reveal that the concentration of the lignin solution has a negligible influence on the oxidation process, and that the optimal oxidation current and temperature are 100 mA and 60 °C, respectively. The activation energy for the electrochemical oxidation of lignin at the$Ti/TiO_2NT/PbO_2$ electrode under 100 mA was determined to be 16.04 kJ/mol. The COD reduction of the lignin solution further demonstrated that the fabricated $Ti/TiO_2NT/PbO_2$ electrode is effective for the oxidation of lignin. Finally, we have studied the intermediates that result from lignin oxidation, which were revealed to be vanillin and vanillic acid. In summary, our study has shown that the PbO_2 nanoparticles photoelectrodeposited on the TiO_2 nanotubes are effective for lignin oxidation. The electrochemical oxidation of lignin is a promising approach for the conversion of lignin into valuable products such as vanillin and vanillic acid, which enhance the potential utility of lignin that is found in the pulp and paper industrial wastewater.

The main recommendation for the future work is to further investigate the lignin model compound reaction in order to study the exact structure of the cross-linking product. The investigation of model compound reaction could thus help understand the modification mechanisms between lignin and glyoxal, which could further lead to a better control of the modification pathways. On the other hand, as kraft lignin modified with glyoxal and epichlorohydrin (LGE) showed an improved reinforcement in rubber, more studies could be made to optimize this modification approach for a better reinforcing effect in rubber. In addition, demonstration of new chemical modification approaches on kraft lignin has potential for adding value to this industrial by-product to meet requirements for more applications. Finally, more studies could be made on electrochemical oxidation of lignin

using different electrode materials. Furthermore, the accelerated lifetime of the fabricated TiO_2NT/PbO_2 electrode could be tested for stability purpose. As lignin is a cheap and renewable by-product from the pulp and paper industry, the development of value-added products from lignin would greatly benefit both the economy and environment.

References

[1] T. Higuchi, Wood Sci. Technol. 40 (2006) 16-25.

[2] T.Q. Hu, Chemical Modifiacation, Properties, and Usage of Lignin, 2002.

[3] J.J. Lundherg, Int. Congr. Pure Appl. Chem. 27 (1980) 373.

[4] P.J. Kopak, D.J. Osteck, W. Foakers, J.J. Kasl, J. Appl. Poly. Sci. 37 (1983) 491.

[5] W.G. Glasser, C.A. Barnett, Y.J. Sano, J. Appl. Poly. Symp.37 (1983) 441.

[6] A.M. Nada, H. El-saied, M.H. Fadl, M. Nassar, Polym. Degrad. Stab. 43 (1994) 55.

[7] A. Gartner, G. Gellerstedt,Nord.Pulp Pap. Res. J. 14 (1999) 163-170.

[8] A.M.A. Nada, M. El-Sakhawy, S.M. Kamel, Polym.Degrad. Stab. 60 (1998) 247-251.

[9] E. Tiainen, T. Drakenberg, T. Tamminen, K. Kataja, A. Hase, Holzforschung 53 (1999) 529-583.

[10] K.V. Sarkanen, C.H. Ludwig, Lignin: Occurrence, Formation, Structure and Reactions, Wiley-Interscience,1971.

[11] K. Freudenberg, A.C. Neish, Constitution and Biosynthesis of Lignin, Springer Verlag, Berling, 1968.

[12] O. Derkacheva, D. Sukhov, Macromol. Symp. 56 (2008) 61-68.

[13] D. Fengel, G. Wegener, Wood Chemistry, Ultrastructure and Reactions, Walter de Gruyter, 1989.

[14] J.G. Buta, F. Zadrazil, G.C. Galletti, J. Agric. Food Chem. 37 (1989) 1382-1384.

[15] A. Sakakibara, Wood Sci. Technol. 14 (1980) 89.

[16] W.G. Gllasser, H.R. Gllasser, Holzforschung 28 (1974) 5.

[17] E. Adler, Wood Sci. Technol. 11 (1977) 169.

[18] O. Derkacheva, D. Sukhov, Macromol. Symp. 56 (2008) 61-68.

[19] N. El Mansouri, J. Salvado, Ind.Cro. Prod. 26 (2007) 116-124.

[20] R. Liu, X. Zhou, J. Phys. Chem. 97 (1993) 9613-9617.

[21] J.M. Yang, D.I. Goring, Can. J. Chem. 58 (1980) 2411.

[22] T. Liitia, T. Tamminen, Holzforschung 61 (2007) 623-627.

[23] G. Huang, J.X. Shi, T.A.G. Langrish, Bioresour. Technol. 98 (2007) 2829-2835.

[24] M.A. Lara, A.J. Malaver, O.J. Rojas, A.M. Gonzalez, J. Bullon, E. Araujo, Int. Biodeterio.Biodegrad. 52 (2003) 167-173.

[25] M. Zaied, N. Bellakhal, J. Hazard.Mater. 163 (2009) 995-1000.

[26] M. Naqvi, J. Yan, E. Dahlquist, Bioresour. Technol. 101 (2010) 8001-8015.

[27] J. Joelsson, L. Gustavsson, Resour.Conserv.Recycl.52 (2008) 747-763.

[28] N. Berglin, H. Eriksson, T. Berntsson, Performance Evaluation of Competing Designs for Efficient Cogeneration from Black Liquor. 2nd Biennial Johan Gullichsen Colloquium. (1999).

[29] M. Ksibi, S. Ben Amor, S. Cherif, E. Elaloui, J. Photochem. Photobiol. 154 (2003) 211-218.

[30] S. Mahesh, B. Prasad, I.D. Mall, I.M. Mishra, Ind. Eng. Chem. Res. 45 (2006) 2830-2839.

[31] E. Larson, S. Consonni, T. Kreutz, J. Engin.Gas.Turb.andPow. 122 (2000) 255-261.

[32] M. Sandberg, O. Holby, J. Environ. Eng. Sci. 7 (2008) 335-344.

[33] M.A. Lara, A.J. Rodriguez-Malaver, O.J. Rojas, O. Holmquist, A.M. Gonzalez, J. Bullon, N. Penaloza, E. Araujo, Int. Biodeterior. Biodegr. 52 (2003) 167-173.

[34] F. Torrades, M. Perez, H.D. Mansilla, J. Peral, Chemosphere 53 (2003) 1211-1220.

[35] O. Wallberg, A. Holmqvist, A.S. Jonsson, Desalination 180 (2005) 109-118.

[36] O. Wallberg, A.S. Jonsson, R. Wimmerstedt, Desalination 156 (2003) 145-153.

[37] O. Wallberg, A.S. Jonsson, Desalination 195 (2006) 187-200.

[38] Q. Zhang, K.T. Chuang, Adv. Environ. Res. 3 (2001) 251-258.

[39] H. Braconnot, Ann. Chim. Phys. 12 (1819) 172.

[40] A. Payen, Compt. Rend. 9 (1832) 149.

[41] P. Klason, Cellulosechem. 4 (1923) 82.

[42] K. Freudenberg, T. Ploetz, Ber. 73 (1940) 754.

[43] P. Klason, Tek. Tidskr. Avd. Kemi. 23 (1893) 55.

[44] F.E. Brauns, The Chemistry of Lignin, Academic Press, 1952.

[45] E. Hagglund, Chemistry of Wood, Academic Press, 1951.

[46] Q. Shen, T. Zhang, M.F. Zhu, Physicochem. Eng. Aspects 320 (2008) 57-60.

[47] X. F. Sun, R. C. Sun, P. Fowler, M.S. Baird, International J. Polymer Anal. Charact. 9 (2005) 317-337.

[48] X. Zhao, L. Dai, D. Liu, J. Appl. Poly. Sci. 114 (2009) 1295-1302.

[49] K. Freudberg, W. Betz, C. Numann, Chem. Ber. 62 (1929) 56.

[50] A.M. Nada, Y. Fahmy, H. El-Bayoumy, Polym. Degrad. Stab. 46 (1994) 293.

[51] W. Thielemans, R.P. Wool, Biomacromolecules 6 (2005) 1895-1905.

[52] N. El Mansouri, A. Pizzi, J. Salvado, Holz Roh Werkst 65 (2007) 65-70.

[53] N. El Mansouri, A. Pizzi, J. Salvado, J. App. Poly. Sci. 103 (2007) 1690-1699.

[54] Y. Nagamatsu, M. Funaoka, Green Chem. 5 (2003) 595-601.

[55] A. Simmons, A. Eisenberg, Polym. Prepr. 27 (1986) 341.

[56] A. Tejado, C. Pena, J. Labidi, J.M. Echeverria, I. Mondragon, Bioresour. Technol. 98 (2007) 1655-1663.

[57] D.K. Setua, M.K. Shukla, V. Nigam, H. Singh, G.N. Mathur, Polym. Compos. 21 (2000) 988-995.

[58] Z. Jin, S. Shao, K.S. Katsumata, T. Ishida, K. Iiyama, JARQ 43 (2009) 71-79.

[59] X.F. Sun, R.C. Sun, J.X. Sun, J. Agric. Food Chem. 50 (2002) 6428-6433.

[60] R. Tolba, M. Tian, J. Wen, Z.H. Jiang, A. Chen, J. Electroanal. Chem. 649 (2010) 9 - 15

[61] J. Yanhua, Q. Weihong, L. Zongshi, C. Lubai, Energy Sources 26 (2004) 409-414.

[62] N. Rattanasom, T. Saowapark, Polym. Test 26 (2007) 369.

[63] M. Tuncan, A. Tuncan, A. Cetin, Waste Manage Res. 21 (2003) 83.

[64] M. Bhattacharya, A.K. Bhowmick, J. Mater. Sci. 45 (2010) 6139-6150.

[65] N. Rattanasom, T. Saowapark, Polym. Test 26 (2007) 369.

[66] W.B. Wiegand, India R. J. 60 (1920) 423.

[67] K.G. Gatos, K. Kameo, J. Express Polym. Lett.1 (2007) 27.

[68] D. Xu, J. Karger-Kocsis, Z. Major, R. Thomann, J. Appl. Poly. Sci. 112 (2009) 1461.

[69] H. Ismail, N.F. Omar, N. Othman, J. App. Poly. Sci. 121 (2011) 1143-1150.

[70] M. Morton, Rubber Technol. 1973.

[71] J.L. Leblanc, Prog. Polym. Sci. 27 (2002) 627-687.

[72] D.K. Setua, M.K. Shukla, V. Nigam, H. Singh, G.N. Mathur, Polym.Compos. 21 (2000) 988-995.

[73] M.G. Kumaran, S.K. De, Kautschuk Gummi Kunststoffe 30 (1977) 915.

[74] Ibid, J. Appl. Poly. Sci. 22 (1978) 1885.

[75] Ibid, Kautschuk Gummi Kunststoffe 31 (1978) 435.

[76] Ibid, J. Poly. Sci. 17 (1979) 399.

[77] R.R. Nichols, U.S. Patent 2845422 (1958)

[78] B. Xiao, X.F. Sun, R.C. Sun, Polym.Degrad. Stab. 71 (2001) 223-231.

[79] M.V. Alonso, J.J. Rodriguez, M. Oliet, F. Rodriguez, J. Garcia, M.A. Gilarranz, J. App. Poly. Sci. 82 (2001) 2661-2668.

[80] S. Witayakran, A.J. Ragauskas, Enzyme Microb. Technol. 44 (2009) 176-181.

[81] E.C. Capanema, M.Y. Balakshin, C.L. Chen, J.S. Gratzl, A.G. Kirkman, Holzforschung 55 (2001) 397-404.

[82] E.C. Capanema, M.Y. Balakshin, C.L. Chen, J.S. Gratzl, A.G. Kirkman, Holzforschung 55 (2001) 405-412.

[83] E.C. Capanema, M.Y. Balakshin, C.L. Chen, J.S. Gratzl, A.G. Kirkman, Holzforschung 56 (2002) 402-415.

[84] A. R. Goncalves, Priscila Benar. Bioresour. Technol. 79 (2001) 103-111.

[85] N. El Mansouri, A. Pizzi, J. Salvado, HolzRohWerkst 65 (2007) 65-70.

[86] F. Bertaud, J.P. Croue, B. Legube, Ozone Sci. & Eng. 23 (2001) 139-148.

[87] G.A. Amaral-Labat, A. Pizzi, A.R. Goncalves, A. Celzard, S. Rigolet, G.J.M. Rocha, J. App. Poly. Sci. 108 (2008) 624-632.

[88] A. R. Goncalves, PriscilaBenar. Bioresour. Technol. 79 (2001) 103-111.

[89] T. Malutan, R. Nicu, V.I. Popa, Bioresources 3 (1) 13-20.

[90] C. Martinez, J.L. Rivera, R. Herrera, N. Flores, J.L. Rica, J. Mol. Model 14 (2008) 77-81.

[91] Y.L. Stephen, Wausau, U.S. Patent 209478 (1980).

[92] H.T. Dellicolli, P. Dilling, S.T. Falkehag, U.S. Patent 654884 (1981).

[93] N. El Mansouri, A. Pizzi, J. Salvado, HolzRohWerkst 65 (2007) 65-70.

[94] W. Thielemans, R.P. Wool, Biomacromolecules 6 (2005) 1895-1905.

[95] R. John, Z. Yinsheng, Tetrahedron 58 (1998) 1349-1354.

[96] D.K. Setua, M.K. Shukla, V. Nigam, H. Singh, G.N. Mathur, Polym.Compos. 21 (2000) 988-995.

[97] A.T. Martinez, J. Rencoret, G. Marques, A. Gutierrez, D. Ibarra, J.C. Delrio, Phytochemistry 69 (2008) 2831-2843.

[98] J.C. Delrio, J. Rencoret, G. Marques, A. Gutierrez, D. Ibara, L.M. Zhang, A.T. Martinez, J. Agric. Food Chem. 56 (2008) 9525-9534.

[99] J. Ralph, J. Nat. Prod. 59 (1996) 341-342.

[100] J. Ralph, F. Lu, J. Agric. Food Chem. 46 (1998) 4616-4619.

[101] F. Lu, J. Ralph, Chem. Commun. (2002) 90-91.

[102] J.C. del Rio, A. Gutierrez, A.T. Martinez, Rapid Commun. Mass Spectrom. 18 (2004) 1181-1185.

[103] J.C. del Rio, G. Marques, J. Rencoret, A.T. Martinez, A. Gutierrez, J. Agric. Food Chem. 55 (2007) 5461-5468.

[104] X. Haibo, K. Alistair, K. Iikka, G. Mari, S.A. Dimitris, Biomacromolecules 8 (2007) 3740-3748.

[105] R.D. Harfield, J.M. Marita, K. Frost, J. Grabber, J. Ralph, F. Lu, H. Kim, Planta 229 (2009) 1253-1267.

[106] G. Chen, Sep. Purif. Technol. 38 (2004) 11-41

[107] J. Iniesta, P.A. Michaud, M. Panizza, G. Cerisola, A. Aldaz, C. Comninellis, Electrochim.Acta 46 (2001) 3573-3578

[108] M. Tian, L. Bakovic, A. Chen, Electrochim.Acta 52 (2007) 6517-6524

[109] B. Adams, M. Tian, A. Chen, Electrochim.Acta 54 (2009) 1491-1498

[110] M. Rafiee, D. Nematollahi, J. Electroanal. Chem. 626 (2009) 36-41

[111] C. Zeng, F. Liu, D. Ping, Y. Cai, R. Zhong, J.Y. Becker, J. Electroanal. Chem. 625 (2009) 131-137

[112] R. Tolba, G. Wu, A. Chen.Bioresources, 6(2) (2011) 1322-1335

[113] S. Carmen, J.H.P. Utley, M. Petrescu, H. Viertler, J. Appl. Electrochem. 19 (1989) 535-539

[114] B. Wang, L. Gu, H. Ma, J. Hazard. Mater. 143 (2007) 198-205

[115] V.A. Smirnov, E.I. Kovalenko, Elektokhimiya 28 (1992) 485-497

[116] L.P. Nagpurkar, A.R. Chaudhari, J.D. Ekhe, Asian J. Chem. 14 (2002) 1387-1392

[117] M. Tian, J. Wen, D. MacDonald, R.M. Asmussen, A. Chen, Electrochem. Comm. 12 (2010) 527-530

[118] M.R. Hoffmann, W. Choi, D.W. Bahnemann, Chem. Rev. 95 (1995) 69-96

[119] K.P. Beh, F.K. Yam, S.S. Tneh, Z. Hassan, Appl. Surf. Sci. 257 (2011) 4706-4708.

[120] C. Xiaobo, J. Chin, Catal. 30 (2009) 839-851.

[121] H. Hou, S. Lo, Sep. Purif. Technol. 58 (2007) 179-191.

[122] G.K. Gopal, O.K. Varghese, M. Paulose, K. Shankar, C.A. Grimes, Sol. Energ.Mater. Sol. 90 (2006) 2011-2075.

[123] K.S. Raja, M. Misra, K. Paramguru, Electrochim.Acta 51 (2005) 154-165.

[124] N.K. Allam, C.A. Grimes, J. Phys. Chem. 111 (2007) 13028-13032.

[125] R. Hahn, J.M. Macak, P. Schmuki, Electrochem. Commun. 9 (2007) 947-952.

[126] J.X. Gao, G. Zhao, W. Shi, Chemosphere 75 (2009) 519-525

[127] M. Panizza, G. Cerisola, Ind. Eng. Chem. Res. 47 (2008) 6816-6820

[128] A. Anglada, A. Urtiaga, Environ. Sci. Technol. 43 (2009) 2035-2040

[129] L. Ciriaco, C. Anjo, M.J. Pacheco, Electrochim.Acta 54 (2009) 1464-1472

[130] C.A. Martinez-Huitle, M.A. Quiroz, Electrochim.Acta 50 (2004) 949-956

[131] X.M. Chen, G.H. Chen, Environ. Sci. Technol. 37 (2003) 5021-5026

[132] Z.C. Wu, M. H. Zhou, Environ. Sci. Technol. 35 (2001) 2698-2703

[133] J. Cao, H. Zhao, F. Cao, Electrochim.Acta 52 (2007) 7870-7876

[134] G. Zhao, Y. Zhang, Y. Lei, J. Gao, D.M. Li, Environ. Sci. Technol. 44 (2010) 1754-1759

[135] A.B. Velichenko, E.A. Baranova, D.V. Girenko, R. Amadelli, S.V. Kovalev, F.I. Danilov, Russ.J.Electrochem. 39 (2003) 615-621

[136] L.V. Taveira, J. M. Macak, L. F. Dick, J. Electrochem. Soc. 152 (2005) B405-B410

[137] J. M. Macak, P.J. Barczuk, H. Tsuchiya, M.Z. Nowakowska, A. Ghicov, M. Chojak, S. Bauer, Electrochem. Commun. 7 (2005) 1417-1422

[138] X. Quan, S.G. Yang, X.L. Ruan, Environ. Sci. Technol. 39 (2005) 3770-3775

[139] J. Feng, D.C. Johnson, J. Electrochem.138 (1991) 3328

[140] T. Chao, X. Bo, Y. Li, J. Fang, M. Huang, J. Chem. Engi. 166 (2011) 15-21

[141] M. Yasumichi, N. Masayuki, M. Tetsuhiro, J. Phys. Chem. B 103 (1999) 7190-7194

[142] M.K. Janet, W. Oleh, R.H. Michael, J. Phys. Chem. B 101 (1997) 2637-2643

[143] C. Crestini, M.C. Caponi, R. Saladino, Bioorg. Med. Chem. 14 (2006) 5292-5302

[144] K.J. Reszka, B.A. Wagner, L.M. Teesch, B.E. Britigan, D.R. Spitz, C.R. Burns, Cancer Res. 65 (2005) 6346-6353